CLM - R 161

CLM - R 161

UKAEA RESEARCH GROUP

Report

PROGRAMMED REVERSED FIELD PINCHES IN HBTX-I

A J L VERHAGE

CULHAM LABORATORY
Abingdon Oxfordshire
1976
Available from H. M. Stationery Office

C.18

PRICE £2.00

U.D.C.
621.039.615.2
621.039.626 HBTXI

CLM-R161

PROGRAMMED REVERSED FIELD PINCHES IN HBTX-I

by

A J L Verhage

ABSTRACT

This report describes experimental studies of Reversed Field Pinches (RFPs) on HBTX-1 (R = 100 cm, a = 6 cm) for different programmed field configurations, principally using electrical diagnostics. Measurements on MHD instabilities, field diffusion, and the final plasma states are compared with theory.

The stability of the RFP is observed to depend on the plasma current and on the ratio of the radius of the conducting wall to that of the plasma. The plasma is stable for currents and compression ratios below certain critical values. When the compression ratio is increased gross m = 1 helical kink instabilities appear, which are predicted by ideal MHD theory, and lead to radial expansion of the plasma. The explanation for gross m = 1 modes observed for currents above the critical value requires the use of MHD instability theory which includes dissipative effects such as finite conductivity. The occurrence of more localized modes during the decay of the plasma is ascribed to the fact that the pressure gradient is too large since the value of β always increases and exceeds the stability limit. The observation that the current decay time does not increase when the peak current is raised above the critical value, as might be expected theoretically, is attributed to MHD instabilities. The field configurations measured later during the decay of the plasma are similar for all RFPs studied in this work and are largely independent of the initial field distribution, which indicates that RFP discharges tend to relax to a particular final state in the experiments.

Euratom UKAEA Association for Fusion Research,
Culham Laboratory,
Abingdon,
Oxfordshire OX14 3DB,
England.

August 1976

SBN: 85311 047 6

CONTENTS

PREFACE AND ACKNOWLEDGEMENTS

The work presented in this report is based on measurements with electrical diagnostics on Reversed Field Pinches in HBTX-1, in which the author was involved between 1971 and 1976. The report should therefore not be read as a review of all the work done on HBTX-1 during this period and the interpretations and conclusions of the measurements are those of the author.

It is a pleasure to acknowledge the help of H. A. B. Bodin under whose direction the work was done, and for whose elaborate comments and suggestions on the manuscript I am much indebted. Many thanks are due to D. C. Robinson, who supervised and guided the work in this report, for the many valuable discussions and suggestions concerning the experiments and the interpretation of data. I am also grateful for his comments on the manuscript. Numerous valuable discussions have taken place with other colleagues of the Toroidal Pinch Group, especially with E. P. Butt, whose data acquisition system was used, C. W. Gowers, A. A. Newton and M. R. C. Watts, who cooperated in the experiments in the last two years and contributed streak photographs to this report. I am very grateful to the following colleagues with whom I worked together on HBTX-1: W. H. Davies, J. A. Fessey, H. T. Fielding, J. Goodenough, R. L. Grant, G. C. H. Heywood, F. C. Jones, P. A. Jones, R. E. King, R. J. Rigley and A. F. Webster.

SUMMARY

Programmed Reversed Field Pinches (RFPs) have been studied for a wide range of plasma parameters in HBTX-1. Most RFP discharges were produced in Deuterium at filling pressures of 40 mtorr and plasma currents (I) between 30 kA and 170 kA. Programmed RFPs in Helium and Argon have also been investigated. The pinch ratio, and hence the compression ratio of the plasma, is controlled in HBTX-1 by varying the amount of trapped longitudinal flux for a given value of the plasma current. The primary circuits are usually crowbarred after the programming stage and the plasma decays.

The time behaviour of β_θ during the decay is found to depend on the value of the plasma current. The value of β_θ usually rises to about 0.6 during the early stages of the decay of RFP configurations. When the plasma current falls below 50 kA ($k\bar{T}_e < 6$ eV) the value of β_θ increases towards 1 during the decay of the plasma. When the current exceeds 50 kA β_θ stays approximately constant at 0.6 for which value the plasma violates Suydam's necessary criterion and is generally found to be unstable. The time-scale for classical plasma diffusion in a stable RFP exceeds the time-scale for ohmic heating, hence β_θ is predicted to increase, which will lead to MHD instabilities (because the pressure gradient becomes too large) and consequently to a reduction in the time-scale of plasma diffusion. The stability observed when β_θ rises above the value of 0.6 for $I < 50$ kA can be explained by dissipative effects.

The generally observed linear decay of the plasma current is interpreted as a result of a continuous increase in the plasma resistance during the decay. Exponential decay, which is observed in radiation dominated plasmas with $k\bar{T}_e < 5$ eV and also after strong MHD instabilities, indicates a constant resistance during decay.

When, in programmed RFPs, the pinch ratio at the plasma boundary

exceeds 2 stabilization by the conducting wall does not occur and a large amplitude m = 1 helical kink instability with origin inside the central plasma column is observed. This gives rise to a redistribution of field and plasma, during which the pinch ratio falls to about 2. The growth of the m = 1 instability agrees with predictions from linear ideal MHD theory, but redistribution of the field can only be explained by a non-linear description of the instability. The m = 1 helical kink instabilities observed in RFPs and in stabilized pinches for the same value of the pinch ratio have very similar properties.

Programmed RFPs with pinch ratios less than 2 are characterized by large gradients of field and plasma pressure near the wall of the vessel. Diffusion eventually leads to an approximately constant current density and a constant pressure gradient and causes the pinch ratio to rise towards 2. Perturbations with m = 1 observed in these RFPs are identified as gross MHD modes, believed to be resistive tearing modes since the configuration is predicted to be stable to ideal MHD instabilities.

Reversed field pinches in HBTX-1 usually diffuse towards a final configuration with a pinch ratio of about 2, independent of the history of the programming stage, provided the total conserved flux has the same sign as the flux trapped by the plasma. If the total flux has the opposite sign diffusion causes the configuration to contract, the pinch ratio changes sign and reaches a value of - 2.

The pinch ratio before and after instabilities can vary by a factor of up to 5 in programmed RFPs. Such variations are typical for HBTX-1 where a large vacuum field region exists outside the plasma. In the theory of the relaxation of a plasma the plasma boundary and flux boundary coincide and the changes in the pinch ratio are predicted to be much smaller.

The value of the decay time of the plasma current averaged over a large fraction of the total decay period, is found to be approximately the same when the peak value of the current is varied between 50 kA and 170 kA. For RFPs with the same values of the plasma inductance and β_θ the decay time is predicted to scale as I^3. However for $I > 60$ kA RFPs are observed to be MHD unstable while the level of field perturbations increases with the current. The instabilities lead to an enhanced loss of plasma energy which increases with the amplitude of the perturbations.

1. INTRODUCTION

The Reversed Field Pinch (RFP) is a diffuse pinch in which the longitudinal magnetic field in the outside region of the plasma has the opposite direction to the field trapped within it. Field reversal provides the necessary shear in magnetic field required for MHD stability which can be obtained, if, in addition, there is a conducting wall sufficiently close to the plasma.

Theoretical predictions[1] of stability with values of β of 0.3 - 0.4 (β is the ratio of the plasma pressure to the magnetic pressure), the observation of improved stability due to self generated reversed field in Zeta[2], and the results from programmed pinch experiments by Ohkawa and colleagues[3], were the main incentives to study the reversed field pinch in HBTX-1.

In the relatively slow Zeta experiment (rise time 1 msec) the field reversal could not be controlled with the external circuit, while β was about 0.1. It therefore seemed desirable to study the influence of the reversed field on pinch configurations systematically using field programming. The High Beta Toroidal Experiment (HBTX-1), which came into operation in 1970, utilises fast programming to set up field configurations on a time-scale which is usually short compared with the time required for instabilities to change the distribution.

Programmed RFPs are now also studied in Los Alamos (ZT-1)[4], Padua (Eta-Beta)[5], and Tokyo (TPE-1)[6]. A review of the RFP has been given by Bodin[7].

The properties of programmed RFPs in HBTX-1 have been investigated in the last five years for a range of different initial parameters. In this report the results of measurements with electrical diagnostics on the RFPs are presented and a comparison is made with theoretical predictions. The limitations of theory and experiment are also indicated. The MHD stability

theory of the RFP is reviewed; and other theoretical topics such as particle effects, MHD equilibrium, field diffusion, and the relaxation to a final state are briefly mentioned.

The behaviour of the main plasma parameters during the decay of programmed RFPs leads to a division of the discharges into two classes, characterized by the ratio of plasma current to trapped toroidal flux (the pinch ratio). The experimental data are therefore divided into two classes; discharges in the first class have a pinch ratio above a critical value, and the ratio of the radius of the conducting wall to the effective plasma radius (compression ratio) is greater than 2. These RFPs are unstable to ideal MHD modes, which lead to a fall in the pinch ratio. The pinch ratio for the second class of RFPs is below the critical value, and the plasma is stable when the plasma current does not exceed about 60 kA (at a filling pressure of 40 mtorr Deuterium). The pinch ratio does not change during instabilities which occur when the current is raised above 60 kA. The time evolution of the pinch ratio indicates that the field configurations for both classes of RFPs tend towards similar final states, which may be compared with the final states predicted by Taylor[8]. The decay time of the plasma current is observed to be approximately constant when the peak value of the current exceeds 50 kA, while theoretically it should increase. This result is discussed and related to instabilities. The diffusion of the fields in an RFP, and also the stability of the plasma during diffusion is discussed and shown to depend strongly on the sign of the total flux in crowbarred experiments.

2. FIELD PROGRAMMING IN HBTX-1 AND PARAMETERS OF THE EXPERIMENT

Reversed field pinches in HBTX-1 are set up by time-programming selected fractions of three separate capacitor banks, charged to the required voltages. The gas in the quartz torus (major radius R = 100 cm, inner radius r_1 = 6 cm, thickness 0.5 cm) is usually ionized by switching one main capacitor bank (C ≤ 360 μF, V ≤ 50 kV, risetime 3 - 17 μsec) to the gaps in the aluminium shell (major radius 100 cm , inner radius r_2 = 7.5 cm, thickness 5 cm). A plasma sheath is formed near the wall, implodes, and compresses the longitudinal field (B_z) which was applied before from a relatively low voltage capacitor bank (C = 34 mF, V ≤ 6 kV, risetime 100 μsec). The B_z-field outside the plasma annulus is then reversed by switching a fast capacitor bank (C ≤ 720 μF, V ≤ 50 kV, risetime 3 μsec), with polarity opposite to that of the slow bank, to the B_z-coils. When the desired magnitudes of plasma current and reversed field are reached the capacitor banks are crowbarred at the load assembly by metal-to-metal switches, and the plasma is left to decay. The programming sequence is illustrated in figure 1a. The amount of flux trapped by the plasma is controlled by the relative timing of the applied field reversal and the plasma current. The power input, measured by the Poynting vector S, reaches a maximum after B_z changes sign and is reduced to zero when the circuits are crowbarred.

In some experiments the gas is partly ionized (30% - 50%) before the main bank is switched into the load assembly by means of a small capacitor bank, which is also connected to the gaps in the shell and induces a plasma current of 15 - 20 kA with an oscillation period of 5 μs.

The amount of trapped flux can be optimized for a given current by adopting a different mode of programming, shown in figure 1b. The reversed field is produced during the second half cycle of the B_z-waveform, while the plasma current is initialized during the first half cycle. The

trapped flux is maximal when I and B_z rise simultaneously. The power input reaches a maximum well before B_z is reversed. Stabilized z-pinches are produced by inducing a plasma current in a gas with a constant B_z-field (stabilizing field). Reversal of B_z in the outside region of stabilized z-pinches occurs spontaneously in some conditions provided the total toroidal flux is conserved by crowbarring the B_z-circuit in advance. The effective radius (r_3) inside which the flux is conserved is 9.8 cm, which is larger than the inside radius of the metal shell due to the flux stored in the transmission lines between coils and crowbar switches.

The filling pressure of the Deuterium gas generally used for programmed RFPs was varied between 10 and 120 mtorr, but most experiments were performed with 40 mtorr, yielding a line density $N_e = 3 \times 10^{19}$ m^{-1} and an average number density $n_e = 2.6 \times 10^{21}$ m^{-3}, when Deuterium is fully ionized. The concentration of impurities, identified as mainly Carbon and Oxygen, was generally less than 1%, hence $Z_{eff} \approx 1$. Programmed RFPs were also studied in HBTX-1 with Hydrogen, Helium, and Argon as a filling gas with pressures between 15 and 40 mtorr.

3. PLASMA DIAGNOSTICS IN HBTX-1

The diagnostic instruments used on HBTX-1 between 1971 and the beginning of 1976, and their application to measurements on Reversed Field Pinches (RFPs) and stabilized z-pinches (SZPs) in that period, are listed in TABLE 1.

TABLE 1

	Measurement	Details of instrument	Measured Quantity	Configuration studied
Optical	90° Thomson scattering	Pulsed ruby laser λ = 694.3 nm Pulse duration 20 ns. Power $\leq$ 500MW maximally 4 pulses with adjustable time intervals. Radial scan with Risley prism, polychromator + P.M.-array.	n_e, T_e	Peak temperatures in RFP for I_{max} = 30 - 160 kA. Detailed scans of n_e, T_e for SZP and RFP with $I_{max} \leq$ 50 kA.
	D_α-emission	Radial scan with Risley prism, monochromator and photomultiplier.	n_o	RFP with known n_e, T_e. $I_{max} \leq$ 50 kA.
	Spectroscopy of visible spectrum.	Ebert-monochromator with P.M. Resolution $\Delta\lambda$ = 0.02 nm	T_e from line ratios. Impurity lines.	RFP: I_{max} = 30-130 kA
	Streak photography	Image converter streak cameras with filters for pass-band selection. Stereo views of plasma with wide-angle lenses at 2 positions 26 cm apart.	Light intensity in space and time. n_e from continuum emission, wavelength from correlations.	Standard technique, applied to all RFP and SZP.
Ultraviolet	Spectroscopy of UV with $\lambda \gtrsim$ 120 nm.	Vacuum UV - spectrometer with normal incidence grating. Resolution $\Delta\lambda \approx$ 0.02 nm.	Radiated power from plasma. Ly α absorption line ratios.	RFP: I_{max} = 30 - 130 kA
	Radiation detection	Photo-multiplier with Sodium salicylate scintillator and selective filters in calibrated set-up.	Radiated power from plasma between 5 nm and 600 nm	RFP: I_{max} = 40 - 120 kA
X-rays	X-ray measurements	X-ray detector. P.M. with lead scintillator and lead filters.	X-ray-spectrum 30 keV - 4 MeV.	RFP: I_{max} = 50 - 120 kA SZP: I_{max} = 50 - 120 kA
Infrared	Line density measurements.	Michelson interferometer with CW - CO_2 laser (10.6 μm)	$\int_{-r_1}^{r_1} n_e \, d\ell$ as a function of time	RFP: I_{max} = 50 - 120 kA SZP: I_{max} = 50 - 120 kA
Neutral particles	Neutral particle detection.	Time-of-flight spectrometer with secondary emission detector 10 eV - 1 keV	Energy spectrum of neutral particles	RFP: I_{max} = 40 kA SZP: I_{max} = 40 kA
Electrical	Outer region parameters	Langmuir double probe.	n_e, T_e	RFP: I_{max} = 50 - 120 kA SZP: I_{max} = 50 - 120 kA
	Electrical measurements	Internal magnetic probes, multicoil (6 or 12) array inserted into plasma along vertical line, radial scans for 3 components of field.	$\vec{B}$ (r, θ = 90°, t)	RFP: I_{max} = 40 - 120 kA SZP: (+ reversal) I_{max} = 60, 100-150kA
		Azimuthal dependence of magnetic field measured with sets of 8 discrete coils, sine-cos coils	$\vec{B}$ (r_2, θ, t)	- do -
		Standard measurements flux-loops, Rogowski-coils	Φ , I	Standard on all experiments.

4. THEORETICAL BACKGROUND

4.1 Plasma states with minimum magnetic energy

Reversed field pinches in HBTX-1 are usually crowbarred after the field programming stage and the plasma is left to decay. The fields are generally redistributed by instabilities and diffusion until a distribution is reached which remains approximately constant during the further evolution of the RFP. Predictions of the final state can be made theoretically by using the principle that a plasma configuration will tend to evolve towards a state of minimum energy under certain constraints imposed by the apparatus and the physical properties of the system. The fewer constraints there are the lower the energy in the final state, as illustrated by Wells[9]. Taylor[8] used the variational principle to minimize the magnetic energy of a plasma with negligible kinetic energy, bounded by an ideally conducting wall. In a plasma without dissipation field line topology must be conserved and the infinite number of local constraints permits any force-free configuration to be the final state. When breaking and rejoining of field lines is assumed without significant dissipation of magnetic energy (i.e. the time-scale for reconnection is much shorter than the diffusion time τ_σ, as was the case in e.g. Zeta) the number of constraints reduces to one: The conservation of the integral of $\vec{A}.\vec{B}$ over the entire plasma volume, or

$$\frac{dK}{dt} = \frac{d}{dt}\int_V \vec{A}.\vec{B}\, d\tau = 0 \quad \text{where} \quad \vec{B} = \vec{\nabla}\wedge\vec{A} \ .$$

This condition is more general than conservation of magnetic flux. For an axisymmetric system:

$$K = \int_0^{r_{wall}} \{\Phi,\chi\}\, dr \quad \text{with } \{\Phi\ \chi\} = \Phi \frac{\partial \chi}{\partial r} - \chi \frac{\partial \Phi}{\partial r}$$

$$\Phi(r) = 2\pi r A_\theta = \int_0^{2\pi} \int_0^{r} B_z\, r\, dr\, d\theta \text{ (longitudinal magnetic flux)}$$

$$\chi(r) = -\ell A_z = \int_0^{\ell} \int_0^{r} B_\theta\, dr\, d\ell \text{ (azimuthal magnetic flux).}$$

The final state in an axisymmetric system is shown to be the Bessel function distribution[10]. In the Force-Free Bessel Function Model (F.F.B.F.M.) with $\vec{j} = \alpha \vec{B}$, and α = constant, B_z is reversed when the pinch ratio $\Theta > 1.2$, where $\Theta(r) \equiv \mu_o r\, I/2\Phi(r)$. The F.F.B.F.M. is unstable to helical m = 1 modes when the effective radius of the current distribution is too small compared with the radius of the conducting wall; the effective radius for marginal stability corresponds to $\Theta = 1.55$ ($\beta = 0$). When the plasma current is increased at this critical value of Θ the extra magnetic energy will be stored in helicity of the fields while Θ remains 1.55. The Force-Free Paramagnetic Model (F.F.P.M.), where $\alpha = \alpha(r) = B_z\,(r)/B^2$ has more magnetic energy for the same value of Θ while B_z in the outside region is not reversed. The F.F.P.M. and the F.F.B.F.M. are extreme cases at either end of the spectrum of force-free field distributions. Rusbridge[11] treated the intermediate cases with less reversal than in the F.F.B.F.M. in his "Tangled Discharge Model", and found satisfactory agreement between data from Zeta and theoretical predictions for the dependence of field reversal on Θ.

The theory mentioned here applies to plasmas in linear geometry with $\beta = 0$ and the plasma boundary coinciding with the flux boundary, assumptions which are not valid on HBTX-1, and the consequences of this are now discussed. Toroidal curvature has little influence on the value of Θ for which B_z reverses in the F.F.B.F.M., even for an aspect ratio of 2[8], and

its effect can be ignored for HBTX-1 with an aspect ratio of 17. The effect of plasma pressure is to raise the value of Θ for which reversal occurs, e.g. for a stable B.F.M. Θ increases from 1.20 to 1.33 while $\beta \leq 0.10$[12,14]. To obtain higher values of β the value of Θ must also be raised to satisfy Suydam's necessary criterion for shear stabilization. The maximum value of β, theoretically possible in the MHD stable B.F.M., is 0.26 for $\Theta = 2.1$[13,14]. If no constraints are applied to the plasma pressure the minimum energy state has $\nabla p = 0$, provided the pressure gradient relaxes on the time-scale of field reconnection, which is assumed to be much shorter than the diffusion time τ_σ, otherwise K is not invariant. In HBTX-1 however, changes in the pressure gradient occur on the time-scale of field diffusion, so the variation principle only applies to a period which is short compared with the field diffusion time. In the theory the plasma boundary coincides with the magnetic boundary at $r = r_2$ and Θ is uniquely defined as $\Theta(r_2)$. In the experiment the plasma is restricted to $r = r_1$, thus the radial velocity at the wall is zero. The vacuum field between r_1 and r_2 can interact with the plasma, which will lead to a discrepancy between $\Theta(r_1)$ and $\Theta(r_2)$. Outside r_2 the value of B_θ is zero and B_z is constant, so $K(r_2)$ is the constraint of the system in HBTX-1 identical to K in the theory. The evolution of a particular RFP is characterized by $\Theta(r_1,t)$, as this parameter usually reflects changes in the distribution of fields inside the plasma. The pinch ratio at the flux boundary $\Theta(r_3,t)$ is directly proportional to the plasma current and gives no extra information, but is useful as a parameter to compare one plasma configuration with another.

4.2 Equilibrium in a reversed field pinch

The quartz torus of HBTX-1 is enclosed by a metal shell at $r = r_2$ and an equilibrium is provided by the surface currents on the shell by which the effect of forces acting on the plasma is countered. Outwardly directed forces due to the toroidal geometry are relatively small since $r_2/R = 0.07$

in HBTX-1 and the maximum equilibrium displacement Δ is usually less than 1 cm ($\Delta/r_2 < 0.13$)[15]. The thin horizontal slit in the shell allows fast programming of the reversed field by means of the external B_z-circuit, but has a negligible effect on the equilibrium of the plasma.

The plasma in an RFP is heated and confined by the longitudinal plasma current. Shock heating of ions is negligible for RFPs in HBTX-1 for typical rise times of the field used[16]. The equipartition time for electrons and ions τ_{ei} is 0.1 μs for T_e = 10 eV and 5 μs for T_e = 100 eV ($n_e = 2.6 \times 10^{21}$ m^{-3} in both cases). For most experiments it is reasonable to assume that after the setting-up stage of the plasma a magnetostatic equilibrium with a scalar pressure ($p_\perp = p_{/\!/}$) is obtained with $T_e = T_i$. Except for cases with fast growing large amplitude instabilities the inertia term can be ignored and the equilibrium equations when the driving electric field is small (e.g. in crowbarred discharges) are:

$$\vec{\nabla} p = \vec{j} \wedge \vec{B} \quad , \quad \vec{\nabla} \wedge \vec{B} = \mu_o \vec{j} \quad , \quad \vec{\nabla} \cdot \vec{B} = 0 \quad .$$

For axisymmetric plasmas knowledge of the magnetic field $\vec{B}(r,t)$ suffices to describe the equilibrium. The current density $\vec{j}(r,t)$ and the pressure $p(r,t)$ are derived from $\vec{B}(r,t)$. This is illustrated by a model of the RFP configuration, shown in figure 2, where the measured fields are approximated by simple functions.

From $p(r) = \frac{1}{\mu_o} \int_r^{r_o} \left(B_z \frac{d}{dr} B_z + \frac{B_\theta}{r} \frac{d}{dr} r B_\theta \right) dr$ the pressure of the given field profile is

$$p(r) = \frac{1}{2\mu_o} \left\{ 2 B_\theta^2(r_o) \left(1 - \left(\frac{r}{r_o} \right)^2 \right) + B_z^2(r_1) - B_z^2(o) \; f(r) \right\}$$

where $f(r)$ is a parabolic function between $r_o - \delta$ and r_o which is required

for a smooth transition of the pressure profile from a parabola to zero at $r = r_o$. The pinch ratio at $r_1 > r_o$ for the model configuration is

$$\Theta(r_1) = \left(\frac{1 - \left(\frac{B_z(r_1)}{B_z(o)} \right)^2}{1-\beta_\theta} \right)^{\frac{1}{2}} \frac{\frac{r_1}{r_o}}{1 + \frac{B_z(r_1)}{B_z(o)} \left(\frac{r_1^2}{r_o^2} - 1 \right)}$$

where $\beta_\theta = \frac{\bar{p}}{B_\theta^2(r_o)/2\mu_o} = \frac{8\pi}{\mu_o} \frac{Nk(\bar{T}_e + \bar{T}_i)}{I^2}$; N is the line density and $k\bar{T}_e$ and $k\bar{T}_i$ are the averaged energy of electrons and ions respectively. A necessary condition for the stability of RFPs in HBTX-1 is $|B_z(r_1)/B_z(o)| \lesssim 0.2$ (Section 4.3) so in the expression for $\Theta(r_1)$ the term $(B_z(r_1)/B_z(o))^2$ can be ignored with respect to 1. For weakly compressed RFPs in HBTX-1 with $r_1/r_o \lesssim 1.5$ $\Theta(r_1)$ reduces to $\frac{r_1}{r_o}(1 - \beta_\theta)^{-\frac{1}{2}}$, and since $B_z(r_1)/B_z(o)$ scales as r_o^2/r_1^2, the pinch ratio $\Theta(r_1)$ can also indicate the compression ratio for more compressed RFPs in HBTX-1.

The equilibrium configuration is determined by the externally adjustable parameters $\Phi(r_1)$, I, $B_z(r_2)$, as illustrated in figure 3. The radius of the plasma column is mainly controlled by $I/\Phi(r_1)$ since stability considerations do not allow much freedom in $B_z(r_2)$ for HBTX-1.

4.3 The stability of reversed field configurations

It has been shown theoretically that in the RFP configuration MHD stable confinement of plasma with high values of beta ($\gtrsim$ 30%) is possible. In this section the stability of the RFP both to ideal MHD modes ($\sigma \to \infty$) and dissipative MHD modes is briefly reviewed.

4.3.1 Stability to ideal MHD modes

Robinson[1] applied the energy principle to test the stability of diffuse pinches with special emphasis on the RFP. The procedure, as

outlined by Newcomb[17], is to separate the perturbation amplitude $\xi(r)$ for an axisymmetric plasma into normal modes $\xi(r) = \xi(r)\, e^{i(m\theta+kz)}$, where $\xi_\theta(r)$ and $\xi_z(r)$ are dependent on $\xi_r(r)$. Instability is expected whenever the perturbed potential energy $\delta W(\xi)$ is negative. To assess this the appropriate Euler-Lagrange equation must be solved. The plasma boundary is assumed to be the conducting wall at $r = r_2$, thus $\xi_r(r_2) = 0$. A marginal stability analysis (i.e. the growthrate $\omega = 0$) is carried out. From Sturm's comparison theorem for the Euler equation the azimuthal modes with mode number $m = 1$ are shown to be the most unstable and in the analysis emphasis is placed on $m = 1$ helical kink modes. The potential energy for gross perturbations with $m = 1$ is represented by the function $g_{m=1,k}(\frac{dp}{dr}, P, B_\theta)$. The pitch function $P = r\, B_z/B_\theta$ is a monotonically decreasing function of radius for the RFP, generally favourable for stability since instability is predicted wherever $dP/dr = 0$. The most unstable wavelengths correspond to longitudinal wave numbers k with $kP = (1 - k^2r^2)/(3 + k^2r^2)$ and $kP = -1$. Gross modes are predicted when the necessary criterion $|P(0)| > |P(r_2)|/3$ is violated. This pitch condition sets a limit to the degree of field reversal. The conducting wall must be sufficiently close to the region where most of the current flows to stabilize modes with $kP = -1$. For a skin current model of the RFP stability demands $\Phi(r_2) > 0$ as a necessary condition. A model configuration of the RFP with diffuse currents and $\beta = 0.31$ requires the conducting wall inside the point with $r_2/r_p = 2.0$, for stability against $m = 1$ modes (r_p is the radius for which the plasma pressure has half the maximum value). The position of the conducting wall is usually computed numerically, although approximate results can be obtained with analytical methods[1]. The flux condition $\Phi(r_2) > 0$ is necessary but not sufficient for wall stabilization. All equilibria with $\Phi(r_2) < 0$ are overcompressed and unstable to $m = 1$ modes. Instead of the compression ratio r_2/r_p the normalized radius $\tilde{r}$ is frequently

used, defined in the F.F.B.F.M. as $\tilde{r} = \alpha r$ where $\alpha = j/B$ (section 4.1). For other models $\tilde{r}$ us defined by normalizing the field components near $r = 0$ to the F.F.B.F.M.. The F.F.B.F.M. is stable to ideal MHD modes if the normalized radius of the conducting wall $\tilde{r}_2 < 3.176$[18]. In this special case $\Theta(r)$ is directly related to $\tilde{r}$ as $\Theta(r) = \frac{\tilde{r}}{2} = \frac{\alpha r}{2}$, thus $\Theta(r_2) < 1.588$ for stability. The relation between Θ and $\tilde{r}$ is only valid for the F.F.B.F.M. In the model configuration with $\beta = 0.31$[1], $\tilde{r}_2 < 2.45$ corresponds to $r_2/r_p < 2$, and the pinch ratio for marginal stability is $\Theta(r_2) = 2.4$. The flux condition $\Phi(r_2) > 0$, which is equivalent to $\Theta(r_2) < \infty$, is already satisfied for $\tilde{r}_2 < 2.60$. The driving energy of the $m = 1$ mode in the RFP mainly comes from the azimuthal magnetic field, although the plasma pressure can also play a role. The upper limits to β_θ for stability against modes with $m = 1$ and $m = 0$ are[1]:

$$\beta_\theta < 1 \text{ for } m = 1$$

$$\beta_\theta - \beta_\theta(B_z = 0) < 0.5 \text{ for } m = 0 \quad [1,19]$$

($\beta_\theta(B_z=0)$ is local value of β_θ at the reversal point).

Suydam's criterion is the local criterion necessary for stability against pressure-driven modes

$$S = \frac{dp}{dr} + \frac{r B_z^2}{8\mu_o}\left(\frac{1}{P}\frac{dP}{dr}\right)^2 > 0 \quad .$$

Stability against gross $m = 1$ modes sets a limit to $\Theta(r_2)$, hence to the maximum overall shear in the magnetic field. The value of β is therefore restricted to a maximum of about 0.3 for RFPs stable to ideal MHD modes including convective modes, although with models for which the pressure gradient is supported by currents near the conducting wall higher values of β are possible[14]. In the analysis of the stability of diffuse pinches Goedbloed and Sakanaka[20] permit instabilities with growth times exceed-

ing the field diffusion time, as such instabilties will not significantly affect energy confinement (they called this σ-stability). Their RFP model is σ-stable for $\beta = 0.20$ ($\beta_\theta = 0.38$), if the conducting wall position satisfies $r_2/r_p < 2.2$, i.e. 10% further out than the model configuration with $\beta = 0.31$ mentioned above. Growth rates of ideal MHD modes have been computed by various authors[20,22]. The most dangerous gross mode is invariably m = 1, originating inside the reversal point (kP = -1). Compressibility allows extra degrees of freedom to the plasma and leads to higher growth rates for a given configuration[22,23]. Properties of instabilities which are readily measurable are $B_r(r)$ and the mode numbers of the magnetic field outside the plasma near the conducting wall (m, k). The radial dependence of the displacement amplitude ξ_r is known in terms of the fields $\xi_r = B_r/(\frac{m B_\theta}{r} + k B_z)$, and the origin of the instability is in general the point where $m B_\theta + kr B_z = 0$ or $kP = -m$, and where also $B_r = 0$.

4.3.2 MHD modes in a dissipative RFP

When finite electrical conductivity effects and other dissipative effects are included in the equations describing MHD instabilities in the RFP, numerical methods have to be used to solve them.

Resistive MHD theory was developed by Rebut[24], Furth, Killeen, and Rosenbluth[25], and Coppi, Green, and Johnson[26]. Three basic types of resistive modes are distinguished in a current layer[25]: Tearing modes (long wavelength modes corresponding to break-up along current lines), Rippling modes (short wavelength modes, break-up across current lines), and G-modes (interchange modes associated with curvature of the magnetic field). The tearing mode (resistive counterpart of the ideal MHD helical kink) and the rippling mode (due to gradients in the conductivity) are governed by the time-scale $\tau_\sigma^{3/5}\ \tau_A^{2/5}$, the g-modes by the time-scale $\tau_\sigma^{1/3}\ \tau_A^{2/3}$ (these modes serve as an analogue of the convective modes). The Lundquist number $S = \tau_\sigma/\tau_A$ defined as the ratio of diffusion time ($\tau_\sigma = \mu_o \sigma r_p^2$) to hydromagnetic transit-time ($\tau_A = r_p(\mu_o \rho)^{\frac{1}{2}}/B$) determines the stability behaviour

and is used as a parameter in numerical computations of resistive instabilities. In HBTX-1 S is about 100 for an RFP with I = 50 kA ($k\bar{T}_e$ = 6 eV) and about 1,000 for I = 100 kA ($k\bar{T}_e$ = 20 eV), in Deuterium (filling pressure 40 mtorr).

To stabilize resistive tearing modes the compression ratio of the plasma must be less than is required for stability against ideal MHD modes. This is illustrated for the F.F.B.F.M. where marginal stability analysis for the tearing mode has been carried out analytically. Voslamber and Callebaut[17] predicted that if the position of the conducting wall is outside $\tilde{r}_2$ = 3.176 m = 1 modes are unstable in the limit of ideal MHD. The limit for purely resistive modes is $\tilde{r}_2$ = 3.104, and m = 1 tearing modes are expected for $3.104 < \tilde{r}_2 < 3.176$ (Gibson and Whiteman[27]). The most dangerous resistive modes in HBTX-1 are also the m = 1 tearing modes, with growth rates that can exceed the growth rate of ideal MHD modes, due to the multiplication factor for the field configuration by which the time-scale $\tau_A S^{3/5}$ is reduced[28]. In the limit $S \to \infty$ ideal MHD modes are the fastest growing modes. Various RFP models in which the compression ratio is optimized for the use in HBTX-1 were tested for stability against MHD modes. Configurations with a maximum value of Θ = 3.6 and $\beta \leq 0.18$ were found to be stable to both ideal and resistive MHD modes[13,14]. The model configuration with β = 0.31, which is stable to ideal MHD modes, appears to be unstable to tearing modes unless the compression ratio is reduced so that $\tilde{r}_2 \leq 2.0$[29]. As a rule less shear is available to stabilize pressure driven instabilities when the value of Θ is reduced for a given model configuration and therefore also the largest average value of β possible for a stable plasma is smaller. The positive gradient of a hollow pressure profile tends to stabilize not only ideal MHD modes, but also tearing modes in that region, provided the current distribution for j_z is not hollow[21,30]. Diffusion will eventually cause the pressure

gradient to become negative everywhere, which is already assumed in the tested field models for HBTX-1. Experimental identification of the tearing mode is possible from the form of the radial distribution of B_r. The difference between $B_r(r)$ for m = 1 tearing modes and ideal MHD modes depends on S and is predicted to be small for HBTX-1, hence difficult to measure. When a measured field configuration is theoretically stable to ideal MHD modes while gross m = 1 instabilities are observed then these modes are likely to be tearing modes[31]. To identify rippling modes and g-modes experimentally is difficult, if at all possible; numerical simulation also encounters severe problems[32].

Localized instabilities associated with the violation of Suydam's criterion are generally stabilized by dissipative effects. In an RFP in HBTX-1 with $S \approx 100$ ($T_e \approx 10$ eV) these localized modes are stablized when Suydam's criterion is violated by a factor of 2, for which ion-viscosity is the most important mechanism but finite conductivity and thermal conduction also play a role, as has been shown with the numerical MHD code GNSTAB[29,33].

4.3.3 Non-linear effects of MHD instabilities

The theory of MHD instabilities reviewed above is linear and applies only when perturbations are small compared with the main components of the magnetic field. Redistribution of flux, observed during the large amplitude stage of m = 1 helical kink instabilities in compressed RFPs and stabilized z-pinches (section 6.1.4), requires a non-linear description of the instability to be explained. The flux enhancement in pinches is understood as the result of the distortion of the current channel from a cylindrical into a helical shape, which occurs during the large amplitude phase of the instability[33,34]. Flux amplification has been found in numerical simulations of the development of the m = 1 helical kink instability with 3-dimensional MHD codes[35,36].

4.3.4 Particle effects

Stringer[37] has shown that the finite Larmor radius of ions in a typical high beta plasma such as the RFP has a stabilizing influence on localized MHD modes. This requires that the ion-ion collision frequency τ_{ii}^{-1} is less than the ion Larmor frequency ω_{ci}, thus $\omega_{ci}\,\tau_{ii} > 1$, an essential assumption of the theory. Finite Larmor radius effects are predicted to raise the stability limit for local m = 1 modes by a factor of 2 for HBTX-1 parameters. If in HBTX-1 the average temperature is $\bar{T}_e = \bar{T}_i = 6$ eV and the average particle density is $\bar{n}_e = \bar{n}_i = 3 \times 10^{21}\ m^{-3}$, parameters typical for an RFP with I = 50 kA in 40 mtorr Deuterium, for which the average value of the field is 0.25 Tesla, then $\overline{\omega_{ci}\,\tau_{ii}}$ (averaged over the plasma) is 0.2 (the Coulomb logarithm is taken as 10). For plasma currents above 75 kA $\overline{\omega_{ci}\,\tau_{ii}} > 1$. The Lundquist number S is proportional to $\omega_{ci}\,\tau_{ii}$ for a given particle density: $\omega_{ci}\,\tau_{ii} = 5.3\times10^{6} S/\ell \bar{n}_i^{\frac{1}{2}}$ (= S/100 for $\bar{n}_i = 3 \times 10^{21}\ m^{-3}$ and $\ell = 10^{-2}$ m). The stabilizing effect of the finite Larmor radius of ions on localized modes would be difficult to detect in the experiment since RFPs with $\overline{\omega_{ci}\,\tau_{ii}} > 1$ are generally unstable to gross MHD modes.

During the setting-up stage the charged particle density outside the annular plasma sheath is relatively low ($n_e \approx 10^{20}\ m^{-3}$) while the strength of the electric field is of the order $10^4\ V\ m^{-1}$. The electric force is then likely to exceed dynamical friction (Dreicer condition[38]) and runaway is expected for the electrons. Relativistic electron beams can build up on a time-scale of 1 μs in HBTX-1 only to be quenched when n_e rises sufficiently and the electric field is reduced, or by destruction of magnetic surfaces through MHD instabilities. The X-ray emission observed[39] during the programming stage of RFPs and stabilized z-pinches indicates that such beams of electrons, which are accelerated to relativistic velocities on the expected time-scale (section 6.1.1), exist in the experiment.

4.4 Diffusion

The decay of the fields in a crowbarred RFP is controlled by dissipation of the plasma currents, although instabilities can influence the decay by changing the inductance through a redistribution of the fields. In this section the influence of field diffusion on the shear and the consequences for instabilities due to the pressure gradient are described theoretically, and expressions relating the plasma resistance and the decay of the total plasma are derived.

4.4.1 Field diffusion and Suydam's criterion for stability

In an axisymmetric configuration with negligible hydrodynamic flow the convection term may be dropped from the induction equation and magnetic field diffusion is governed by the equations[40]:

$$\frac{\partial B_z}{\partial t} = \frac{1}{r}\frac{\partial}{\partial r}\left(\eta_{zz}\, r\, \frac{\partial B_z}{\partial r}\right) - \frac{1}{r}\frac{\partial}{\partial r}\left(\eta_{z\theta}\, \frac{\partial}{\partial r}\,(r\, B_\theta)\right)$$

$$\frac{\partial B_\theta}{\partial t} = \frac{\partial}{\partial r}\left(-\eta_{\theta z}\, \frac{\partial B_z}{\partial r}\right) + \frac{\partial}{\partial r}\left(\eta_{\theta\theta}\, \frac{1}{r}\frac{\partial}{\partial r}\,(r\, B_\theta)\right) .$$

The electrical conductivity along the magnetic field is $\sigma_{/\!/}$, across the field $\sigma_\perp$. The resistivity tensor in terms of the electrical conductivity reads:

$$\eta_{zz} = \frac{1}{\mu_o \sigma_{/\!/}}\left\{1 + \frac{(\sigma_{/\!/}-\sigma_\perp)}{\sigma_\perp}\,\frac{B_z^2}{(B_z^2 + B_\theta^2)}\right\}$$

$$\eta_{\theta\theta} = \frac{1}{\mu_o \sigma_{/\!/}}\left\{1 + \frac{(\sigma_{/\!/}-\sigma_\perp)}{\sigma_\perp}\,\frac{B_\theta^2}{(B_z^2 + B_\theta^2)}\right\}$$

$$\eta_{z\theta} = \eta_{\theta z} = -\frac{1}{\mu_o \sigma_{/\!/}}\left\{\frac{(\sigma_{/\!/}-\sigma_\perp)}{\sigma_\perp}\,\frac{B_\theta\, B_z}{(B_z^2 + B_\theta^2)}\right\} .$$

The ratio $\sigma_\perp/\sigma_{//}$ is determined by $\omega_{ce}\,\tau_{ee}$, i.e. the product of the gyro-frequency of the electrons ω_{ce} and the electron-electron collision time τ_{ee}. In nearly all experimental conditions in HBTX-1 $\omega_{ce}\,\tau_{ee} \gg 1$, thus $\sigma_\perp/\sigma_{//} = 0.5$ and $(\sigma_{//} - \sigma_\perp)/\sigma_\perp = 1$. The anisotropy of the electrical conductivity gives rise to two different characteristic diffusion times in a cylinder $\tau_{\sigma_{//}} = \mu_o\,\sigma_{//} r^2$ and $\tau_{\sigma_\perp} = \mu_o\,\sigma_\perp r^2$. In the centre of an RFP $B_\theta \ll B_z$, hence $\eta_{z\theta} \approx 0$ and $\eta_{zz} = 2\eta_{\theta\theta}$, and B_z diffuses twice as fast as B_θ. Near the field reversal point $B_z \ll B_\theta$, here B_θ diffuses faster by a factor of 2, so diffusion in the RFP causes a rapid decrease in the gradients of the magnetic field and reduces the shear. In force-free configurations $\vec{j} \wedge \vec{B} = 0$, thus $\vec{j}$ is parallel to B, and $\sigma_\perp$ is effectively zero. Very rapid diffusion is then possible wherever $|B_\theta/B_z| \ll \sigma_\perp/(\sigma_{//}-\sigma_\perp)$ and $|B_z/B_\theta| \ll \sigma_\perp/(\sigma_{//}-\sigma_\perp)$. These conditions can only be met near the points where $B_\theta = 0$, $B_z \gg 0$ (the centre) and $B_z = 0$, $B_\theta \gg 0$ (field reversal point). In the RFP the current density perpendicular to $\vec{B}$ is comparable with $j_{//}$ and values of $\sigma_\perp/\sigma_{//}$ below 0.5 are not expected if the plasma is stable[41].

When the initial magnetic field distribution of an axisymmetric plasma is given the evolution of the discharge for which the conductivity profile and the time dependence is known follows from the diffusion equations. In the RFP with $\sigma_{//}(r) = 2\,\sigma_\perp(r)$ the conductivity is related to the electron temperature as $\sigma(r) \propto T_e^{3/2}$. The equations have been solved numerically[22,39,41] for the RFP and the solutions for $\vec{B}(r,t)$ are characterized by a rapid reduction of magnetic shear. The sign of B_z after a few diffusion times becomes positive everywhere when the total conserved toroidal flux is positive, otherwise it becomes uniformly negative. Thus the reversal point of B_z will eventually move outwards when $\Phi(r_3) > 0$, or move inwards for $\Phi(r_3) < 0$. The result of the reduction of the shear due to diffusion in an RFP will be the violation of Suydam's criterion unless also the pressure

gradient is reduced. It is therefore necessary to consider the effect of plasma diffusion during the diffusion of magnetic field. The relation between electrical conduction and thermal conduction is directly obtained from the generalized version of Ohm's law. The diffusion across the magnetic field is separated into plasma drift, diffusion driven by Ohmic dissipation (v_{dif}) and thermal diffusion ($v_{th\ dif}$)[42]. When the external E-field is zero as in crowbarred discharges and the diffusion velocity across the field (in radial direction in an axisymmetric plasma) is $v_{dif} + v_{th\ dif} = (-\nabla p + 3/2\ nk\nabla T_e)/\sigma_\perp B^2$. Since $\nabla p = \nabla\ nk(T_e + T_i)$ and ∇n and $\nabla T_{e,i}$ have the same sign during decay in an RFP the diffusion velocity across the field is less than $|\nabla p/\sigma_\perp B^2|$. From the definition for β and τ_σ the time-scale for the decay of ∇p is $2\tau_\sigma/\beta$, which is a factor β^{-1} longer than the decay time of the fields. For RFP configurations the shear of the magnetic field decreases on the same time-scale as the magnetic field, so Suydam's criterion will be violated during the decay phase at a time which depends on the initial value of the Suydam function $dp/dr + r\ B_z^2\ (dP/dr)^2/P^2\ 8\ \mu_o$. The value of β is therefore predicted to increase during field diffusion until a critical value is reached at which instabilities occur. Butt and Pease[43] calculated this "overheating" time for a stationary plasma with constant dissipation for Zeta-like parameters and also found this to occur on a time-scale short compared with τ_σ. An RFP with very steep gradients obtained by fast programming in ZT-1 (an order of magnitude faster than in HBTX-1) diffuses rapidly towards a configuration with $\beta \approx 1$ so that no equilibrium is possible in this case[44].

4.4.2 The decay of the plasma current during field diffusion

An estimate of the average value of the plasma conductivity is obtained from the decay of the plasma current in a crowbarred discharge. The total current through a cross-section of the plasma is

$I = \int \vec{j} \circ d\vec{A} = \int_0^{2\pi} \int_0^{r_1} j_z \, r\,dr\,d\theta$. In an RFP the conductivity is anisotropic and j_z is generally coupled to both longitudinal and azimuthal components of the fields. If thermal effects are neglected Ohm's law reduces to $\vec{j}_{/\!/}/\sigma_{/\!/} = \vec{E}_{/\!/}$ and $\vec{j}_{\perp}/\sigma_{\perp} = \vec{E}_{\perp}$ where $\vec{E}_{\perp}$ is the component of the effective electric field perpendicular to B. In an axisymmetric plasma with anisotropic conductivity

$$j_z = (\sigma_{/\!/} - \sigma_{\perp})\, E_{/\!/}\, \frac{B_z}{|B|} + \sigma_{\perp} E_z$$

which reduces to $j_z = \sigma_{/\!/} E_z$ for $\sigma_{\perp} = \sigma_{/\!/}$ or $B_\theta << B_z$. The plasma current in the case of isotropy is only related to the change in azimuthal flux χ, in a crowbarred discharge with $E_z(r_2) = 0$, since

$$E_z(r) = \frac{1}{\ell}\left(\frac{\partial \chi(r)}{\partial t} - \frac{\partial \chi(r)}{\partial t}\right) ,$$

where ℓ is the unit length, hence

$$I = \int_0^{r_1} E_z \sigma(r)\, 2\pi r dr = \frac{1}{R}\left(-\frac{\partial \chi(r_2)}{\partial t} + \left\langle \frac{\partial \chi(r_1)}{\partial t} \right\rangle\right)$$

The plasma resistance R is defined by

$$\frac{\ell}{R} = \int_0^{2\pi} \int_0^{r_1} \sigma(r)\, r dr d\theta = \pi\, r_1^2 \langle \sigma(r_1) \rangle \quad , \quad \text{and}$$

$$\frac{\ell}{R} \left\langle \frac{\partial \chi(r_1)}{\partial t} \right\rangle \equiv \int_0^{r_1} \frac{\partial \chi(r)}{\partial t} \quad \sigma(r) 2\pi r dr \quad .$$

The equation for the plasma current can be rewritten as the longitudinal circuit equation

$$IR + \frac{d}{dt}(L_{eff}\, I) = 0 \quad , \quad \text{where}$$

$$\frac{d}{dt}(L_{eff}\, I) \equiv \frac{d}{dt}\chi(r_2) - \left\langle \frac{\partial \chi(r_1)}{\partial t} \right\rangle \quad .$$

The plasma resistance R is a function of the effective plasma inductance L_{eff} and the current decay time $\tau_I = - I/(dI/dt)$:

$$R = \frac{L_{eff}}{\tau_I} - \frac{d\, L_{eff}}{dt} \quad .$$

The determination of L_{eff} requires assumptions about the azimuthal field and the conductivity profile. For example, for a profile with constant current density and electrical conductivity between $r = 0$ and $r = r_o$, and vacuum for $r > r_o$: $L_{eff} = (\chi(r_2) - \frac{1}{2}\chi(r_o))/I$. In the case of isotropic conductivity a relation between τ_I and R can also be obtained from the energy equation, as the power dissipated by the plasma current is provided by the azimuthal field:

$$I_z^2\, R_z = - \frac{d}{dt}(\tfrac{1}{2}\, L_z\, I_z^2) \quad \text{with } \tfrac{1}{2}\, L_z\, I_z^2 = \int_V \frac{B_\theta^2}{2\mu_o}\, d\tau \quad ,$$

where the integral is over the volume V inside the conducting shell. However part of the longitudinal field energy will be dissipated in the same volume and contributes to the heating of the plasma, and knowledge of $\sigma(r)$, $B_\theta(r)$, and $B_z(r)$ is required to relate R to R_z. In the anisotropic case with $\sigma_\perp = \sigma_{/\!/}/2$, relevant for RFPs in HBTX-1, where $j_z = \frac{\sigma_{/\!/}}{2}(E_{/\!/}\, B_z/|B| + E_z)$, the expression for the circuit equation incorporates both the toroidal and the poloidal flux. To compute L_{eff} the field distribution and conductivity profiles must be known as functions of time. In the centre of the RFP $B_\theta\ (r,t) \ll B_z\ (r,t)$ and $j_z \approx \sigma_{/\!/} E_z$, whereas in the outside region $B_z\ (r,t) \ll B_\theta\ (r,t)$ hence

$j_z \approx \frac{\sigma_{//}}{2} (E_\theta + E_z)$. For RFP configurations the effect of the anisotropy on the value of L_{eff} is generally less than a factor of 2 if $\Theta(r_1) \lesssim 2$.

The current decay time is expected to be sensitive to the plasma temperature since $\langle\sigma\rangle \propto \bar{T}_e^{3/2} \propto I^3$ in the case of plasmas heated by dissipation of the current; more precisely, if $\frac{d}{dt} L_{eff} = 0$, and $\beta_\theta(t)$ and $N(t)$ are constant:

$$\tau_I(t) = \alpha \left(\frac{\mu_o}{8\pi k} \right)^{3/2} \pi r_1^2 L_{eff}(r_1) \left(\frac{\beta_\theta}{2N} \right)^{3/2} I^3$$

where $\alpha = 1.53 \times 10^{-2} / \ell n \Lambda$. (The Coulomb logarithm $\ell n \Lambda$ is about 10 for most experiments in HBTX-1). A comparison of RFPs with similar values of $L_{eff}(r_1,t)$, $N(t)$, and $\beta_\theta(t)$, but different values of the plasma current are thus expected to yield widely differing values of the current decay time. The value of L_{eff} depends on the pinch ratio, which can be controlled by field programming. The line density N is observed to be approximately constant for the same filling pressure[45], but the detailed functional dependence of β_θ (on the current) has to be obtained from direct measurement (sections 6.1.1, 6.2.2).

If β_θ and the average value of β are known as a function of time, the energy confinement time in a crowbarred discharge can be related to the current decay time. The energy balance in a plasma described by fluid equations reads

$$\frac{\partial}{\partial t} \int_V \tfrac{1}{2} \rho v^2 \, d\tau + \frac{\partial}{\partial t} \varepsilon + \frac{\varepsilon}{\tau_E} - \int_V \vec{E} . \vec{j} . d\tau = 0 \quad ,$$

where $\varepsilon = \frac{3}{2} Nk(\bar{T}_e + \bar{T}_i)$ is the total thermal energy of the plasma. Energy loss not accounted for explicitly (radiation, conduction to the wall) is incorporated in the term $\frac{\varepsilon}{\tau_E}$, with τ_E defined as the energy confinement time. In a crowbarred discharge in magneto-static equilibrium for which inertial terms and power input from the external circuit are negligibly small:

$$\tau_E = \varepsilon \Big/ \left(\frac{\partial}{\partial t} \varepsilon + \frac{\partial}{\partial t} \varepsilon_{magn} \right) \; ; \quad \text{where } \varepsilon_{magn} = \int_V \frac{B^2}{2\mu_o} \, d\tau \quad .$$

From the definitions of β and β_θ:

$$\tau_E = \frac{\beta \tau_I}{2(1 + \beta) + \tau_I \left(\frac{\dot{\beta}}{\beta} - \frac{\dot{\beta}_\theta}{\beta_\theta} \right) - \frac{\dot{\beta}_\theta}{\beta_\theta} \beta \tau_I}$$

If β and β_θ are assumed to be constant during the discharge:

$$\tau_E = \frac{\beta \tau_I}{2(1 + \beta)} \lesssim \frac{\beta \tau_I}{2}$$

So the energy confinement time in a decaying plasma such as the crowbarred RFP in HBTX-1 for which the initial value of β is about 0.2 will be an order of magnitude smaller than the current decay time if β stays constant during the decay.

5. CHARACTERISTIC PARAMETERS OF RFPs IN THE EXPERIMENT

The behaviour of a reversed field pinch during setting-up and decay is characterized by the directly measureable quantities I, $\Phi(r_2)$, $B_z(r_2)$ as is illustrated in figure 3. The pinch ratio at the plasma boundary is a derived parameter calculated as $\Theta(r_1) = \mu_o r_1 I/2(\Phi(r_2) - \pi(r_2^2 - r_1^2)\ B_z(r_2))$. This is an important parameter for HBTX-1 since RFPs are observed to evolve until a configuration is reached for which $\Theta(r_1)$ has a value of about 2. A similar behaviour of the pinch ratio has been observed before[46].

Parameters of RFPsattainable by fast programming in HBTX-1, evaluated when the crowbars are applied (typically between 3 and 10 μs after the start of the current) are limited to the hatched region in the I - $\Phi(r_1)$ plane shown in figure 4. The boundary at the right hand side of the diagram is set by m = 1 helical kink modes with growth times shorter than the programming time. During the setting-up period of RFP configurations with large values of $\Theta(r_1)$ and I the increase in $\Phi(r_1)$ associated with instabilities reduces the value of $\Theta(r_1)$, thus keeping the parameters inside the hatched region. The field reversal point is always inside r_1 = 6 cm, whereas the flux boundary is at r_3 = 10 cm, which leads to a practical lower bound on $\Theta(r_1)$ of about 1.5 for RFPs in HBTX-1. Further reduction in $\Theta(r_1)$ leads to increased wall contact and probably rapid cooling of the plasma. When the current is increased for $\Theta(r_1) \approx 1.5$ the gradient in the magnetic field near the wall becomes very large, since the field reversal point is located nearby $r = r_1$. The shear varies rapidly with radius from a large value to near zero in this region and localized instabilities are predicted with growth rates increasing with I. The value of $\Theta(r_1)$ rises as the instabilities smooth the gradients of the field, causing the boundary on the left hand side of the parameter region to curve away from the Θ = constant line. The most

suitable parameters for RFPs in HBTX-1 are characterized by $\Theta(r_1) = 2$ for then the Θ-value of the configuration is observed to remain approximately stationary.

The practical limit for $B_z(r_2)$ is imposed by the condition $\Phi(r_2) > 0$ (section 4.3.1), thus $|B_z(r_2)| < \Phi(r_1)/(\pi r_2^2 - \pi r_1^2)$. When $\Phi(r_2) = 0$ RFPs in HBTX-1 are observed to be highly compressed and unstable to m = 1 modes. It is possible to program RFPs to have $\Phi(r_2) < 0$ but the plasma becomes unstable during the setting-up stage. A further increase in $|B_z(r_2)|$ leads to highly unstable pinches which decay rapidly (Section 6.1.3). If initially $\Phi(r_2) > 0$ but $\Phi(r_3) < 0$ field diffusion will eventually cause a change in the sign of $\Phi(r_1)$, while $\Theta(r_1)$ changes sign through infinity. Pinches with $\Theta(r_1) \approx 2$ always satisfy $\Phi(r_3) > 0$.

The $\Theta(r_1) = 2$ line in figure 4 separates RFPs at the end of the programming stage into two classes:

1. RFPs unstable to gross m = 1 modes. The field configuration changes on the MHD time-scale, and $\Theta(r_1) > 2$. Stabilized z-pinches in which field reversal occurs spontaneously during gross m = 1 helical kink instabilities also belong to this class.
2. RFPs initially stable to gross m = 1 modes. Redistribution of the configuration takes place on the diffusion time-scale, and $\Theta(r_1) < 2$.

Although the initial, programmed, value of the pinch ratio $\Theta(r_1)$ can vary between 1.5 and more than 10 the final RFP configurations reached after a diffusion time of 20-30 μs are observed to be very similar; the parameter diagram for RFPs at that time is reduced to a narrow strip at either side of the line $\Theta(r_1) = 2$[47].

6. EXPERIMENTAL STUDIES OF RFPs

6.1 Reversed field pinches unstable to gross m = 1 helical kink modes

In this section RFPs of class 1 (chapter 5) are discussed for which the initial programmed value of the pinch ratio $\Theta(r_1)$ exceeds 2.

6.1.1 Experimental study of an unstable RFP with I_{max} = 50kA

A detailed study of a programmed RFP with a maximum plasma current of 50 kA is presented, in order to illustrate the behaviour of compressed RFPs which are unstable to gross m = 1 helical kink instabilities as predicted with ideal MHD theory. The maximum plasma current is somewhat higher than in the grossly stable RFPs with I ≤ 40 kA, which were reported by Robinson[41].

The RFP is produced using the programming sequence of figure 1(a). The power input into the plasma shown in figure 5(a) is given by the integrated Poynting vector $S(r_2)$, where

$$S(r_2) = -\frac{1}{2\pi r_2}\left(\frac{B_z(r_2)}{\mu_o}\,\frac{\partial\Phi(r_2)}{\partial t} + \frac{V.I}{2\pi R}\right)$$

is dervied from electrical diagnostics outside the plasma. The magnetic energy of the B_z-field inside the torus is reduced during the initial stages of programming since $\partial\Phi/\partial t < 0$ while I is still small. When $B_z(r_2)$ reverses both terms in the expression for $S(r_2)$ have the same sign and the power input increases rapidly. The total energy input is controlled by crowbarring the primary circuits at t = 3 μs. The total energy and the magnetic energy in the RFP configuration evaluated from magnetic probe data are compared in figure 5(b), with the total energy input from the external circuit. The kinetic energy of the plasma is deduced from the magnetic fields assuming pressure balance. The difference between the energy input and the kinetic and magnetic energy is accounted for by the 80 J/m required to ionize the Deuterium gas completely, with a filling

pressure of 40 mtorr. If the kinetic energy of the plasma is assumed to be thermalized at t = 3 μs thus $\frac{3}{2} N mv^2 << \frac{3}{2} Nk(\bar{T}_e + \bar{T}_i)$, where v is the velocity of directed motion, the value of β averaged over the volume inside $r = r_2$ at that time is 0.14. The errors in figure 5(b) are about 20%.

The evolution of the main parameters $I, \Phi, B_z(r_2)$ as functions of time is shown in figure 6(a). After setting-up and crowbarring the plasma current is seen to decay approximately linearly, and on average $B_z(r_2)$ also decays linearly but significant deviations from the average decay are observed. The increase in $\Phi(r_2)$ between $t \approx 4$ μs and $t \approx 15$ μs is followed by a decay similar to that of the plasma current. As shown in figure 6(a) the pinch ratios $\Theta(r_1)$ and $\Theta(r_2)$ fall as the trapped flux increases between t = 6 μs and t = 10 μs, while the plasma current decays. During the fall in the pinch ratio the first harmonic of the B_θ-field derived from sine and cosine coils is seen to increase by more than 1.0×10^{-2} T (corresponding to a displacement of 4 mm). The mean level of $B_{\theta 1}$ is due to the toroidicity, which causes an outward shift in the equilibrium position of the plasma.

The main parameters of a similarly programmed RFP, but with a gas filling of Helium, are shown in figure 6(b). The plasma current decays approximately exponentially with a shorter average decay time than in Deuterium and the fall in the values of $\Theta(r_1)$ and $\Theta(r_2)$ between t = 4 and t = 10 μs is mainly due to the fall in plasma current since the increase in flux is relatively small. The amplitude of $B_{\theta 1}$, measured with respect to its average level, is less than half the amplitude observed for the RFP in Deuterium, which indicates that the plasma is less unstable to the m = 1 mode.

The magnetic field profiles, measured for RFPs programmed as in figure 6a, evolve rapidly on a time-scale of 1 μs, as seen in figure 7.

The radial velocity due to the electric field $v_r = (E_\theta B_z - E_z B_\theta)/B^2$ is generally less than, but comparable to, the ion thermal velocity until the fields are crowbarred and the kinetic energy in the non-thermal motion can amount to a sizable fraction of the thermal energy. In a right-handed coordinate system (B_r, B_θ, B_z) the value of B_z is negative in the centre and positive outside the plasma (inverted in figure 7 for convenience of drawing), so the direction of v_r is inwards before crowbarring at t = 3.2 μs. The contribution of the non-thermal motion cannot be ignored to $t \leq 3.2$ μs and the computed pressure profiles do not only represent the thermal pressure but also the effect of directed plasma motion. At t = 3.6 μs the equilibrium is expected to be thermal since v_r will be negligible small compared with the thermal velocity of the ions ($\tau_{ei} \lesssim 0.1$ μs, section 4.2). The value of β_θ, derived from the pressure profile, is 0.4 at t = 3.6 μs and increases with time.

The time development of the RFP configuration between t = 2.6 μs and t = 3.6 μs is characterized by the contraction of the annular pressure distribution and the current distribution. The pitch of the magnetic field, $P = rB_z/B_\theta$, is reduced on average while the pressure gradient increases and at t = 3.6 μs Suydam's criterion is violated by a factor of 2 between r = 3 cm and r = 4.5 cm. The occurrence of a radial magnetic field B_r in this region indicates that the plasma is unstable. Later during the decay phase, e.g. at t = 24 μs (figure 7(b)) the gradient of the pitch has become very small while the value of β_θ has risen to 0.75, leading to the violation of Suydam's criterion by a large factor over the whole of the region where the pressure gradient is negative. Large amplitude radial field components (B_r) are observed in this region.

The average plasma temperature derived from the pressure distribution at t = 3.6 μs corresponds to $k(\bar{T}_e + \bar{T}_i)/2 = 5$ eV. The electron temperature profile can also be derived from the magnetic field profiles by

computing the electrical conductivity $\sigma_{//} = \vec{J}.\vec{B}/\vec{E}.\vec{B}$. For classical collision processes the electron temperature is proportional to $\sigma_{//}^{2/3}$, but the error in $\sigma_{//}$ is large wherever $\vec{E}.\vec{B} \approx 0$ ($E_\theta B_\theta \approx - E_z B_z$) and can reach 100% for the peak values of $\sigma_{//}$ in figure 7, whereas for the wings of the profiles the errors are about 30%. Peak values of $\sigma_{//}$ of 2×10^4 mho/m correspond to $kT_e = 5$ eV for $Z_{eff} = 1$. The pressure distribution coincides with the electron temperature distribution for t = 3.0 μs and t = 3.6 μs, although for t = 2.6 μs the calculated electron temperature distribution is peaked outside the pressure distribution. Thomson scattering data presented elsewhere[41] indicate that the electron temperature distribution is peaked outside the electron density profile at t = 3 μs. This observation can be compared with the results from probe data if the pressure distributions for electrons and ions are the same, but errors in $\sigma_{//}$ are generally too large for the conclusions of such a comparison to be relevant. Directly measured peak values of kT_e between 10 and 14 eV have been obtained, while the average over the radial distribution of T_e is 7 eV. Assuming equipartition of energy between electrons and ions (equipartition time less than 0.1 μs) the value of 7 eV can be compared with 5 eV derived from probes. Since the error in the measurements is about 20% and the error in the time correlation is 0.5 μs during which time β_θ rises rapidly, the discrepancy lies within the errors.

The pressure distribution deduced from probe data is initially hollow but gradually fills in as illustrated in figure 8, and at t = 6 μs the pressure gradient is negative everywhere. This is equivalent to a skin diffusion time $\mu_o \sigma r \delta$, for a plasma with $\sigma = 10^4$ mho/m, skin thickness $\delta = 1.5$ cm and radius r = 3 cm. This value for σ corresponds to 3.5 eV, a reasonable value for the core of the plasma where the density of neutral particles is high initially and ionization will maintain the temperature low. The regions where neutrals are being ionized, the inside and outside

of the annular pressure profile, are the major sources of emission in the visible spectrum (largely D_α) as observed from the streak photographs of figure 9. Abel inversion of the luminosity profile reveals a hollow distribution of light emission[48]. The m = 1 instability causes a displacement of the light emitting column and these observations agree approximately with those from electrical measurements[48].

The amplitude of $B_{\theta 1}$ at the conducting wall is observed to grow between t = 7 μs and t = 9 μs until $B_{\theta 1}(r_2)/B_{\theta 0}(r_2)$ is about 0.1 ($B_{\theta 0}(r_2) = \mu_o I/2\pi r_2$), when the m = 1 instability reaches maximum amplitude.

The first harmonic of the B_θ-field is defined $B_{\theta 1} = (B_{\theta s}{}^2 + B_{\theta c}{}^2)^{\frac{1}{2}}$, where $B_{\theta s} = \frac{1}{\pi}\int_0^{2\pi} B_\theta \sin\theta d\theta$ is measured with a sine coil and $B_{\theta c} = \frac{1}{\pi}\int_0^{2\pi} B_\theta \cos\theta d\theta$ with a cosine coil. The wave-number k of the m = 1 mode is determined at the conducting wall from the amplitudes of the first harmonics of the field outside the plasma where $kr_2 = B_{z1}(r_2)/B_{\theta 1}(r_2)$; see also[33]. The ratio $B_{z1}(r_2)/B_{\theta 1}(r_2)$, which is measured with discrete coils outside the plasma for two RFPs similar to the discharge in figure 6(a), is plotted as a function of time in figure 10. During the growth of the m = 1 perturbations in the outside region ($r \approx r_2$): $kr \approx 2$, or $k \approx 30\ m^{-1}$ (wavelength 20 cm). After the instability has saturated kr_2 falls to about 1. The m = 1 instability starts to grow in the region near r = 2 cm, at $t \approx 5$ μs as observed from B_r - signals shown in figure 11. The pitch $P = rB_z/B_\theta$ is 4 cm at r = 2 cm, so that the wave-number of the perturbation resonant with the main field, for which $mB_\theta + krB_z = 0$ or $kP = -m$ (section 4.3), is $k = 25\ m^{-1}$ for m = 1. This is similar to the value measured near the wall, where the sign of kr_2 is opposite to the sign of rB_z/B_θ in agreement with kP = -1. The region with maximum growth rate is seen to shift towards the centre where the pitch is larger, so the k-number of the m = 1 mode associated with the fastest

growth becomes smaller. This trend is also observed in figure 10. The maximum amplitude of B_r in the centre is reached at t = 7 μs, about 1 μs earlier than at the wall. The relation between the displacement Δ of the centre of a straight current filament with respect to the geometrical axis, due to an instability or toroidal displacement, is given by $\Delta/r_2 = B_{\theta 1}(r_2)/2B_{\theta 0}(r_2)$, yielding 4 mm for the measured values of the instability at maximum amplitude. In the centre of the discharge the shift of the magnetic axis is proportional to rB_r/B_θ, yielding values between 10 and 20 mm for t > 7 μs. As pointed out elsewhere [49] the displacement derived at the wall requires a correction for a helical plasma, by which the value of Δ is raised (in this case to about 6 mm), but the effect of the finite size of the plasma current distribution can lead to errors of interpretation for the shift of the magnetic axis [50], which can account for the difference between the two measurements. The toroidal displacement derived from $B_{\theta 1}$ in figure 6(a) is 3 mm.

When the instability grows to large amplitude and B_r becomes comparable to B_θ and B_z axisymmetric computations of the pressure and other quantities derived from the fields are no longer valid. Discontinuities are seen to occur at t = 7 μs in figure 12(a), where the kinetic and magnetic energy derived from probe measurements, assuming axisymmetry, are plotted as a function of time. They are mainly due to the effect of the helical m = 1 mode not included in the calculations. The differences in the toroidal flux $\Phi(r_2)$ derived from magnetic flux loops and from the magnetic probes, where $\Phi(r_2) = \int_0^{r_2} B_z \, 2\pi r dr$, in figure 12(b) correlate well with the measured m = 1 amplitude.

The evolution of the toroidal (longitudinal) flux $\Phi(r_2,t)$ and the poloidal (azimuthal) flux $\chi(r_2,t)$ are compared in figure 12(b), and flux conversion is observed during the instability. The error in the computation of $\chi(r_2,t)$ from the probe data during the m = 1 instability is of the

order Δ/r_2, where Δ is the shift of the magnetic axis. If $\chi(r_1,t)$ is normalized for a wavelength of 25 cm ($k = 25\ m^{-1}$) the helical flux $\psi(r_1,t) = \Phi(r_1,t) + \chi(r_1,t)$ is conserved between t = 7 μs and t = 9 μs, from which is concluded that the average wavenumber of the m = 1 helical kink instability is $25\ m^{-1}$.

The plasma energy, deduced from the measured magnetic field and shown in fig. 12(a), increases until the m = 1 instability occurs at $t \approx 7$ μs, after which a rapid fall in the energy of the field and plasma is observed, which is mainly due to the effect of the instability on the axisymmetry. (The plasma energy in figure 12(a) is the total kinetic energy for 3 degrees of freedom, but in calculations of β only the pressure perpendicular to the axis is used, thus $\beta < 1$ for the whole of the plasms decay). The value of β_θ derived from the magnetic field rises to 0.8 at t = 7 μs, as shown in figure 12(c) where the time evolution of β_θ, calculated in two different ways[47], is compared. For $t \gtrsim 7$ μs errors due to the instability are large (30-40%) but for t > 35 μs the axisymmetry is restored, and the error in β_θ is then estimated to be less than 15% so the value of β_θ at t = 40 μs is 0.9 ± 0.1. The quantity K where $K = \int_0^{r_2} \vec{A}.\vec{B}\ 2\pi r dr$ (section 4.1) is calculated for the decay phase of the RFP. As shown in figure 12(d) K is not constant during the decay but decreases by a factor 5 between t = 7 μs and t = 40 μs, and can only be considered as a constant of the system on a time-scale short compared with the diffusion time.

The plasma current in the RFP with Deuterium as a filling gas decays linearly in time as seen in figure 6(a). The energy confinement time τ_E (section 4.4.2) falls from a value of 10 μs at t = 10 μs to about 7 μs at t = 30 μs after which time τ_E increases when β_θ rises.

Exponential decay is observed for RFPs where radiation effects are important as illustrated by figure 13, which shows a comparison between

the current wave-forms of similarly programmed RFPs in Deuterium, Helium, and Argon. When the filling pressure of Helium is reduced to 15 mtorr the decay changes from exponential to linear.

6.1.2 Unstable RFPs with I_{max} = 75 kA

In this section programmed RFPs with $\Theta(r_2) > 2$ (class 1, see chapter 5) are described, with a maximum plasma current of 75 kA, i.e. a doubling of the magnetic energy with respect to the RFP with I ≤ 50 kA described in the previous section. For the same values of β_θ the average plasma energy will also be twice as high with $k(\bar{T}_e+\bar{T}_i)/2 \gtrsim 10$ eV. The main parameters of three RFPs with I ≤ 75 kA are presented in figure 14, (a) and (b) are discharges in Deuterium with 10% difference in the applied reverse field, (c) is an RFP in Helium.

The initial values of the parameters I, $\Phi(r_2)$, $B_z(r_2)$ in figure 14(a) are obtained by increasing those in figure 6(a) by about 50%. The programmed value of $\Theta(r_1)$ is the same in both cases, but in the discharge with I ≤ 75 kA a more rapid fall in $\Theta(r_1)$ associated with a helical m = 1 instability is observed. The fluctuations of the $B_z(r_2)$ wave-form as a result of instabilities are larger for the RFP of figure 14(a) and the plasma current decays faster by about 10% in spite of the increase in its maximum value. The increase in flux is larger than in the discharge of figure 7(a), while the amplitude ratio $B_{\theta 1}(r_2)/B_{\theta 0}(r_2)$ reaches a maximum value of 0.2, which is twice as high. The difference in output of two B_z-coils and two B_θ-coils, positioned diametrially opposite each other in the direction for which the initial signal due to the m = 1 mode is maximal, is also shown in figure 14(a). The ratio $\Delta B_z(r_2)/\Delta B_\theta(r_2)$, which is the tangent of the angle of the field perturbations at the wall with wavenumber k, yields k-values between 25 and 35 m^{-1} during the growth of the instability, similar to the values found for the RFP with I_{max} = 50 kA. The pressure profile, derived from the measured fields at

$t = 3\ \mu s$, before an instability is observed, is already too compressed for stability since the compression ratio r_2/r_p exceeds the theoretically predicted stability limit of 2 (figure 14(a)).

The sensitivity of the RFP to the programming parameters is illustrated in figure 14(b) where the programmed value of $\Theta(r_1)$ is larger than its comparable value in figure 6(a) by a factor of two, due to an increase in the reversed field by 10%. Flux amplification during the instability again leads to a fall in $\Theta(r_1)$ to a value of about 2. The amplitudes of $\Delta B_z(r_2)$ and $\Delta B_\theta(r_2)$ indicate that the instability is stronger and the wavelength shorter than in the case of figure 14(a). During the early growth phase k reaches 60 m^{-1} while at maximum amplitude $k \approx 34\ m^{-1}$. The fluctuations in the main signals of the RFPs are a result of continuing instabilities throughout the decay phase.

An RFP programmed as in figure 14(b), but with Helium as filling gas is shown in figure 14(c). The plasma is less unstable, less flux is generated and consequently the drop in $\Theta(r_1)$ is smaller. After the instabilities the main parameters $B_z(r_2)$, I, $\Phi(r_2)$ decay exponentially and the value of $\Theta(r_1)$ falls to about 3 but rises again and changes sign through infinity when $\Phi(r_2)$ reaches zero and becomes negative. This is also the case in the Deuterium discharge of figure 14(b) but there the sign change of $\Theta(r_1)$ through infinity occurs for $t > 40\ \mu s$.

6.1.3 Collapsing RFP configurations

Instabilities with a disastrous effect on the RFP configuration are observed when the current is raised above 100 kA and the programmed value of $\Theta(r_1)$ exceeds 2 while the total flux $\Phi(r_3)$ is negative. In the RFP in figure 15 where the maximum current is 130 kA, and $\Theta(r_1)$ reaches 4 at the time of crowbarring the plasma is rapidly compressed, and a large amplitude m = 1 instability occurs during which the plasma interacts strongly with the wall. At that time $\Phi(r_2) = 0$ hence the necessary condition for

stability to m = 1 modes (section 4.3) is violated. The plasma current decays exponentially with an e-folding time of 4.5 μs, meanwhile 750 J/m of the azimuthal field is lost to the walls. During the instability the confining configuration is destroyed and within 5 μs after the start of the decay B_z is approximately constant throughout the discharge with a negative value equal to $\Phi(r_3)/\pi r_3^2$. When $\Phi(r_1)$ changes sign $\Theta(r_1)$ also changes sign through infinity after which $\Theta(r_1)$ decays to zero proportionally to the plasma current.

6.1.4 Self reversal of magnetic field during m = 1 helical kink instabilities

In compressed RFPs with $\Theta(r_1) > 2$ an m = 1 helical kink instability is observed to grow from the region inside the reversal point, and amplification of toroidal flux appears to be associated with the instability. An instability with the same characteristics is also observed in a stabilized z-pinch (SZP) with a similar value of $\Theta(r_1)$ but without programmed field reversal. When the total flux is conserved in such an SZP the field in the outside region reverses when the trapped flux increases.

The total toroidal flux in the SZP of figure 16(a) is conserved by crowbarring the primary circuit before the plasma current is induced. During an m = 1 helical kink instability the value of $\Theta(r_1)$ is reduced from 2.2 to 1.5 and stays constant during the decay of the configuration. The plasma current is seen to vary in figure 16(a) during the flux enhancement, which reflects the effect of the instability on the plasma inductance, because the driving electric field is zero. The relation between the instability and field reversal is illustrated in figure 17. The radial field starts to grow near r = 2.5 cm and the field at the wall reverses when the instability affects the whole of the plasma column. The gross features of the instability agree well with the observations

on the RFP in section 6.1.1 for which the plasma current is similar.

Detailed studies of self reversal in SZPs with initial values of $\Theta(r_1)$ above 3 have been published elsewhere[33]. In SZPs with peak plasma currents between 125 and 150 kA spontaneously occurring reversed field is observed to last for 40 μs, and no fundamental difference is found between these self reversed pinches and programmed RFPs with similar initial values of $\Theta(r_1)$ and peak plasma current.

The field in the outside region of a SZP can also be controlled by field programming, examples of which are shown in figures 16(b) and 16(c), where the maximum values of I are 60 kA and 75kA respectively. Flux enhancement and field reversal are always correlated, but the azimuthal average of B_z outside the plasma exhibits features which are due to local effects and disappear when $B_z(r_2)$ is also averaged over many wavelengths[33,47]. After the initial instability $\Theta(r_1)$ stays almost constant at about 1.5, and field reversal disappears when the current decays. The decay of the plasma current is very similar to the decay in the RFPs in figures 7(a) and 14(a). The value of the pinch ratio after the instability is lower in these examples than in most RFPs. This is due to the larger amount of total flux $\Phi(r_3)$ in flux conserving SZPs which leads to a relatively rapid diffusion of field reversal, so the field between the plasma column and the wall becomes positive and adds to $\Phi(r_1)$, whereas in the RFPs $\Phi(r_1)$ is reduced.

6.2 Weakly compressed RFPs

When more longitudinal flux is trapped during the programming stage the compression ratio is reduced and RFPs become less unstable to gross m = 1 helical kink modes. The main plasma parameters I, Φ, and $B_z(r_2)$ of programmed RFPs with $\Theta(r_1) < 2$ (class 2, chapter 5) decay continuously and $\Theta(r_1)$ stays approximately constant or changes gradually on the diffusion time-scale during the decay of the plasma depending on the

current. In such weakly compressed RFPs instabilities have been observed but they do not lead to a major redistribution of the field. When the maximum plasma current is less than 60 kA the RFP is observed to be stable[34,48]. Two cases of weakly compressed RFPs are studied in more detail in this section, one with a maximum current of 60 kA the other with a peak current of 120 kA.

6.2.1 Weakly compressed RFPs with I_{max} = 60 kA

The programming mode of figure 1(b) has been used to produce RFPs with a low compression ratio and $\Theta(r_1) < 2$ for I_{max} = 60 kA. The wave-form of $\Theta(r_1)$ in figure 18 shows a smooth increase in pinch ratio during the programming period of 10 μs. The dynamics of the programming phase is controlled by the time dependence of the power input represented by $S(r_2)$ in figure 1(a) and figure 1(b) (wave-form 1) where most of the energy input for the programming sequence of figure 1(b) is seen to occur earlier in time. The final configuration is therefore better controlled when the RFP is programmed according to the sequence of figure 1(b). The relatively slow rise in $\Theta(r_1)$ is due to the efficient trapping of longitudinal flux during the setting-up stage and RFPs with $r_2/r_p < 2$ can be produced, which are predicted to be stable in the limit of ideal MHD. The main parameters in figure 18 are characterized by a continuous decay, which is linear for the plasma current but faster than linear for the flux, hence $\Theta(r_1)$ increases slowly in time. This means that the plasma gradually contracts during the decay phase (section 4.2), because for weakly compressed RFPs $\Theta(r_1)$ is proportional to r_1/r_p.

In figure 19 parameters in particular case are shown for an RFP with I_{max} = 60 kA, and $\Theta(r_1)$ = 1.9 at the time of crowbarring. The plasma is not completely stable in this case, for magnetic field perturbations at the wall and inside the plasma are observed which are smaller than in RFPs with $\Theta > 2$ and I_{max} = 60 kA. A series of B_r wave-forms at different

radial positions inside the plasma is also shown in figure 19, where the maximum amplitude of B_r reaches a value of 4×10^{-2} T in the centre ($\delta B/|B| \approx 0.2$), compared with 2.6×10^{-1} T ($\delta B/|B| \approx 0.7$) for the RFP with I_{max} = 50 kA in figure 11. During the early stages of programming the B_r distribution corresponds to a shift in the magnetic axis with respect to the geometrical axis, which is ascribed to the equilibrium displacement. In the centre B_r is seen to grow in the opposite direction with a growth time of about 4 μs, while a similar growth time is observed for the $B_{\theta 1}$-amplitude at the wall, which is also shown in figure 19. The development of the radial distribution of B_r indicates a rotation of the m = 1 displacement which causes B_r in the centre to change sign while $B_{\theta 1}$ reaches a maximum amplitide. The second maximum of $B_{\theta 1}$ at t = 35 μs is not strongly correlated with B_r. Local effects may play a role in this case and the discrepancy may be due to the fact that $B_{\theta 1}$ and B_r were not measured at the same position along the torus.

The field distributions at the time of crowbarring, t_o, and 5.5 μs and 18 μs later are given in figure 20. At $t = t_o$ the pressure distribution is found to be hollow, but 5.5 μs later the pressure profile has filled in and a shift of the magnetic axis is observed. The displacement Δ of the point where B_θ is zero, derived from $\Delta = rB_r/B_\theta$, is 8 mm near the centre. The point where B_r is zero is at r = 4.5 cm where $B_z \approx 0$. From the condition kP = _1 at this point a large wave-number is predicted ($k >> 100\ m^{-1}$), but at the wall $k \approx 25\ m^{-1}$ for m = 1, which corresponds to the position of the origin at r = 2 cm. Dissipation can cause the point where B_r is zero to shift with respect to the origin of the instability[23]. A test with an ideal MHD stability code[14] shows that the configuration is stable to gross m = 1 modes at this time, although the B_r-profile indicates a gross instability. At $t = t_o + 18$ μs the compression ratio is too large for stability no gross m = 1 modes as predicted with ideal

MHD theory, while also Suydam's necessary criterion is violated by about a factor 5 between r = 1 cm and r = 6 cm. However, the B_r-signals at $t = t_o + 18$ μs do not indicate a strong instability. The contraction of the pressure profile due to diffusion predicted from the increase in $\Theta(r_1)$ is indeed observed between $t = t_o$ and $t = t_o + 18$ μs, while β_θ computed from the pressure profiles rises from 0.6 to 0.75.

The development of a decaying RFP depends on the sign of the total trapped flux inside a flux conserving system as discussed in section 4.4 and in[22]. The process of field diffusion is studied for two RFPs with $I \leq 60$ kA and a different sign of $\Phi(r_3)$ by measuring the time evolution of the magnetic field at different positions inside the plasma. The main parameters of these RFPs together with the wave-forms of B_r and B_z near the centre and B_z at r = 36 cm are shown in figure 21. When $\Phi(r_3) > 0$ the reversal of B_z disappears during the decay phase as seen in figure 21(a) and B_z inside r = 36 mm decays with uniform sign. The maximum amplitude of B_r in the centre is 2×10^{-2} T, or about half the maximum value found in similar conditions shown in figure 19. Figure 21(b) shows an RFP with a much larger value of the reversed field such that $\Phi(r_3) < 0$ but with $\Phi(r_2) > 0$ at the time of crowbarring ($t = t_o$ in figure 21), while the field reversal point is outside r = 36 mm. Diffusion of the configuration leads to the contraction of the plasma column and the field reversal point reaches r = 36 mm at $t = t_o + 6$ μs. At that time, 10 μs before $\Phi(r_2)$ changes sign, a large radial field component B_r is observed in the inside region but no effect is observed outside the plasma in spite of the large amplitude of B_r which grows until it exceeds the amplitude of the main field. When the value of B_r reaches a maximum in the centre at $t = t_o + 12$ μs the value of B_z in the centre is observed to change sign although the flux trapped inside the plasma boundary $\Phi(r_1)$ is still positive. Outside the plasma still no perturbations are observed, but at r = 36 mm B_z becomes approximately zero whereas

between r = - 4 mm and r = 36 mm B_z is predominantly positive, in agreement with $\Phi(r_1) > 0$. The decay of the plasma current is accelerated during the growth and saturation of the B_r amplitude and at $t = t_o + 22$ μs large amplitude perturbations with m = 0 and m = 1 are observed at the wall, after which B_z is uniform throughout the discharge. The final destruction of the configuration is preceded by a perturbation of B_z at r = 36 mm and near the centre. The pinch ratio $\Theta(r_1)$ changes sign when field perturbations occur at the wall.

6.2.2 Weakly compressed RFPs with I_{max} = 120 kA

When the plasma current is raised above 60 kA for $\Theta(r_1) \lesssim 2$ the onset of MHD instabilities shifts to an earlier time until the plasma becomes unstable during the programming stage. For the RFP with I_{max} = 120 kA the standard mode of programming of figure 1(a) is used, which has the advantage that the setting-up stage is faster.

The main parameters of a weakly compressed RFP with a maximum current of 120 kA are shown in figure 22. The plasma starts as an SZP, while 3μs after the start of the current $B_z(r_2)$ is reversed which leaves enough time for the current sheath to trap sufficient flux so that $\Theta(r_1) \lesssim 2$. The pinch ratio can be reduced further by delaying the reversal of $B_z(r_2)$, but by that time unstable modes have grown to sufficient amplitude to affect the field configuration. The flux, current, and field at the wall shown in figure 22 are seen to decay approximately linearly without the flux enhancement typical in RFPs with higher values of $\Theta(r_1)$. However for $t > 20$ μs $\Theta(r_1)$ increases slowly and deviations of $B_z(r_2)$ from the extrapolated decay are observed.

The end of the programming stage is reached at t = 4 μs when both circuits are crowbarred. At that time the B_r-amplitude at r = 42 mm has started to grow, as seen in figure 23, but in the centre no radial field occurs until t = 5 μs, when also sine and cosine coils produce large

amplitude signals. The B_r-signals and the signals from the sine and cosine coils show a common component between t = 5 μs and t = 7 μs, modulated with more rapidly (1 - 2 MHz) fluctuating signals in the outer region of the plasma. The main perturbation is ascribed to a gross m = 1 helical kink instability, which is however not accompanied by flux enhancement. The mode numbers of the fluctuations have not yet been fully resolved, but modes with m > 1 are seen. The ratios $B_{\theta 1}/B_{\theta 0}$ and $B_{z1}/B_{\theta 1}$ have been determined at the conducting wall for the gross m = 1 mode observed between t = 5 μs and t = 7 μs. At maximum amplitude $B_{\theta 1}/B_{\theta 0}$ = 0.25, which for a thin column model yields a displacement of 1 cm. The ratio $B_{z1}/B_{\theta 1}$ is about 1 at maximum amplitude of the instability with an error of 50% due to the inaccuracy in the measurement of B_{z1}. The corresponding k-number is 15 m^{-1} i.e. a wavelength of 40 cm. The position of the origin of the m = 1 mode derived from the resonance condition kP = -1 is met at r = 4 cm for t = 5 μs; but at t = 6 μs this condition is approximately satisfied over the whole of the central region (0 < r < 3 cm).

The contraction of the plasma radius as a result of diffusion is deduced from the magnetic field configurations of figure 24 where the measured points are connected by a line. At t = 3 μs the plasma has an annular shape with a radius r_p of 4.8 cm. At t = 7 μs the deduced pressure is still hollow with r_p = 4.2 cm (it has filled in at t = 10 μs) while at t = 16 μs the plasma radius has contracted to r_p = 3.8 cm. The pressure gradient between the centre and r = 6 cm becomes approximately constant later in time. During the growth of the instability at t = 5 μs the compression ratio r_2/r_p is 1.7, whereas the predicted stability limit for gross ideal MHD modes with m = 1 is about 2.0. The value of β_θ is derived by integrating the computed pressure profiles over the cross-section of the tube (assuming axisymmetry) and is also computed from the total plasma current and the energy of the B_z-field. The results obtained with both

methods are shown in figure 25 where β_θ is seen to rise to a value of about 0.65 at t = 10 μs, after which it stays approximately constant until t = 25 μs when β_θ increases again. The fluctuations in β_θ in figure 25, which are especially large for the wave-form derived from the internal fields, are a result of the field perturbations due to instabilities. The increase of β_θ for t > 25 μs occurs when the plasma current falls below 50 kA. Optical data from streak photographs (figure 26) shows an abrupt reduction in the light emission at t ≈ 6 μs. The radial light distributions, representing the plasma density, computed from similar streak photographs of the RFP discussed here, have been published in ref. (48) . The luminosity profiles are generally shifted with respect to the axis of the tube for t ≳ 5 μs, but no coherent displacement could be derived. The luminosity changes as a function of radius with a typical scale length of 5 - 10 mm, which is similar to the correlation length of the fluctuations in the B_r signals.

6.2.3 Observations of current decay in weakly compressed RFPs

The decay of the plasma current in RFPs with programmed values of $\Theta(r_1)$ of about 2 has been studied for peak values of the current between 50 kA and 155 kA. The decay is linear during the observation time of about 50 μs, while the time-constant of the decay is approximately independent of I_{max}, as seen in figure 27. The current decay time $\tau_I(t)$ is derived from the empirical relation $I(t) = I(t_o)(t_1-t)/(t_1-t_o)$, so $\tau_I(t) = t_1-t$ where $t_1 \approx 60$ μs. The current decay time decreases while the RFP decays but near $t = t_1$ the decay is usually exponential and τ_I becomes a constant. For Helium and Argon radiation cooling and the higher values of Z lead to a more rapid and exponential decay unless the filling pressure in Helium is lowered (section 6.1.1). As seen in figure 27 RFPs in Deuterium also decay exponentially when the filling pressure is raised, which leads to increased radiation cooling while less energy per particle

is available for the same value of β_θ.

The relation $\tau_I \propto I^3$ was obtained with the assumption that at a particular point in time the values of β_θ, L_{eff}, and N are constant, and $dL_{eff}/dt = 0$, when I is varied. This is a reasonable assumption for N[45], while for similar values of $\Theta(r_1)$ also L_{eff} is approximately independent of I. From probe data on the RFPs with $\Theta(r_1) < 2$ and $I_{max} = 60$ kA and 120 kA the values of β_θ are found to be approximately the same at a given time during the decay, but especially in the 120 kA discharge of section 6.2.2 the errors due to instabilities are large. Independent measurements of the total energy content of RFPs with I > 60 kA during the decay are not yet available, although there is evidence from Thomson scattering that β_θ decreases with I when the plasma is unstable[14]. The decay of the CV-line at 227.1 nm has been monitored for RFPs with $\Theta(r_1) \approx 2$ and 90 kA $\leq I_{max} \leq$ 160 kA. The line is expected to be observable when $k\bar{T}_e >$ 30 eV (I = 110 kA if $\beta_\theta = 0.5$). For a peak current of 90 kA it is not seen, for $I_{max} = 140$ kA the CV-line disappears within 15 μsec when the current falls below 110 kA and for $I_{max} = 160$ kA the intensity decays exponentially with a decay time of 10 μs, and becomes comparable to the noise level after 25 μs when the current is less than 100 kA. Although models for the excitation of the CV-line depend on a number of assumptions that could not be checked, the data still lead to the conclusion that the plasma temperature increases with the peak current. (Peak electron temperatures obtained from Thomson scattering scale as I_{max}^2 (31)).

The contraction of the configuration, observed during the first 20 - 30 μs of the decay of RFPs with $\Theta(r_1) < 2$, leads to an increase in inductance. For example: the inductance L_z (defined in section 4.4.2) of the RFP of figure 20 is 53 nH/m at $t = t_o$, has increased to 71 nH/m at $t = t_o + 5.5$ μs, and is 94 nH/m at $t = t_o + 18$ μs, so dL_{eff}/dt exceeds

2 mΩ/m, which is comparable with a typical value of the resistance. If dL_{eff}/dt is the same for the RFPs with different values of the peak current, the relative values of the plasma resistance current can still be deduced from the decay times.

7. DISCUSSION

7.1 MHD instabilities

The characteristics of the gross m = 1 helical kink instabilities observed in RFPs of class 1 ($\Theta(r_1) > 2$, as defined in chapter 5), indicate that the plasma is unstable to modes predicted with ideal MHD theory, and that the energy is provided by the azimuthal field. The compression ratio r_2/r_p, which is deduced from the magnetic field configurations of RFPs of class 1 (section 6.1), is too large for stabilization of gross m = 1 (ideal MHD) modes by the wall to occur. The predicted ratio r_2/r_p for marginal stability varies between 2.0 and 2.2 for typical RFP configurations in HBTX-1 with a vacuum field between r_1 and r_2 (section 4.3.1). The observed m = 1 modes are helical, with wave-numbers (k) between 20 and 40 m^{-1} and the position of their origin lies inside the field reversal point, usually at $r \approx 2$ cm, in agreement with the resonance condition kP = -1 (section 4.3.1). Similar results are predicted with an ideal MHD instability code[22]. The instabilities are observed to lead to an increase in the pitch of the magnetic field, which causes a reduction of k during their growth to large amplitude. The minimum growth time of gross ideal MHD modes driven by the energy in the azimuthal field is the Alfvén transit time $\tau_A = r_p(\mu_o\rho)^{\frac{1}{2}}B_\theta^{-1}$ which is 0.6 μs for the RFP with I_{max} = 50 kA (section 6.1.1) at the time of instability, when $r_2/r_p \approx 2.5$. The growth time τ_g is predicted to vary with I^{-1} for gross ideal MHD modes, which is verified for the discharges of section 6.1, as shown in table 2.

TABLE 2

Programmed type	I_{max}(kA)	τ_g (μs)	$I_{max} x \tau_g$ (kAμs)	Reference
reversed field pinch	50	1.0	50	section 6.1.1
	75	0.5	38	section 6.1.2
	130	0.2-0.3	33	section 6.1.3
stabilized z-pinch	50	1.0	50	section 6.1.4
	90	0.4	36	(33)

In RFPs of class 2 ($\Theta(r_1) < 2$, chapter 5) gross m = 1 helical kink instabilities have also been observed, although theoretically, for ideal MHD, they are predicted to be stabilized by the conducting wall. The value of the compression ratio for the examples in section 6.2 is 1.7 at the time the gross m = 1 helical kink instabilities start to grow. The field profiles of the RFPs with I_{max} = 60 kA (section 6.2.1) and I_{max} = 120 kA (section 6.2.2) have been tested with a linear ideal MHD instability code and are predicted to be stable to gross m = 1 modes but unstable to local modes outside r = 4 cm where Suydam's criterion is violated. Field perturbations are detected in this region before the gross m = 1 mode occurs, as seen in for example in figure 23. The observed gross m = 1 helical kink instabilities are deduced to be resistive tearing modes, but more data is needed for a positive identification. This requires the use of an MHD code, which includes resistivity[14]. The growth time of the gross m = 1 instability in the RFP with I_{max} = 60 kA is about 4 μs, a factor of 5 longer than expected for an ideal MHD mode (table 2). This is ascribed to dissipative effects ($S \approx 10^2$ in this case). The gross m = 1 instability observed for the RFP with I_{max} = 120 kA ($S \approx 10^3$) has a growth time of 0.4-0.5 μs, similar to values expected for ideal MHD instabilities (table 2). Since dissipative MHD modes can grow as fast as ideal MHD modes in some cases (section 4.3.2), it is still possible that the instability is due to resistive tearing. Another possible explanation is the coupling of the instability in the outer region with the energy in the azimuthal field, which can lead to a gross MHD instability[20].

The enhancement of the flux, observed during the large amplitude stage of gross m = 1 helical kink instabilities in pinches of class 1 is associated with a major redistribution of the field configuration, which does not take place in RFPs of class 2. The flux amplification in stabilized z-pinches and RFPs of class 1 has been explained by the transition

of the plasma from a cylindrical to a helical state[33]. For example, the increase in flux in the RFP with I_{max} = 75 kA shown in figure 14b (section 6.1.2) is accounted for by a helical plasma current with a radius of 2 cm and k = 40 m^{-1}, in agreement with experimental data. In RFPs of class 1 fluctuations in $B_z(r_2)$ are observed which do not appear on the $\Phi(r_2)$-trace in e.g. figure 14b. Such fluctuations are usually not seen in RFPs of class 2. The $B_z(r_2)$ signal represents the average of B_z over a thin annulus around the torus, and deviations from the mean B_z-field in the outside region are ascribed to local effects of large amplitude instabilities[33].

The fluctuations in the field components of the RFP of class 2 with I_{max} = 120 kA ($S \approx 10^3$) are expected to be due to local MHD modes associated with the excessive pressure gradient when Suydam's criterion is violated (convective modes)[51]. At lower values of the Lundquist number ($S \approx 10^2$) localized modes are predicted to be stabilized by dissipative effects, which explains why these fluctuations are not observed in the RFP of class 2 with I_{max} = 60 kA (section 6.2.1). Dissipative stabilization also provides an explanation for the increase in β_θ when the plasma current falls below 40 kA, while Suydam's criterion is violated by a large factor.

7.2 Plasma decay

The decay of the plasma current in RFPs with I ≥ 40 kA in Deuterium (filling pressure 40 mtorr) is generally observed to be linear in time. In RFPs of class 1 ($\Theta(r_1) > 2$) the decay rate fluctuates in time about the average value (figures 6 and 14), a phenomenon ascribed to the gross m = 1 helical kink instabilities, which cause a redistribution of the fields. In RFPs of class 2 ($\Theta(r_1) < 2$) the field configuration evolves gradually (on the time-scale of field diffusion) and the decay of the plasma current stays linear, as seen in figures 18, 22 and 27.

Exponential decay is observed when the energy input from the dissipation of magnetic field is comparable to the energy loss by radiation. It is also observed in the RFPs of class 1 with I_{max} = 130 kA and a negative value of the total flux which leads to plasma contraction (section 6.1.3). In discharges in Deuterium with a filling pressure of 40 mtorr the radiation losses balance the energy input from Ohmic heating for plasma currents below about 30 kA[52]. This limiting current increases with the filling pressure as illustrated in figure 27 where an RFP in Deuterium is seen to decay exponentially for $I \leq 50$ kA. Radiation losses also increase when a filling gas with a higher atomic charge number Z is used. (The power radiated in the continuum varies as Z^2, the radiative power due to recombination and to line radiation as Z^4 and Z^6, respectively). This is demonstrated by the exponential decay of RFPs of class 1 in Helium (figures 6, 13 and 14) and in Argon (figure 13). Linear decay is seen in figure 13 for a Helium discharge with a filling pressure of 15 mtorr for which the average energy per particle is estimated to exceed 10 eV and the radiation losses are less important.

In order to calculate the time dependence of the plasma energy from the plasma current β_θ should be known as a function of time. The time variation of β_θ can be estimated from the energy balance of the plasma. At the beginning of the decay values of β are typically about 0.2 for both classes of RFPs. The value of β_θ will increase during the decay of the fields since the power input by Ohmic heating will exceed the loss of plasma energy by a factor of β^{-1} (section 4.4.2). (Energy loss is assumed to be due to classical plasma diffusion). The characteristic growth time of β_θ at the beginning of the decay is approximately $\beta\tau_I/2$ (or about 6 μs since the value of the current decay time τ_I is then usually about 60 μs). Instabilities driven by the pressure will occur when β_θ exceeds a critical value, which will lead to an increase in the loss of plasma energy, and the rise

in the value of $\beta_\theta(t)$ is expected to cease. A further rise in β_θ will be possible when the plasma is stabilized by dissipative effects, which become increasingly important when the value of S falls. This qualitative prediction is confirmed by the time dependence of β_θ, deduced from the field profiles of an RFP of class 1 (figure 12c) and an RFP of class 2 (figure 24). A more quantitative estimate of $\beta_\theta(t)$ can be made when the empirical result that the current decay time is linear is used, and classical resistivity is assumed throughout the decay. From

$I(t) = I(t_o)(t_1-t)/(t_1-t_o)$ (section 4.4.3) it follows that $\tau_I(t) \propto I(t)$.

If the value of L_{eff} is assumed to be constant in time, then:

$\tau_I(t) \propto R^{-1}(t)$ section (4.4.2); when τ_I is eliminated:
$R(t) \propto I^{-1}(t)$ i.e. the resistive voltage drop is contant.

With the assumption of classical resistivity $R(t) \propto T_e^{3/2}$, hence

$$T_e(t) \propto I(t)^{2/3}$$

From the definition of β_θ: $\beta_\theta(t) \propto T_e(t)\ I(t)^{-2}$ (if N(t) is constant so

$$\beta_\theta(t) \propto I(t)^{-4/3} \propto (t_1-t)^{-4/3}.$$

The value of β_θ is found to increase monotonically with time. When the initial value of β_θ is 0.4 and the duration of the total current decay (t_1) is 60 μs, typical values for the RFP in section 6.1.1, the time required to reach $\beta_\theta = 1$ is 30 μs. In the experiment the predicted increase in β_θ only occurs during the later stages of the current decay, as shown in

figure 12c. The assumptions of classical resistivity and constant L_{eff} will be violated during instability and agreement between the predicted and experimental time dependence of β_θ is not expected for the whole of the decay period.

The observation that the rate of decay of the plasma current is independent of its peak value (section 6.2.3) cannot be ascribed to the effect of the primary circuits. (The decay time of the current in the primary circuit is 1 ms). If differences in L_{eff} are ignored then the constant rate of decay observed when the peak current is varied implies that the resistance (R) does not depend on the current (I) at comparable points in time. Thus $\beta_\theta(I) \propto I^{-2}$ if the resistivity is classical. This does not appear to be the case for the values of β_θ in figure 12c ($I \leq 60$ kA) and figure 24 ($I \leq 120$ kA). The constant decay rate as a function of I_{max} indicates that also the plasma temperature at comparable times during the decay of the current is independent of the value of I_{max}. This may be attributed to the increased level of instability observed when the current is raised[51]. The time variation of L_{eff} during the decay of a particular discharge is often comparable to R and should be corrected for (section 6.2.3). A comparison of the current decay times τ_I, at a given point in time, for discharges with similar values of L_{eff} and dL_{eff}/dt, will however still yield the relative values of the plasma resistance in these discharges.

The diffusion of the field distribution in an RFP depends on the sign of the total toroidal flux as demonstrated in section 6.2.1 (figure 21). When the total conserved flux ($\Phi(r_3)$) is negative the plasma contracts radially and the area inside which B_z is positive shrinks progressively. The contraction of the plasma leads to loss of wall stabilization, hence to gross m = 1 helical kink instabilities. For the RFP with $I_{max} = 60$ kA (section 6.2.1, figure 21b) the contraction occurs on the time-scale of classical field diffusion with a value of σ corresponding to a temperature

of $k\bar{T}_e$ = 6 eV and $\sigma_\perp/\sigma_{//}$ = 0.5. The gross m = 1 instability occurs after a decay period of 25 μs. In the RFP of class 1 with I_{max} = 130 kA (section 6.1.3, figure 15) the process of contraction and destruction of the configuration takes place on a time-scale which is shorter by an order of magnitude. The average value of $\sigma_{//}$ is expected to be higher than in the RFP with I_{max} = 60 kA, but if the ratio $\sigma_\perp/\sigma_{//} \ll 1$ the rapid contraction can be explained (section 4.4.1). This was demonstrated by Hobbs [40] for Babychev's data[53], which could be simulated numerically for $\sigma_\perp/\sigma_{//}$ = 0.05. A value of $\sigma_\perp/\sigma_{//}$ much less than 0.5 is unlikely to occur in HBTX-1[41], unless the effective value is reduced by processes which invalidate a classical description of the plasma, such as turbulence in Babychev's experiment. The rapid decay of the fields in the RFP of figure 15 appears to be similar to the decay in reversed bias theta pinches[54], in which the oppositely directed B_z-fields cancel. The energy of the field is transferred to the plasma which can reach velocities close to the Alfvén speed[55]. In the region where the fields cancel the effective value of $\sigma_\perp/\sigma_{//}$ is about zero (section 4.4.1).

7.3 The final states of RFPs

The pinch ratio $\Theta(r_1)$ in both classes of RFPs becomes approximately constant at 2 during the decay of the plasma, provided the total conserved flux $\Phi(r_3)$ is positive but small compared with $\Phi(r_1)$. The field reversal point remains fixed in space while the plasma decays with approximately homogeneous current density and a constant pressure gradient. The field distribution measured later during the decay for an RFP of class 1 with an initial value of $\Theta(r_1)$ of 4, shown in figure 7 (t = 24 μs), is similar to the field profile of the RFP of class 2 in figure 20 ($t = t_o$ + 18 μs), although the programmed value of $\Theta(r_1)$ is 1.7 in this case. From these and other examples of final configurations[47] it is concluded that the state of the plasma later during the decay is independent of the initial

configuration obtained by field programming, provided $\phi(r_3) > 0$. In HBTX-1 a final configuration is reached after a period of field diffusion and instabilities(in RFPs of class 1 and class 2 when $I \geq 60$ kA) during which a large fraction of the magnetic energy is lost. In the relaxation of field configurations, predicted with Taylor's theory, dissipative effects are unimportant since $\int_V \vec{A}.\vec{B}\, d\tau$ must be conserved, which is not the case in HBTX-1 (e.g. figure 12d). Because of this and differences such as the effects of β and of vacuum fields outside the plasma, theory and experiment agree only qualitatively[34]. The main principle, the minimization of energy under constraints, will naturally also apply to the experiment.

8. CONCLUSIONS

1. The field configuration measured later during the decay of programmed RFPs in HBTX-1 is characterized by a value of the pinch ratio at the plasma boundary of about 2, and the field distribution is observed to be largely independent of the initial field programming used.

2. The reduction of the shear of the magnetic field and the increase in β_θ due to diffusion of magnetic field during the decay of programmed RFPs in HBTX-1 leads to instabilities which can be ascribed to the increasing violation of Suydam's criterion for the shear stabilization of pressure-driven instabilities.

3. Programmed RFPs and also "stabilized" z-pinches for which the pinch ratio at the plasma boundary is initially greater than 2 are unstable to gross MHD m = 1 helical kink instabilities, since the plasma is too compressed for stabilization by the conducting wall to be effective. The pinch ratio falls to about 2 during the large amplitude stage of such an instability while a major redistribution of the field configuration is observed, which leads to field reversal in a stabilized z-pinch.

4. Programmed RFPs with an initial pinch ratio less than 2 are stable, when $I < 60$ kA, while for $I > 60$ kA gross m = 1 MHD instabilities occur for which resistive effects are believed to be important, but no major redistribution of field is observed. For average plasma energies above 10 eV ($I > 75$ kA) more localized instabilities are also detected, which are attributed to too high a value of β.

5. The current decay time averaged over a large fraction of the period of plasma decay for programmed RFPs in HBTX-1 is approximately independent of the peak plasma current for values between 50 kA and 170 kA. This result is ascribed to the effect of pressure - and current-driven MHD instabilities.

REFERENCES

1. ROBINSON, D. C., Plasma Physics 13, (1971) 439.

2. ROBINSON, D. C. and KING, R. E., Proc. of the 3rd Int.Conf. on Plasma Physics and Controlled Nuclear Fusion Research, Novosibirsk, 1968, I.A.E.A. CN-24/B-8.

3. OHKAWA, T., FORSEN, H. K., SCHUPP, Jr. A. A. and KERST, D. W., Physics of Fluids 6, (6), (1963) 846.

4. BURKHARDT, L. C., DI MARCO, J. N., FORMAN, P. R., HABERSTICH, A., KARR, H. J. and PHILLIPS, J. A., Proc. 5th European Conf. on Controlled Fusion and Plasma Physics, Grenoble 1972, Vol.1, p.45.

5. BUFFA, A., COSTA, S., FELLIN, L., MALESANI, G., MONDINO, P. L., NALESSO, G. F., ORTOLANI, S., ROSTAGNI, G. and STELLA, A., Proc. 5th Int.Conf. on Plasma Physics and Controlled Fusion Research, Tokyo, 1974, I.A.E.A. CN-33/E9-3.

6. OGAWA, K., KIYAMA, S., MAEJIMA, Y., SHIMADA, T., HIRANO, Y., HIROTA, I., SATO, Y., TAKEDA, S., YAHAGI, E. and TAMARO, T., Proc. 5th Int.Conf. on Plasma Physics and Controlled Nuclear Fusion Research, Tokyo, 1974, I.A.E.A, CN-33/E9-4.

7. BODIN, H. A. B., Proc. 3rd Topical Conf. on Pulsed High Beta Plasmas, Culham 1975, invited paper B1.1.

8. TAYLOR, J. B., Phys.Rev.Letts. 33, (19), (1974) 1139.

9. WELLS, D., Proc. 3rd Topical Conf. on Pulsed High Beta Plasmas, Culham, 1975, paper A1.8.

10. WOLTJER, L., Proc.Natl.Acad.Sci. U.S. 44 (1958) 489.

11. RUSBRIDGE, M. A., to be published, also: COLGATE, S. A., in Culham Memorandum M-21, edited by Rusbridge, M. A. and Saunders, P. A. H. (1963).

12. NEWTON, A. A., LI, YIN-AN, LONG, J. W. and YEUNG, B. C., Proc. 3rd Topical Conf. on Pulsed High Beta Plasmas, Culham, 1975, paper B2.6.

13. ROBINSON, D. C., Bull.Am.Phys.Soc., October 1975, 4118, p.1297.

14. To be published at the 6th Int.Conf. on Plasma Physics and Controlled Nuclear Fusion Research, Berchtesgaden, 1976. (HBTX-1 contribution).

15. BODIN, H. A. B., BUTT, E. P., CROW, J. E., IRONS, F. E., JUNKER, J., NEWTON, A. A. and ROBINSON, D. C., Proc. 4th Int.Conf. on Plasma Physics and Controlled Nuclear Fusion Research, Madison, 1971, Vol.1, p.225-249.

16. GOWERS, C. W., NALESSO, G. F., NEWTON, A. A., ROBINSON, D. C., WOOTTON, A., and BODIN, H. A. B., Theoretical and experimental study of heating and energy losses in pinch discharges. Proc. 2nd Topical Conf. on Pulsed High Beta Plasmas, Garching 1972, IPP-report 1/127, pp.29-32.

17. NEWCOMB, W. A., Physics of Fluids 4 (1961) 391.

18. VOSLAMBER, D. and CALLEBAUT, D. K., Phys.Rev. 128, (1962) 2016.

19. BAKER, D. A., MANN, L. W., Report LASL-5656-PR (1974) 96, Los Alamos Scientific Laboratories.

20. SAKANAKA, P. H. and GOEDBLOED, J. P., Phys.Fluids 17, (5) (1974) 919.

21. AMANO, T., TAMAI, T. and WAKATANI, M., J.Phys.Soc. Japan, 32, (5), (1972) 1385.

22. CROW, J. E. and ROBINSON, D. C., Proc. 2nd Topical Conf. on Pulsed High Beta Plasmas, Garching 1972, IPP-report 1/127, pp.83-86.

23. CROW, J. E. and ROBINSON, D. C., Proc. 3rd Int.Symp. on Toroidal Plasma Confinement, Garching, 1973, paper A4.

24. REBUT, P. H., Plasma Physics (J.Nucl. Energy C) 4, (1962) 159.

25. FURTH, H. P., KILLEEN, J. and ROSENBLUTH, M. N., Physics Fluids 6, (1963) 459.

26. COPPI, B., GREEN, J. M. and JOHNSON, J. L., Nuclear Fusion 6, (1966) 101.

27. GIBSON, R. D. and WHITEMAN, K. J., Plasma Physics 10, (1968) 1101.

28. CROW, J. E., KILLEEN, J. and ROBINSON, D. C., Proc. 6th European Conf. on Controlled Fusion and Plasma Physics, Moscow, 1973, Vol. 1, pp.269-272.

29. DIBIASE, J. A., Numerical studies of resistive instabilities in diffuse pinches. Ph.D. Thesis, University of California. UCRL-51591, May 1974.

30. GOWERS, C. W., LONG, J. W., NEWTON, A. A., ROBINSON, D. C., VERHAGE, A. J. L. and BODIN, H. A. B., Proc. of the 6th European Conf. on Controlled Fusion and Plasma Physics, Moscow, 1973, Vol. 1, pp.265-268.

31. BUTT, E. P., GOWERS, C. W., GRIBBLE, R. F., LI, YIN-AN., NEWTON, A. A., ROBINSON, D. C., VERHAGE, A. J. L., BODIN, H. A. B., TAYLOR, J. C. and SHARP, W. J., Proc. of the 5th Int.Conf. on Plasma Physics and Controlled Nuclear Fusion, Tokyo, 1974, I.A.E.A. CN-33/E9-2.

32. DIBIASE, J. A., KILLEEN, J., ROBINSON, D. C. and SCHNACK, D., 3rd Topical Conf. on Pulsed High Beta Plasmas, Culham, 1975, paper B1.9.

33. VERHAGE, A. J. L., FURZER, A. S., ROBINSON, D. C., Culham Laboratory Preprint 463, submitted to Nuclear Fusion.

34. BUTT, E. P., BODIN, H. A. B., GOWERS, C. W., MOHRI, A., NEWTON, A. A., ROBINSON, D. C., VERHAGE, A. J. L., WATTS, M. R. C. and LI, YIN-AN., 7th European Conf. on Controlled Fusion and Plasma Physics, Lausanne 1975, paper 39.

35. WESSON, J.A., Proc. 2nd Europ. Conf. on Comp. Physics, Garching, 1976, to be published in Comp. Phys. Comm.

36. To be published at 6th Int.Conf. on Plasma Physics and Controlled Nuclear Fusion Research. Berchtesgaden, 1976.

37. STRINGER, T. E., Nuclear Fusion 15 (1975). 125

38. DREICER, H., Electron and ion runaway in a fully ionized gas I, Phys.Rev. 115 (1959) 238, II, ibid 117 (1960) 329.

39. GOWERS, C. W., LONG, J. W., NEWTON, A. A., NORTON, B. A., ROBINSON, D. C., VERHAGE, A. J. L., BODIN, H. A. B., 6th European Conf. on Controlled Fusion and Plasma Physics, Moscow, 1973, Supplementary paper.

40. HOBBS, G. D., Culham Laboratory Preprint CLM-P19 H.M.S.O. 1963.

41. ROBINSON, D. C., CROW, J. E., GOWERS, C. W., NALESSO, G. F., NEWTON, A. A., VERHAGE, A. J. L. and BODIN, H. A. B., Proc. 5th European Conf. on Controlled Fusion and Plasma Physics, Grenoble 1972, Vol.2, pp.47-58.

42. SHAFRANOV, V. D., in: Reviews of Plasma Physics, vol 2, p.142, Atomizdat, Moscow 1963, and Consultants Bureau New York, 1966.

43. BUTT, E. P. and PEASE, R. S., Culham Report CLM-R 30. H.M.S.O. 1963.

44. BAKER, D. A. and PHILLIPS, J. A., Phys.Rev.Lett. 32, (5), (1974) 202.

45. DUTT, T. L., EVANS, D. E., THOMAS, C. D.V. and WILCOCK, P. D., 3rd Topical Conf. on Pulsed High Beta Plasmas, Culham 1975, paper C2.7.

46. LEES, D. J. and RUSBRIDGE, M. G., Proc. 4th Int.Conf. on Ionization Phenomena in Gases, Uppsala 1959, pp.954-960.

47. VERHAGE, A. J. L. and ROBINSON, D. C., 3rd Topical Conf. on Pulsed High Beta Plasmas, Culham 1975, paper B1.5.

48. WATTS, M. R. C. and VERHAGE, A. J. L., 3rd Topical Conf. on Pulsed High Beta Plasmas, Culham 1975, paper C2.6.

49. KING, R. E., ROBINSON, D. C., VERHAGE, A. J. L., J.Phys.D:Appl.Phys., 5 (1972) 2015.

50. BOBELDIJK, C., OOMENS, A. A. M., VAN DER LAAN, P. C. T., Nuclear Fusion(Letters) 13 (1973) 121.

51. ROBINSON, D. C., 3rd Topical Conf. on Pulsed High Beta Plasmas, Culham 1975, paper B1.7.

52. BUNTING, C. A., NEWTON, A. A. and WATTS, M. R. C., 3rd Topical Conf. on Pulsed High Beta Plasmas, Culham 1975, paper C2.4.

53. BABICHEV, A. P., KARCHEVSKII, A. I., MUROMKIN, Yu. A., SOKOLSKII, V. V., Soviet Physics - JETP, 14 (1962) 983.

54. BODIN, H. A. B., GREEN, T. S., NIBLETT, C. B. F., PEACOCK, N. J., QUINN, J. M. P., REYNOLDS, J. A., Nuclear Fusion Suppl. 2 (1962) 521.

55. YEH, T., AXFORD, W. I., J. Plasma Physics 4 (2) (1970) 207.

GLOSSARY OF SYMBOLS

$\vec{A}(A_r, A_\theta, A_z)$	vector potential and cylindrical components
a	radius of quartz wall
$\vec{B}(B_r, B_\theta, B_z)$	magnetic field and cylindrical components
$B_{\theta 0}, B_{\theta 1}$	Fourier components of the azimuthal magnetic field
B_{z1}	first Fourier component of the longitudinal magnetic field
C	Capacitance
CV	Carbon, 4 times ionized
$\vec{E}(E_r, E_\theta, E_z)$	electric field and cylindrical components
D_α	Balmer line of Deuterium
I	toroidal plasma current
I_{max}	peak value of the toroidal plasma current
$\vec{j}(j_r, j_\theta, j_z)$	current density and cylindrical components
K	Integral of $\vec{A}.\vec{B}$ over the volume of the torus
k	wave-number of longitudinal modes
L_{eff}	the effective value of the plasma inductance
ℓ	unit length
$\ell n \Lambda$	Coulomb logarithm in transport theory
m	azimuthal mode-number
N	line-density (= number density n integrated over a cross-section of the plasma)
N_e	line-density for the electrons
n_e, n_i, n_o	number density of electrons, ions, and neutral atoms respectively
P	magnetic pitch
$p, p_{/\!/}, p_\perp$	plasma pressure and its components parallel and perpendicular to the direction of the magnetic field
R	major radius of torus
R(t)	plasma resistance for the toroidal plasma current
r	radius (with respect to the axis of a toroidal tube)
r_1	radius of the quartz wall
r_2	radius of the metal wall
r_3	effective radius of the toroidal flux boundary
r_p	outer radius for which the plasma pressure has half the maximum value (= effective plasma radius)
$\tilde{r}$	dimensionless radius (in the Bessel Function Model)
S	Lundquist number
S(r)	Poynting vector, integrated over a surface with radius r
T_e, T_i	electron and ion temperature
t	time
V	voltage; also volume
v	hydrodynamic velocity in the plasma
v_{dif}	diffusion velocity across the magnetic field
$v_{th\ dif}$	velocity due to thermal diffusion
Z, Z_{eff}	(effective) charge of the ions in the plasma
α	proportionality factor for force-free configurations
β	ratio of kinetic to magnetic pressure
β_θ	ratio of plasma energy to magnetic energy due to the plasma current
Δ	displacement of the magnetic axis
$\varepsilon, \varepsilon_{magn}$	plasma energy and total magnetic energy
$\eta_{\theta\theta}, \eta_{\theta z}, \eta_{z\theta}, \eta_{zz}$	components of the resistivity tensor
$\Theta, \Theta(r)$	pinch ratio (evaluated at different positions)
λ	wave-length
μ_o	magnetic permeability (in vacuum)
$\xi(\xi_r, \xi_\theta, \xi_z)$	displacement of plasma (in stability theory) and cylindrical components
ρ	mass density (of plasma)
$\sigma, \sigma_{/\!/}, \sigma_\perp$	electrical conductivty and its components parallel and perpendicular to the direction of the magnetic field
τ	variable for integration over a volume

τ_A	hydromagnetic (Alfvén) transit-time	$\Phi(r)$	toroidal (longitudinal) magnetic flux
τ_E	energy confinement time	$\chi(r)$	poloidal (azimuthal) magnetic flux
τ_g	growth time of instabilities	ω	growth rate of instabilities
τ_I	current decay time	ω_{ce}, ω_{ci}	Gyro frequencies of electrons and ions in a magnetic field
τ_σ	resistive diffusion time		
$\tau_{ii}, \tau_{ei}, \tau_{ee}$	ion-ion, electron-ion, and electron-electron collision time		

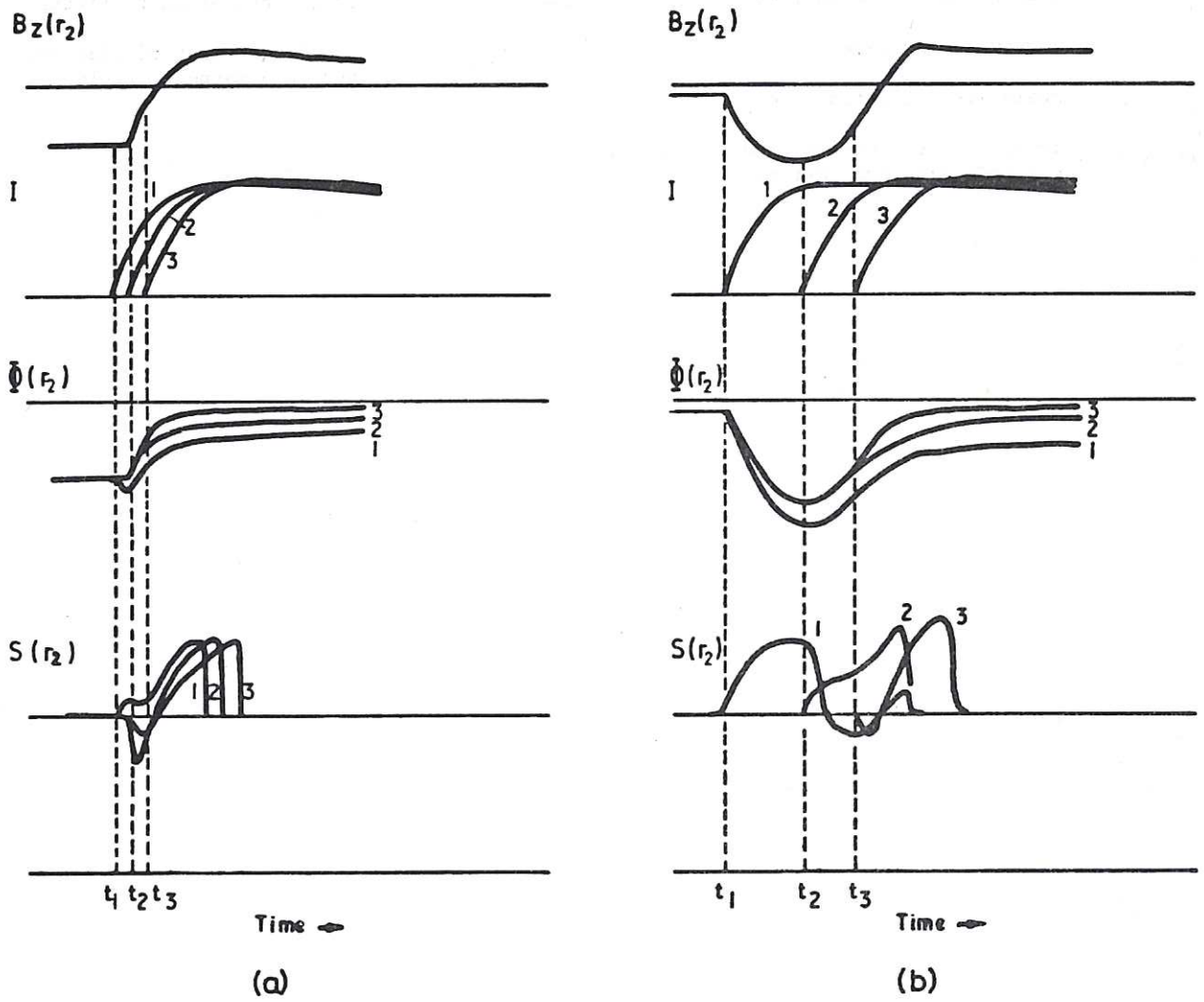

Fig. 1 Programming modes as used in the experiments. $B_z(r_2)$ is the magnetic field applied to the outside region of the plasma, I is the plasma current, $\Phi(r_2)$ is the toroidal flux inside the conducting boundary, and $S(r_2)$ the Poynting vector integrated over the surface of the boundary.

(a) Programming mode used in most experiments. The amount of trapped flux is controlled by the time of I and the initial level of $B_z(r_2)$.

(b) Programming mode with more control on $S(r_2)$, utilized to optimize the level of $\Phi(r_2)$. The amount of trapped flux is maximal when the plasma current starts at $t = t_1$.

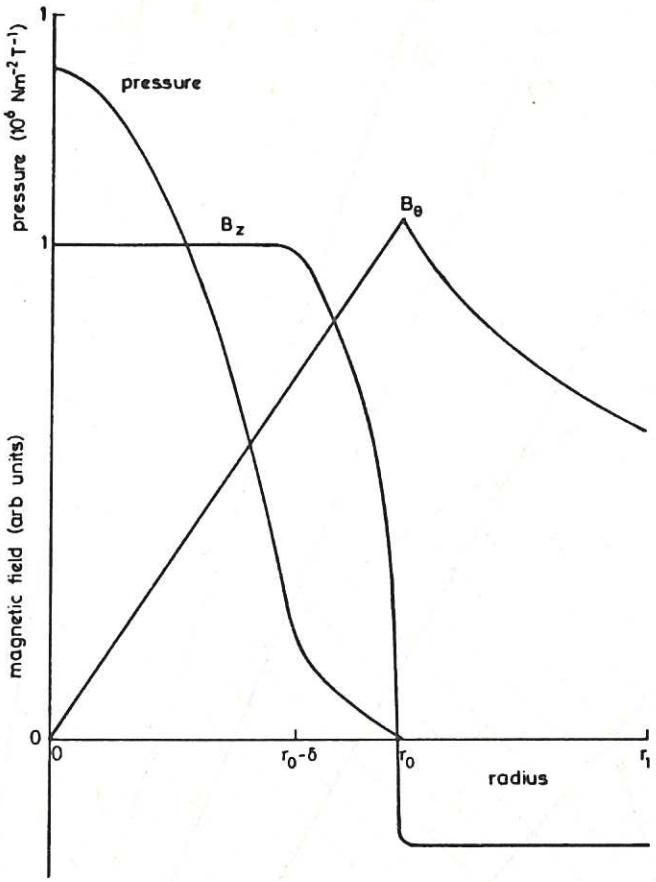

Fig. 2 Model field configuration of the RFP with derived pressure profile. The magnetic field is in arbitrary units.

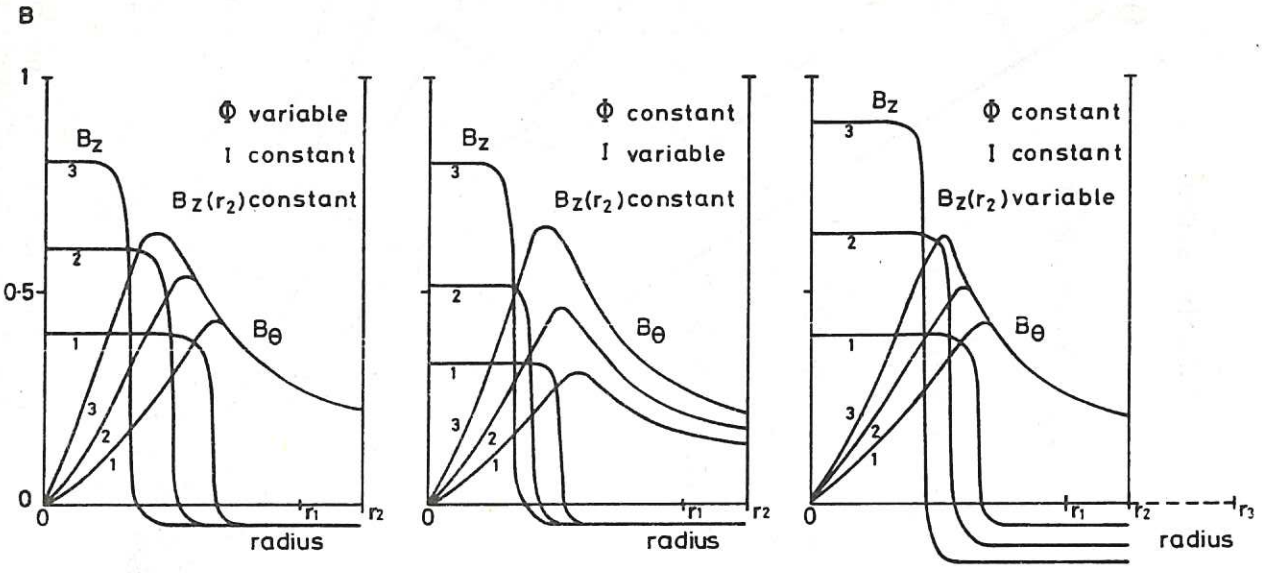

Fig. 3 Model configurations of the RFP with boundaries as in HBTX-1 (quartz wall at r_1, metal wall at r_2, flux boundary at r_3). In each picture the magnetic field components are shown for three different values of the varied parameter marked 1, 2, 3, while the other two parameters and β_θ are kept constant. The meaning of the parameters is as in figure 1.

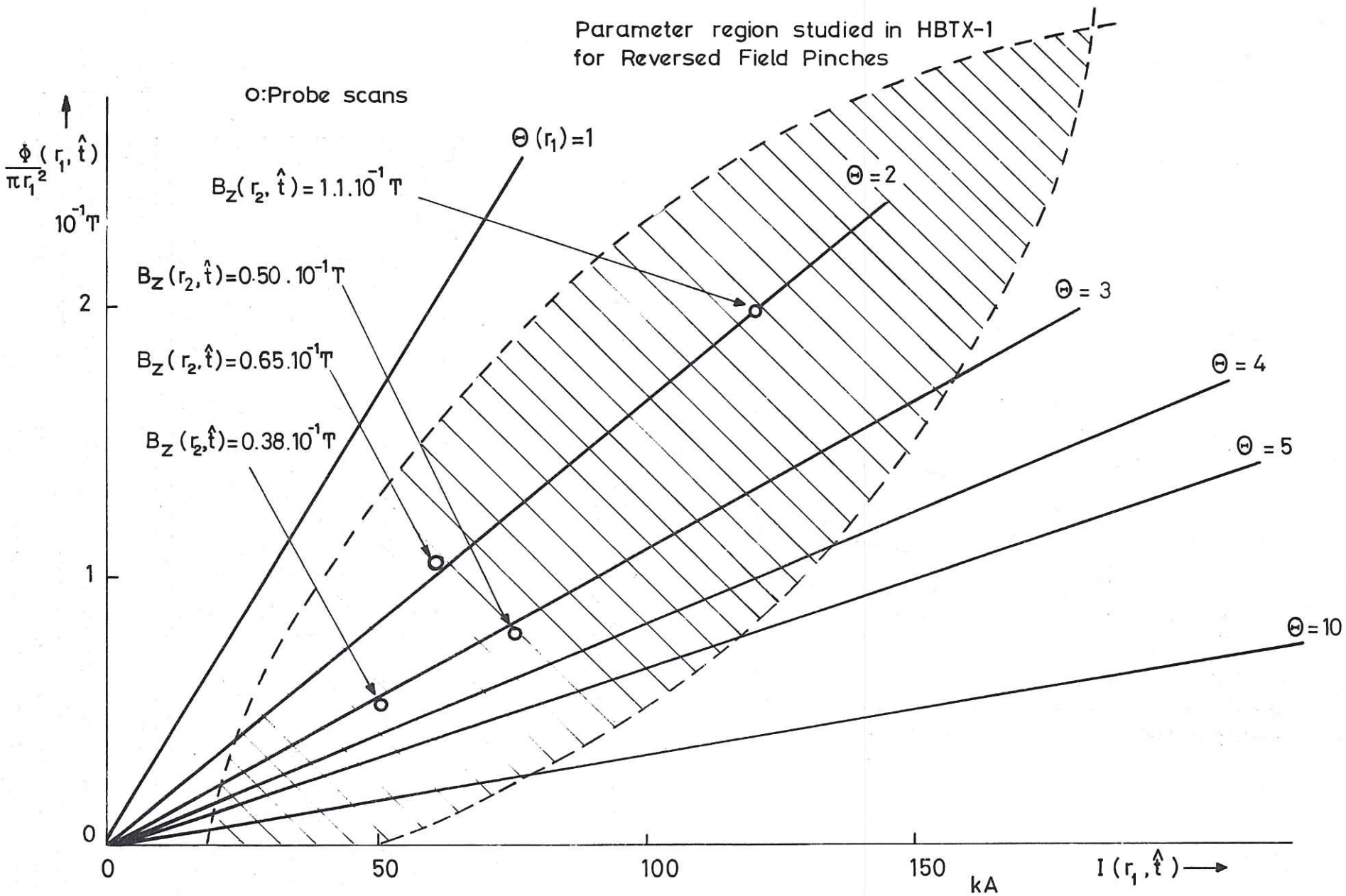

Fig. 4 The values of the plasma current (I) and trapped flux ($\Phi(r_1)$) attainable in RFP experiments in HBTX-1 at the time of current maximum (the time of crowbarring). The lines of constant pinch ratio $\theta(r_1)$ are shown and the values of the reversed field are given for 4 configurations studied.

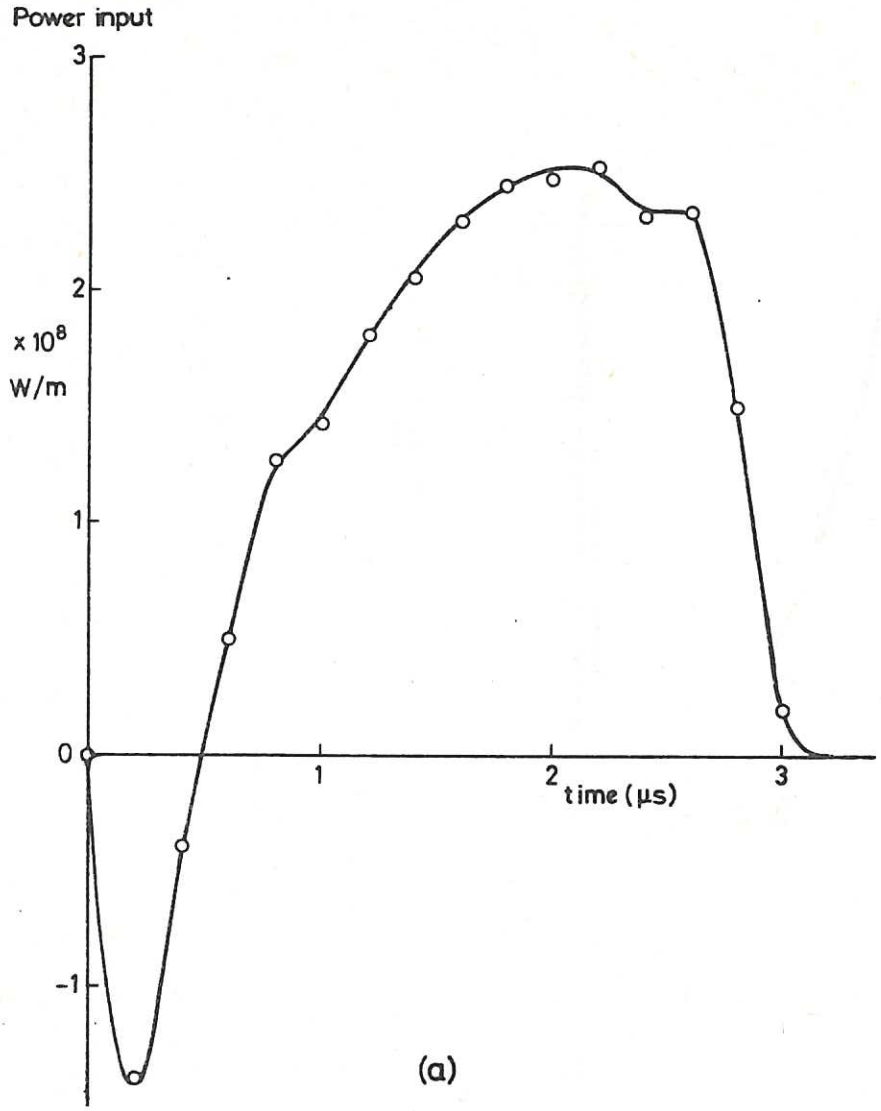

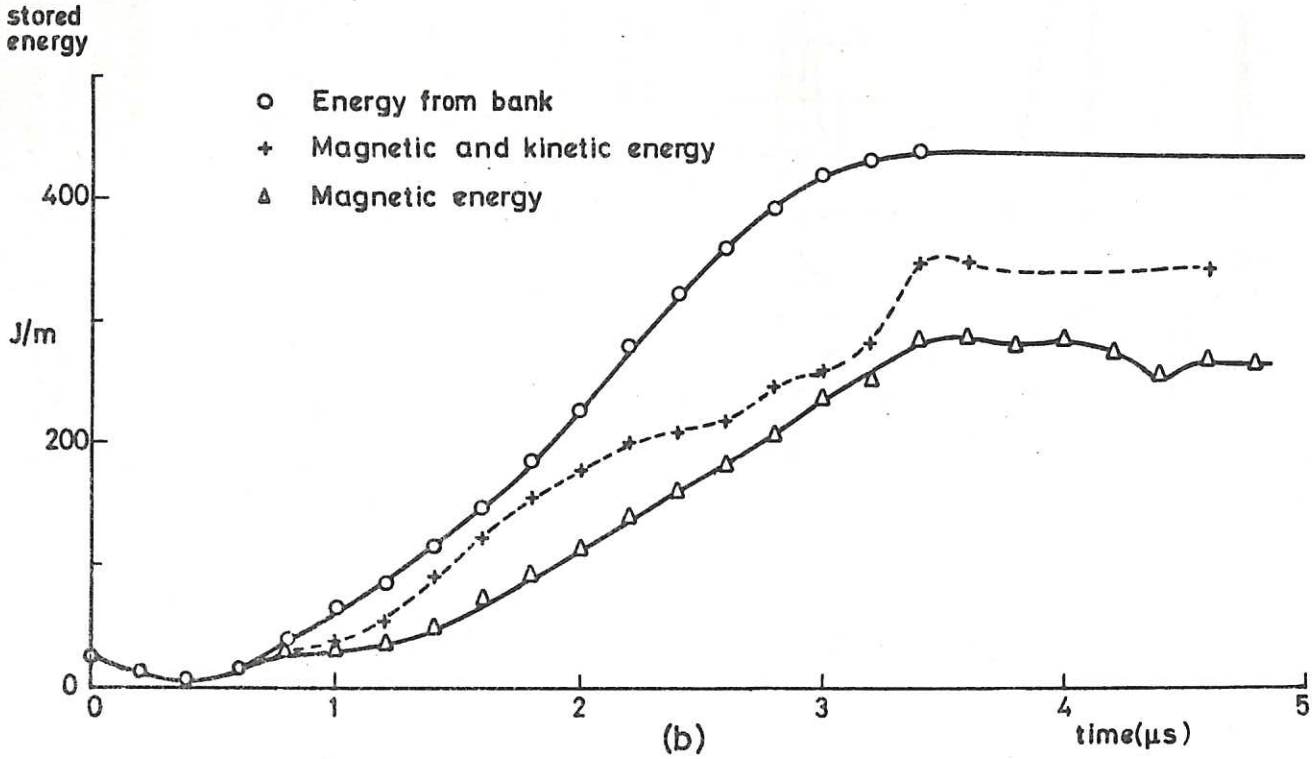

Fig. 5 (a) The time dependence of the Poynting vector, integrated over the plasma boundary, for the RFP of figure 6, obtained with the programming mode of figure 1(a).
(b) The energy inside the torus (i.e. the integral of the waveform of figure 5(a) in time) compared with the magnetic and kinetic energy of the RFP configuration of figure 6(a), evaluated from magnetic probe data. The error in the kinetic energy is about 20%.

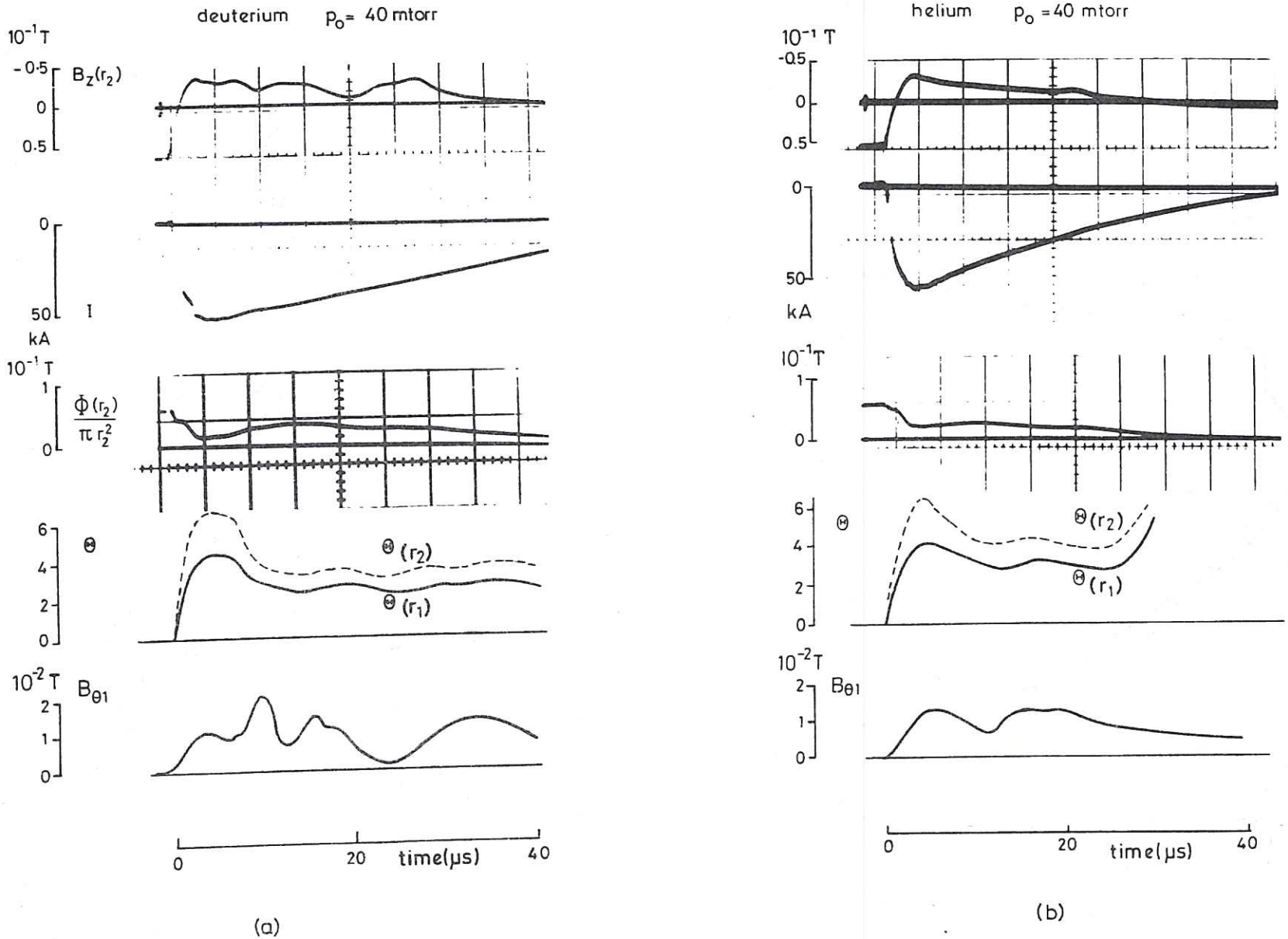

Fig. 6 Main parameters of the RFP discussed in section 6.1.1, measured outside the plasma as a function of time, (a) in Deuterium (filling pressure 40 mtorr), (b) in Helium (40 mtorr). From top to bottom: The B_z-field outside the plasma; the plasma current I; the toroidal flux inside the conducting wall, expressed as the averaged magnetic field; the pinch ratios derived at the plasma boundary $r = r_1$ and at the conducting wall $r = r_2$; the amplitude of the first azimuthal harmonic of the β_θ-field (m = 1) as measured with sine and cosine coils.

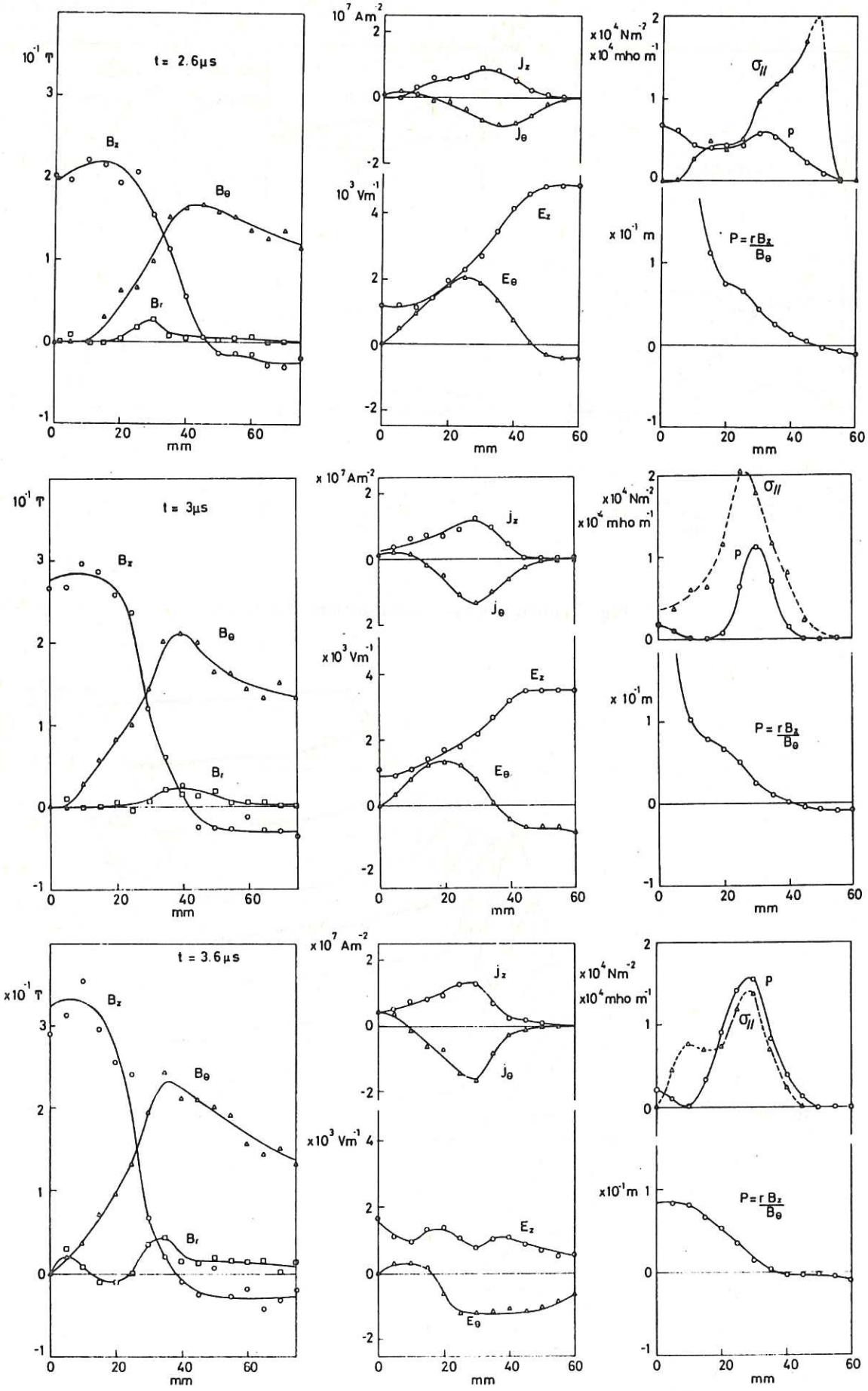

Fig. 7 Magnetic field profiles of the RFP of figure 6(a) and radial profiles of quantities derived from the magnetic field measured at t = 2.6 μs, t = 3.0 μs, and t = 3.6 μs (before and after the time of crowbarring) (a), and later (at t = 24 μs) during the decay of the plasma (b). At each point in time profiles are shown for:
The three components of the magnetic field (B_r, B_θ, B_z); the current density (j_θ, j_z); the electric field (E_θ,E_z); the plasma pressure (p); the parallel electrical conductivity ($\sigma_{//} = \frac{\vec{j}.\vec{B}}{\vec{E}.\vec{B}}$); and the pitch of the magnetic field ($P = rB_z/B_\theta$).

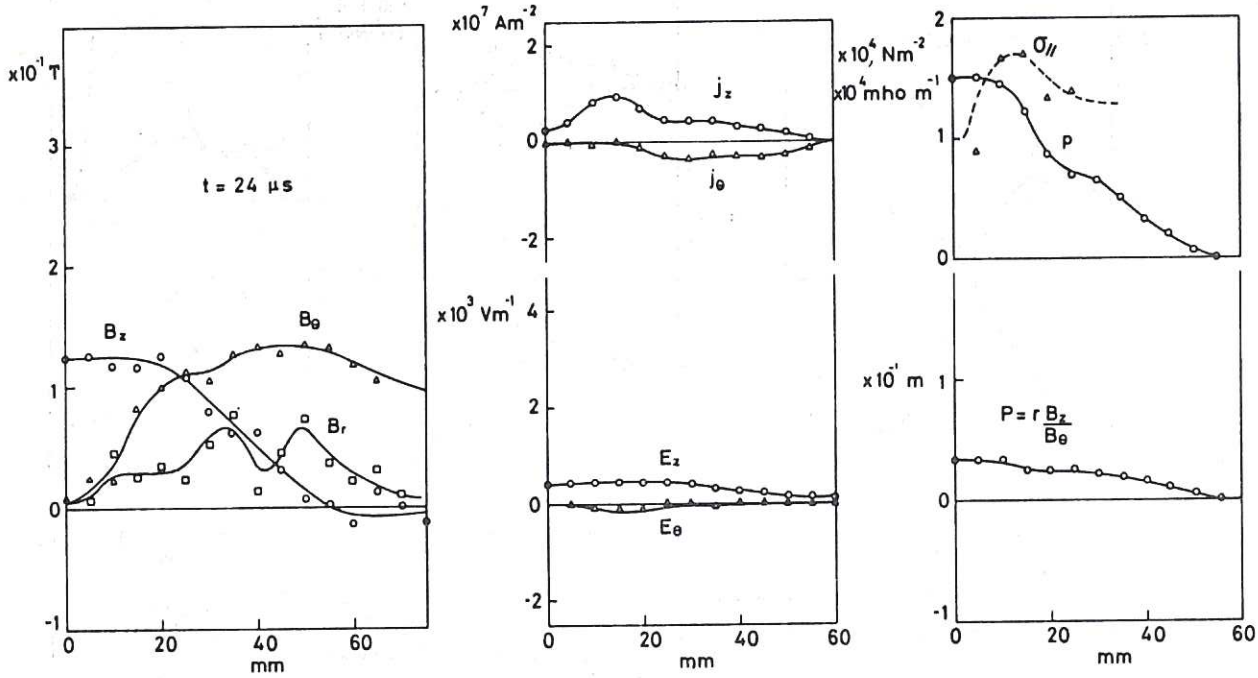

(b)

Fig. 7 continued (see previous page for Caption)

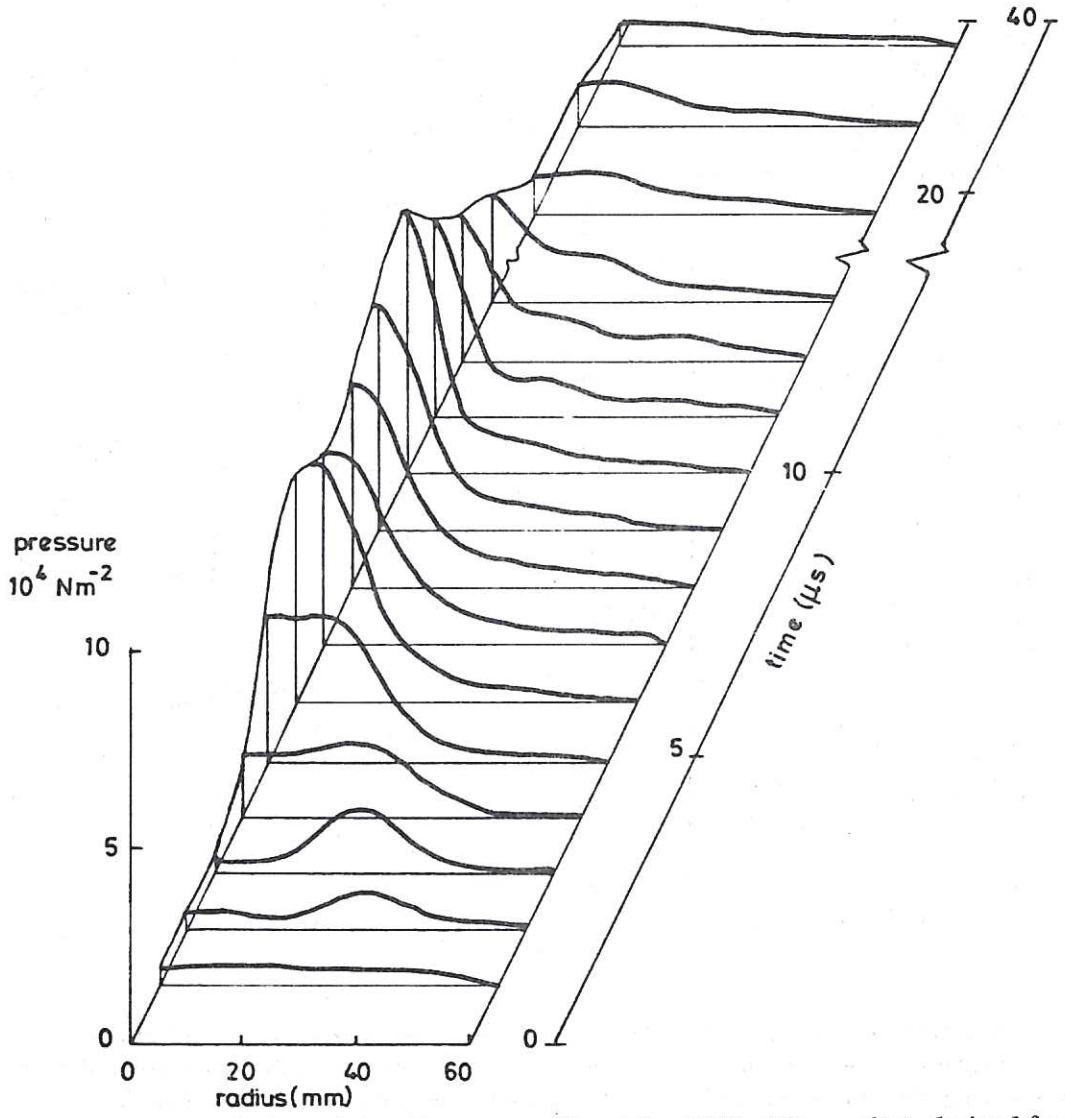

Fig. 8 The time evolution of the pressure profile of the RFP of figure 6(a), derived from the magnetic field at intervals of 1 μs between the start of the plasma current (t = 0) and t = 13 μs; and in steps of 10 μs later during the decay (t = 18,28, and 38 μs).

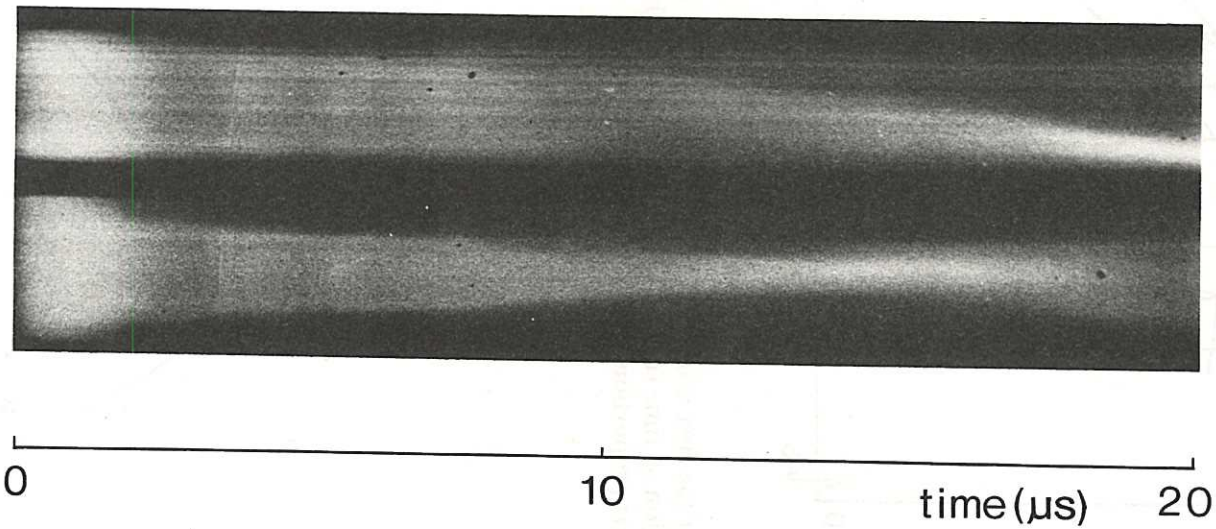

Fig. 9 Streak photographs of the RFP of figure 6(a) taken in two cross-sectional planes 26 cm apart. Because no filters were used, most of the light intensity is due to D_α. Each of the streak photographs covers the diameter of the quartz tube (radius 6 cm).

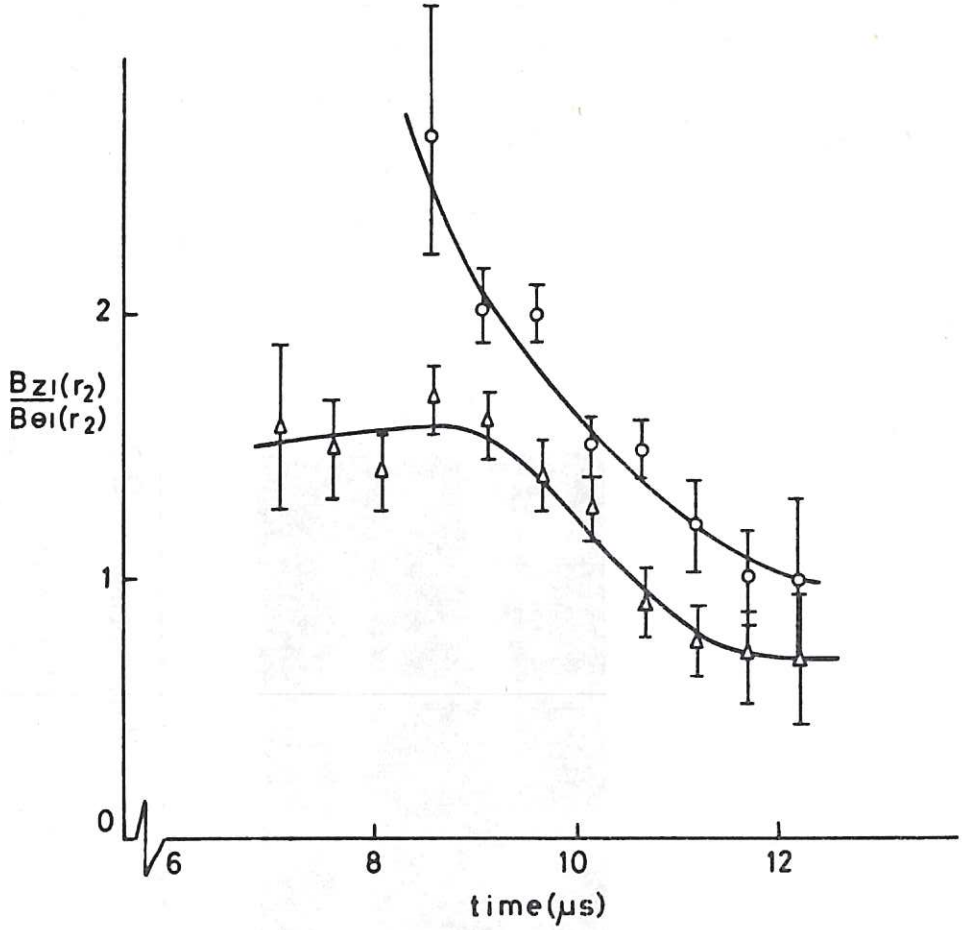

Fig.10 The ratio of the first azimuthal harmonic (m = 1) of the B_z-field to that of the B_θ-field at the wall, as a function of time for two discharges similar to the RFP of figure 6(a). The wavenumber of the m = 1 mode is proportional to $B_{z1}(r_2)/B_{\theta 1}(r_2)$.

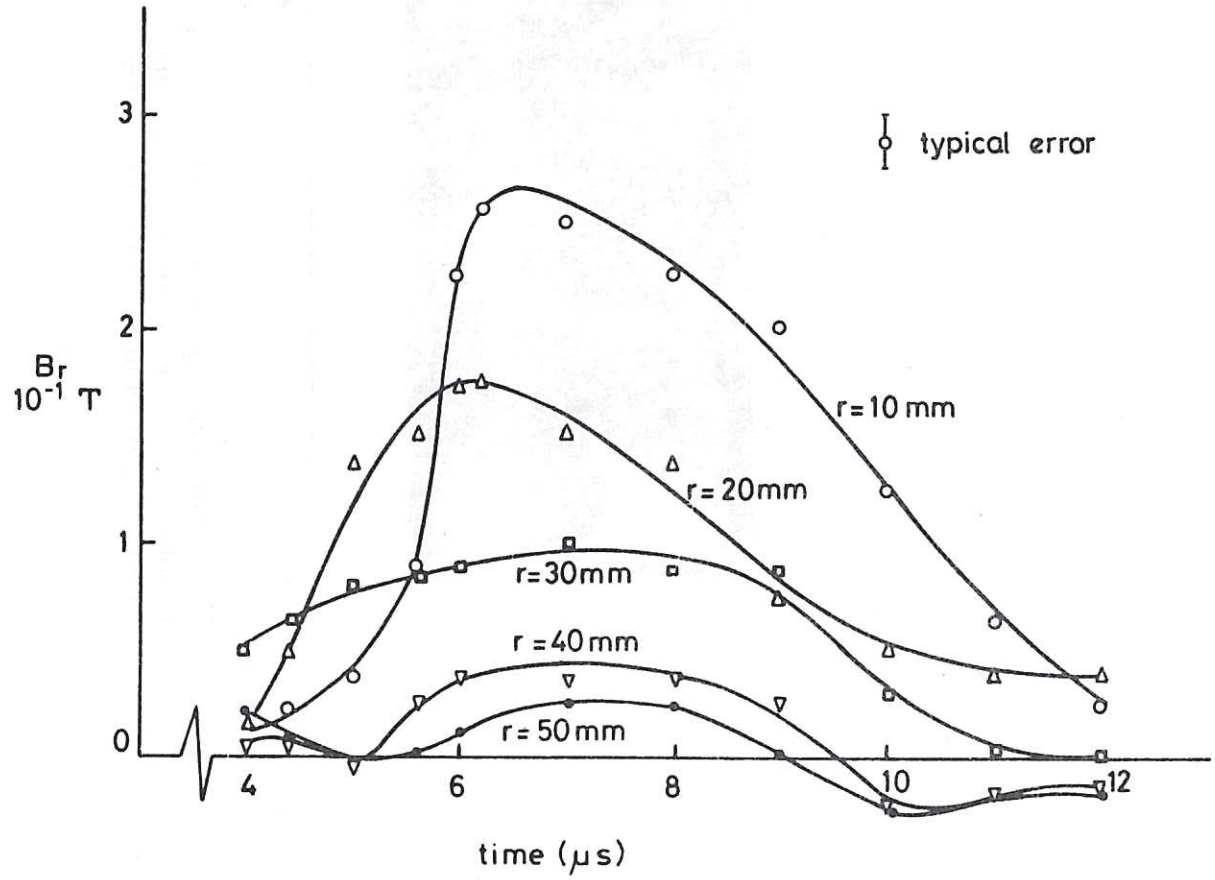

Fig.11 The amplitude of the radial magnetic field B_r at different positions inside the plasma, as a function of time. The B_r signals are due to a gross m = 1 helical kink mode in the RFP of figure 6(a).

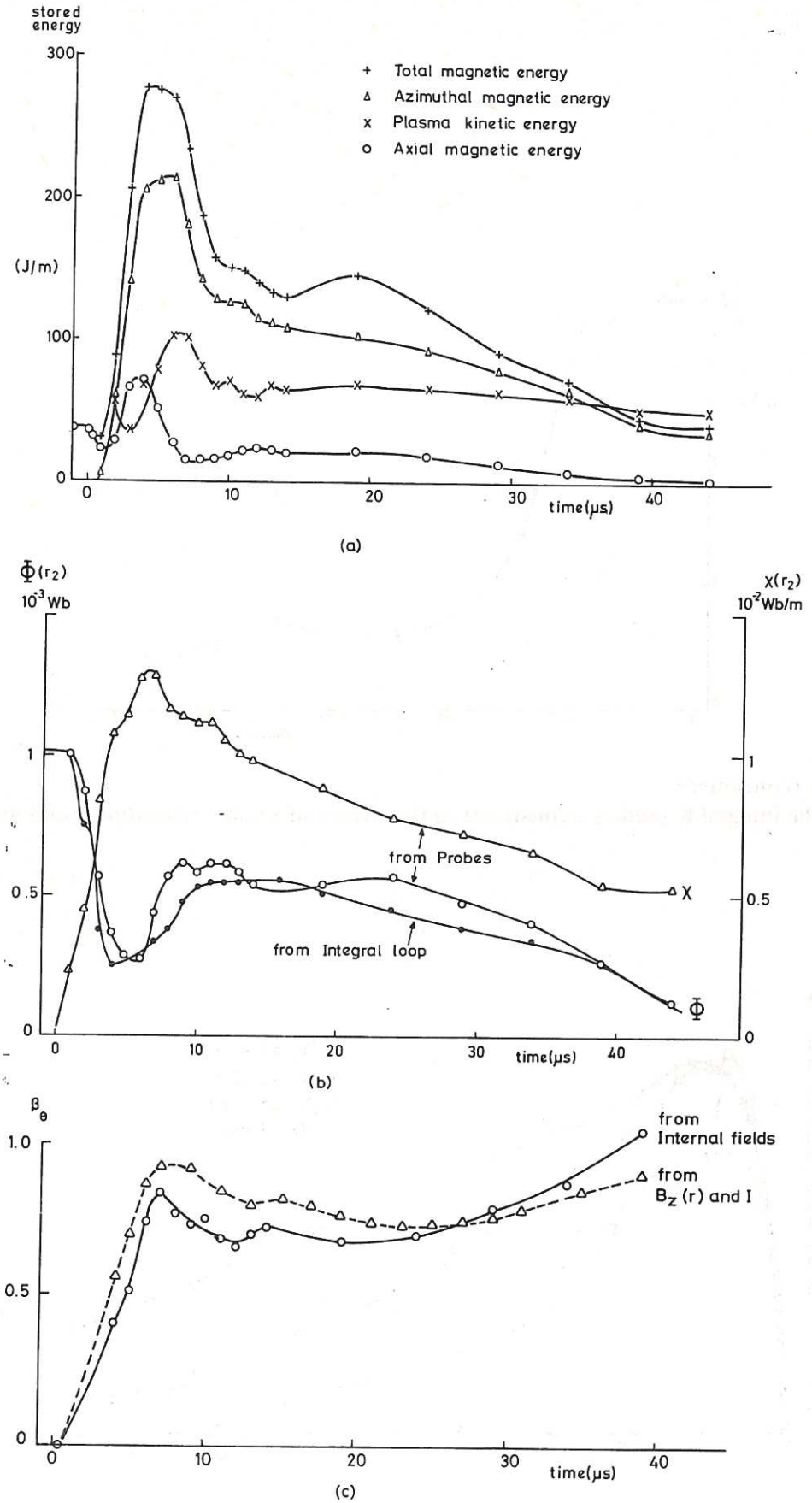

Fig. 12 The time dependence of integral quantities derived from the magnetic field for the RFP of figure 6(a).

(a) The total energy of the magnetic field inside the conducting shell, the energy of the two main components of the magnetic field, and the total plasma energy derived from the fields for 3 degrees of freedom $\frac{3}{2}$ Nk $(\overline{T}_e + \overline{T}_i)$.

(b) The toroidial flux $\Phi(r_2)$ and the poloidal flux $\chi(r_2)$ deduced from magnetic field data, compared with $\Phi(r_2)$ from a flux loop.

(c) The evolution of β_θ derived directly from the field distributions; also β_θ from the B_z-profile and the externally measured plasma current. (Large amplitude instabilities occur between t = 7 μs and t = 9 μs).

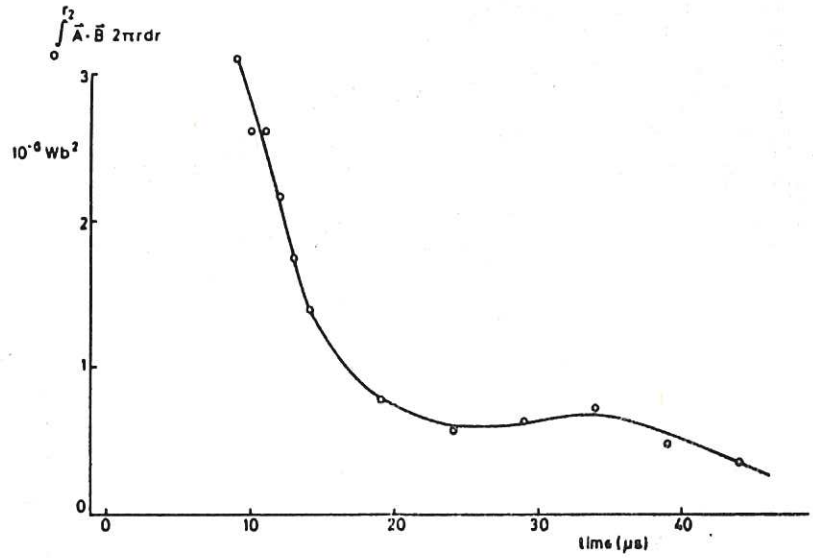

Fig. 12 (continued)
(d) The integral K used as a constraint in the theory of plasma relaxation (section 4.1).

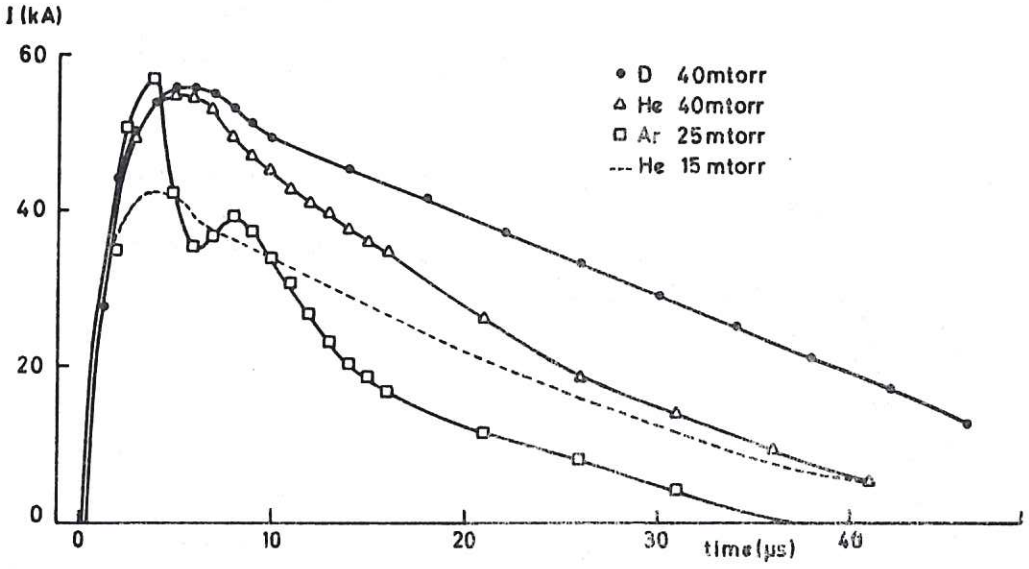

Fig. 13 Decay of the plasma current for different types of filling gas, using the same programming mode as for the RFP of figure 6(a).

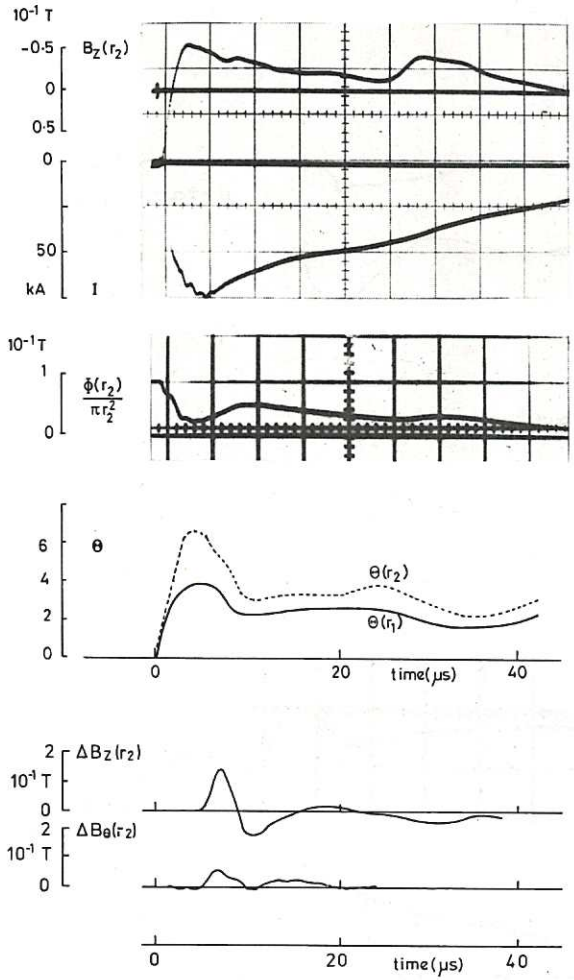

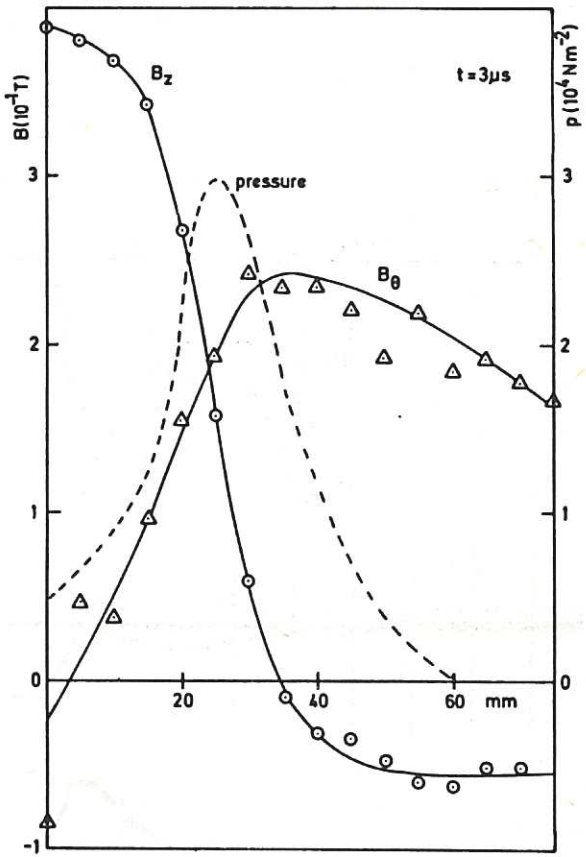

(a)

Fig. 14 Main parameters and pinch ratios, similar to those in figure 6, for RFPs with a maximum current of 75 kA (section 6.1.2). The differences between two B_z coils diametrically opposite each other and two opposite B_θ coils at the same position, are used to detect modes with m = 1; the wavenumber follows from $kr_2 = \Delta B_z(r_2)/\Delta B_\theta(r_2)$.

(a) RFP in Deuterium, unstable to a gross m = 1 mode, and the magnetic field profile at t = 3 μs (the pressure is calculated for the drawn field profile).

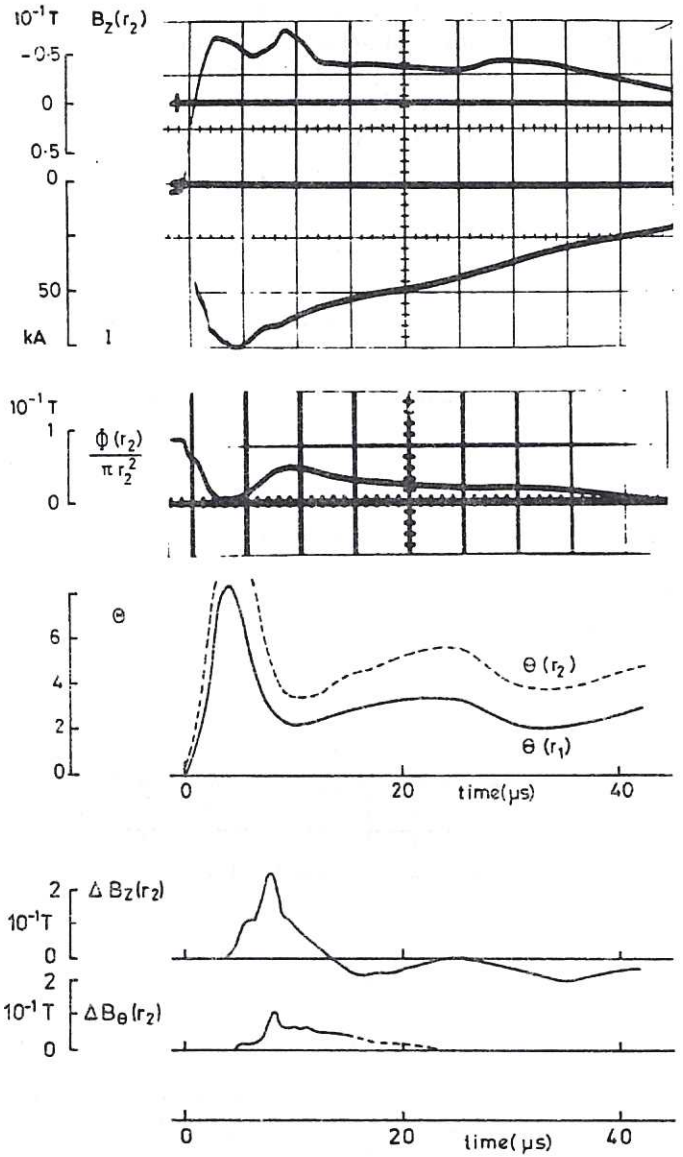

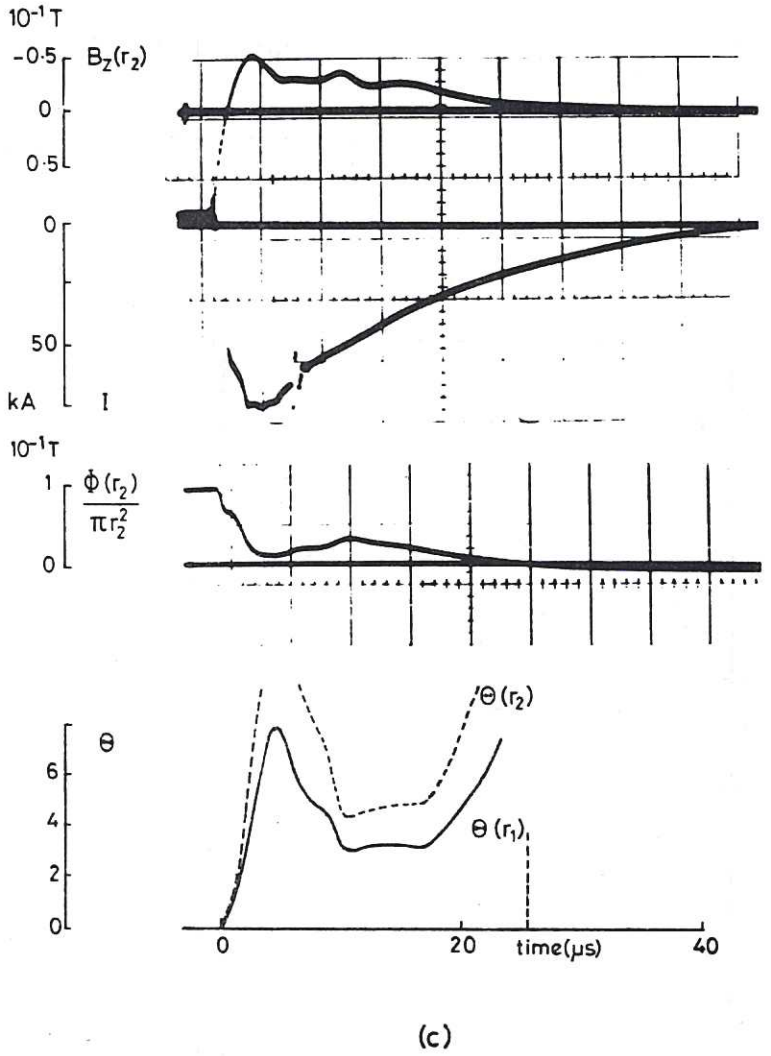

Fig. 14 (continued)

(b) A similar RFP in Deuterium but with 10% more reversed field.

(c) RFP in Helium with the same programming as in 14(a).

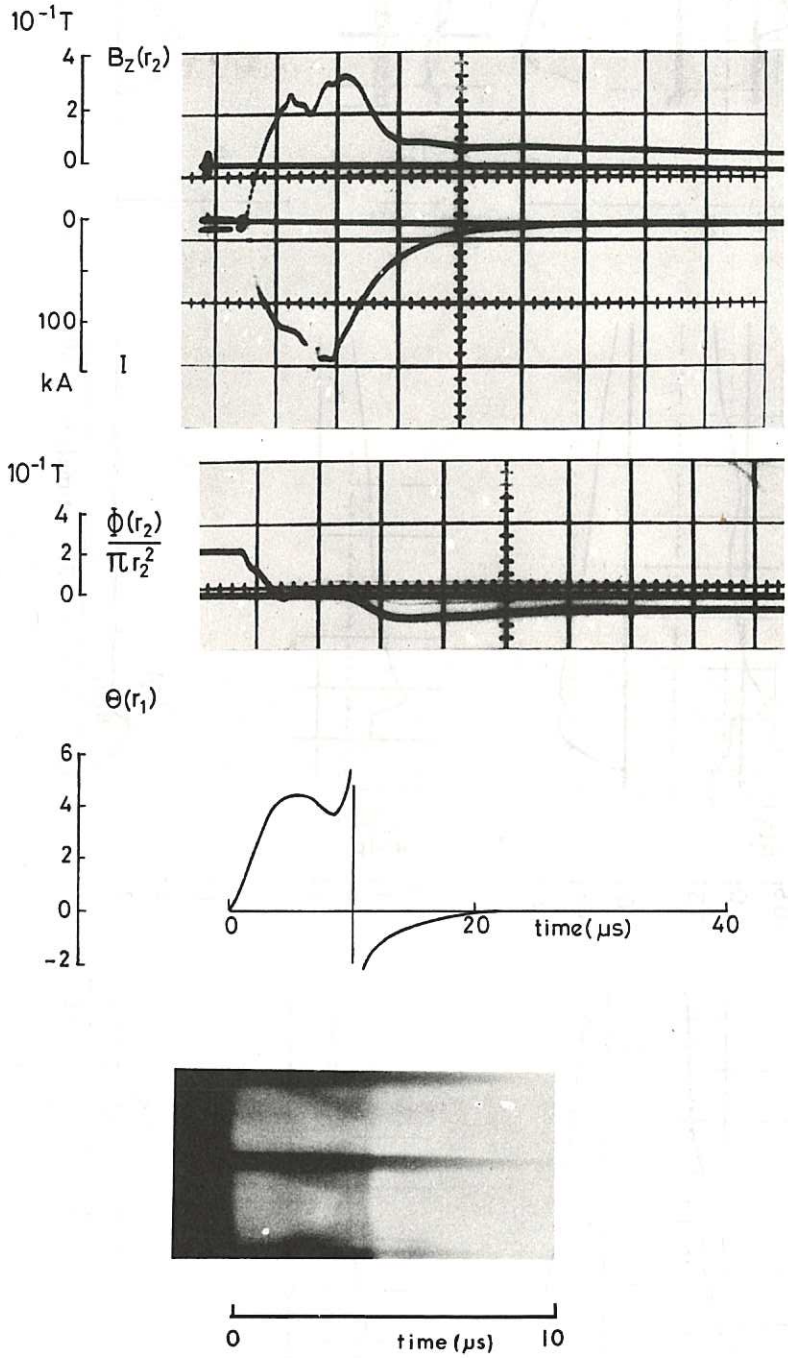

Fig. 15 Main parameters (as in figure 6) and pinch ratio $\Theta(r_1)$ of a rapidly contracting unstable RFP configuration. The streak photographs obtained in the same way as for figure 9 show a large increase in luminosity associated with the collapse of the field configuration (section 6.1.3).

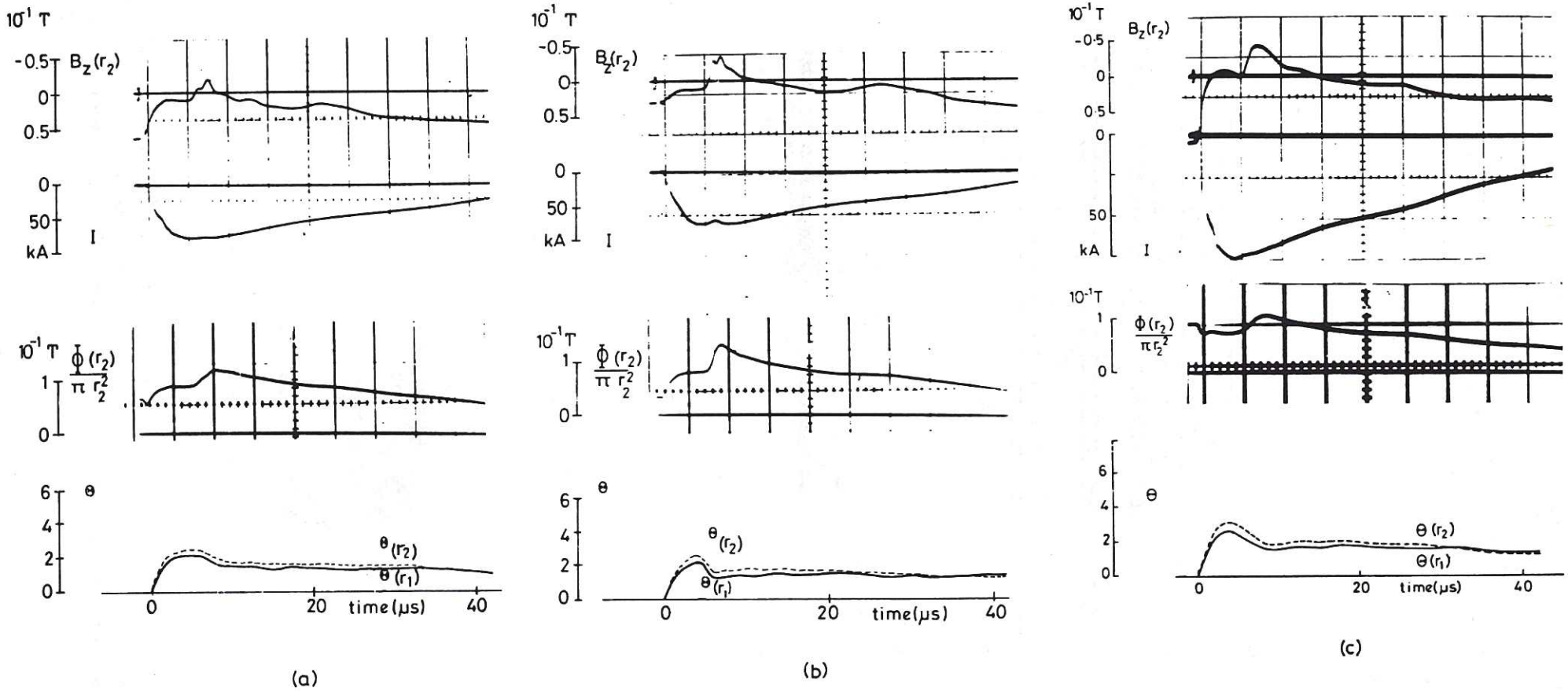

Fig. 16 Main parameters and pinch ratios (explained for figure 6) in discharges for which $B_z(r_2)$ is reversed during instabilities. (Section 6.1.4).

(a) A stabilized z-pinch with conserved total toroidal flux.

(b) A stabilized z-pinch with partially programmed B_z-field.

(c) As in 16(b), but $B_z(r_2)$ is reduced to about zero, and the peak current is increased to 75 kA.

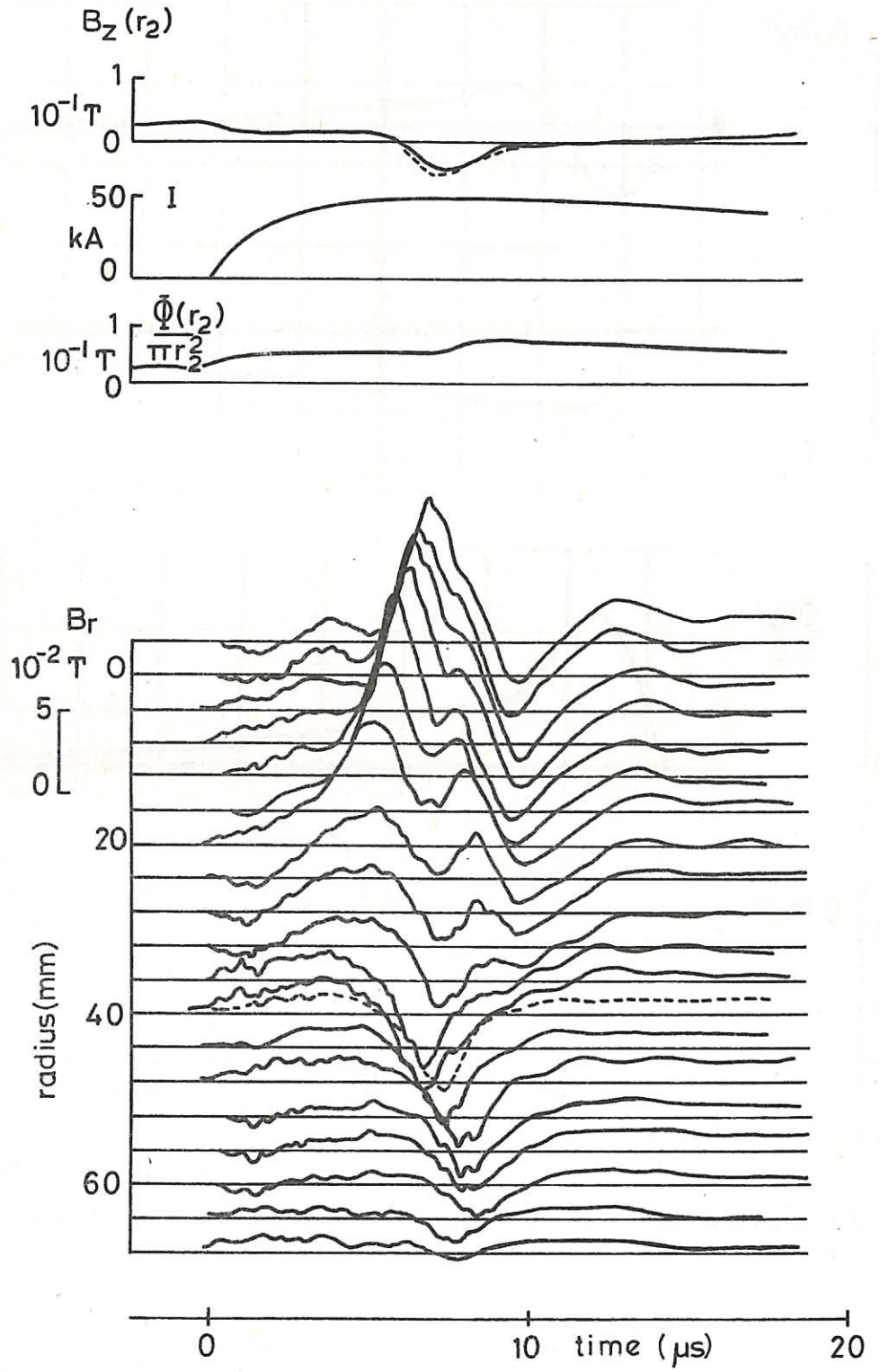

Fig. 17 The radial magnetic field B_r as a function of time for different radial positions inside the plasma. The main parameters, similar to those in figure 16(a), are also shown. The reversal of $B_z(r_2)$ correlates with B_r. (The dashed line indicates the overlap for the two discharges used to acquire a complete radial profile).

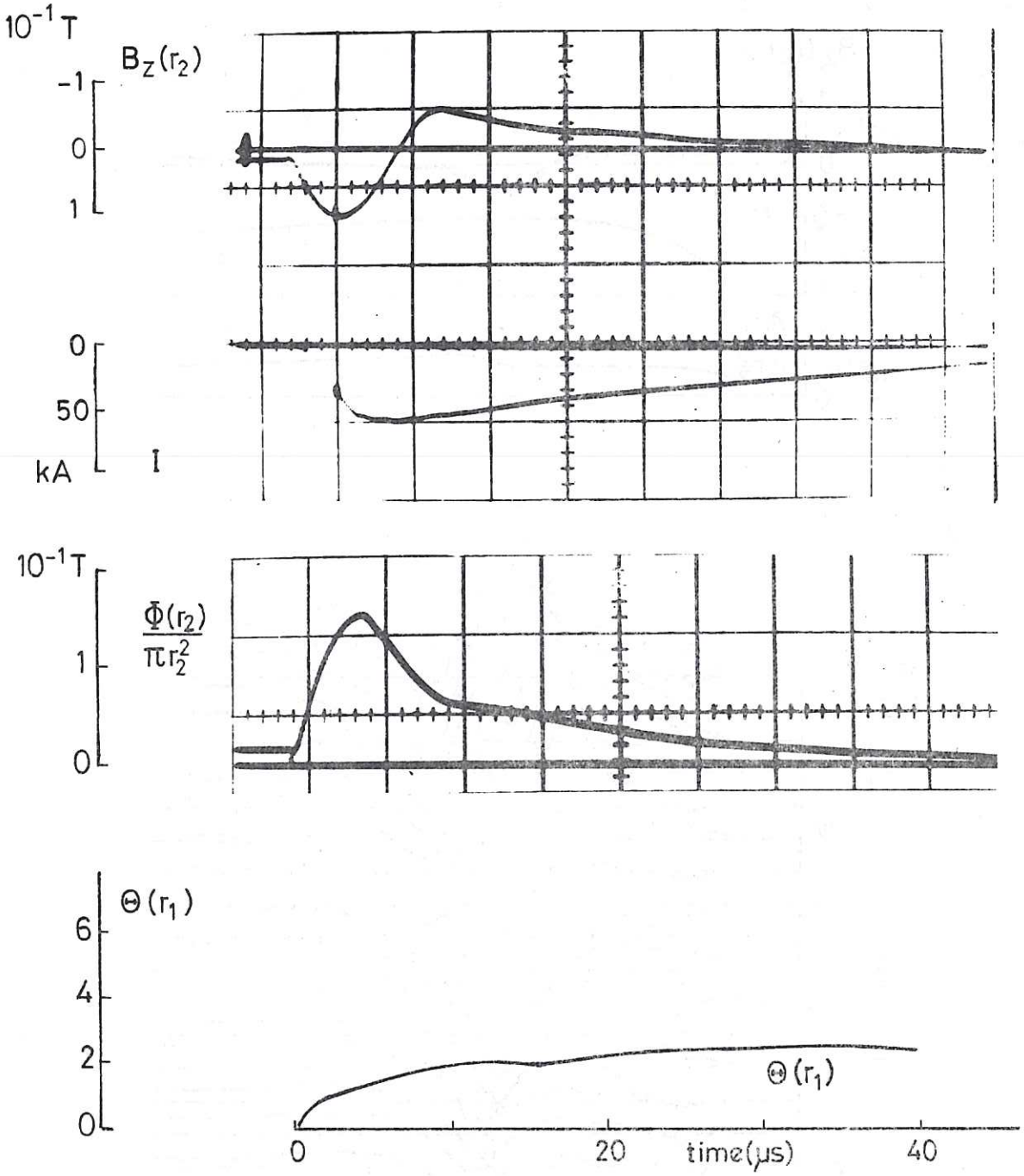

Fig. 18 Main parameters and pinch ratio (legend as for figure 6) for a relatively weakly compressed RFP produced with the programming mode of figure 1(b). (Section 6.2.1).

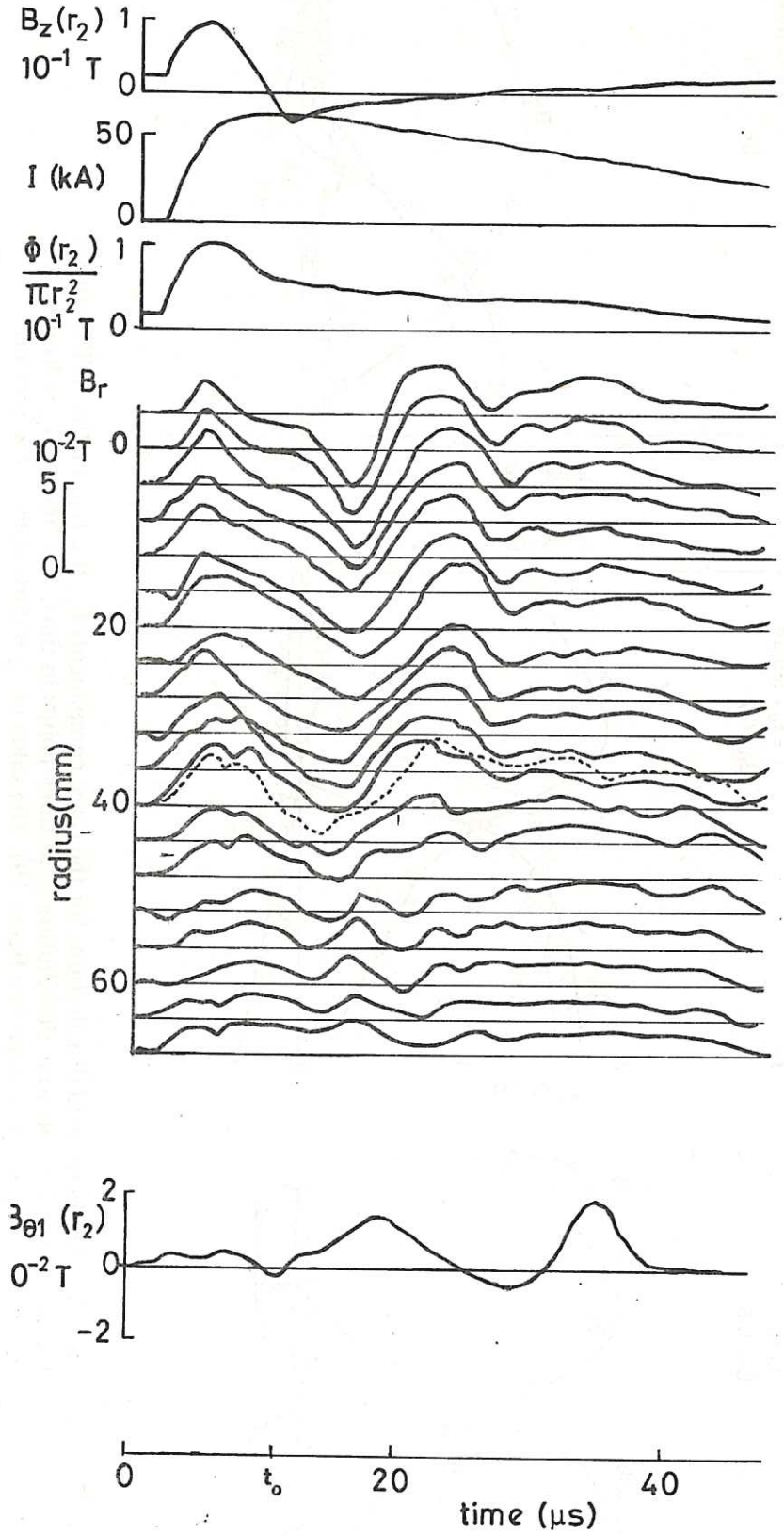

Fig. 19 The time dependence of the radial magnetic field B_r at different radial positions, for an RFP similar to the one in figure 18, together with the m = 1 perturbations in the B_θ-field at the wall and the main parameters. (The dashed line indicates the overlap for two subsequent discharges, as in figure 17; the end of the programming stage is marked t_o).

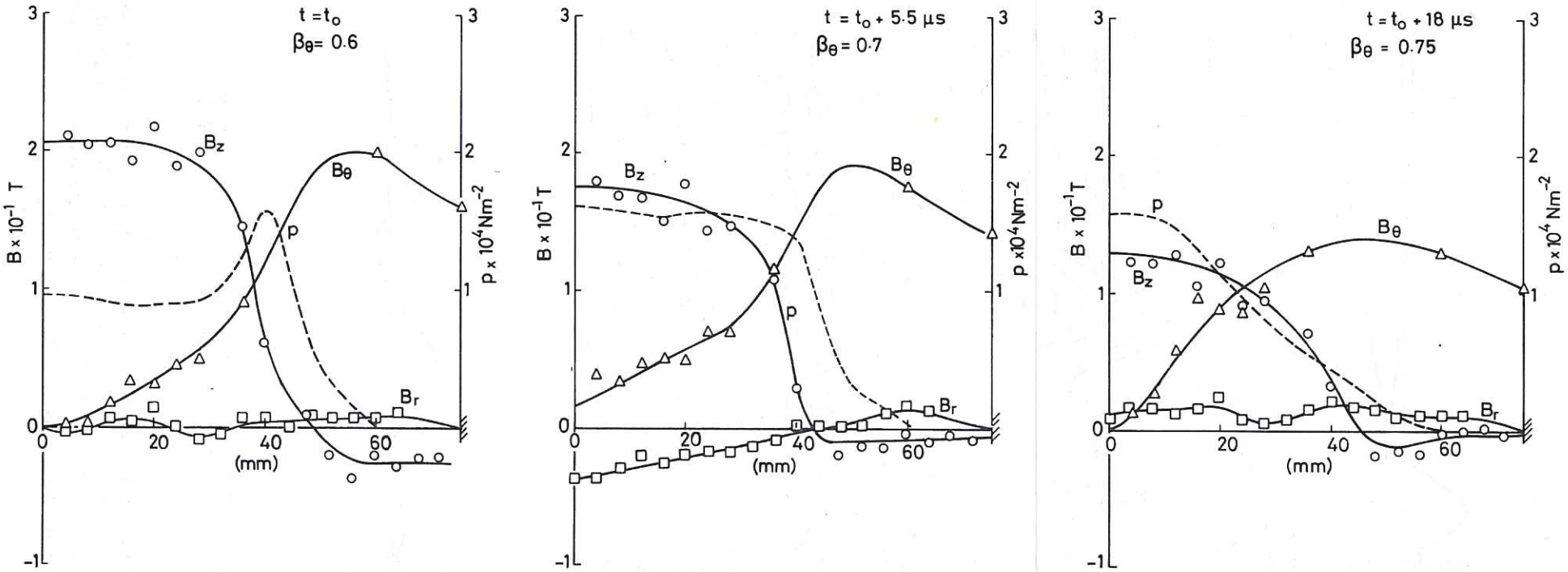

Fig. 20 Magnetic field distributions for the three components B_r, B_θ, B_z, for the RFP of figure 19, and the derived pressure distribution ρ, at three points in time. The time $t = t_o$ indicates the end of the programming stage (see figure 19). The value of β_θ is derived from the pressure.

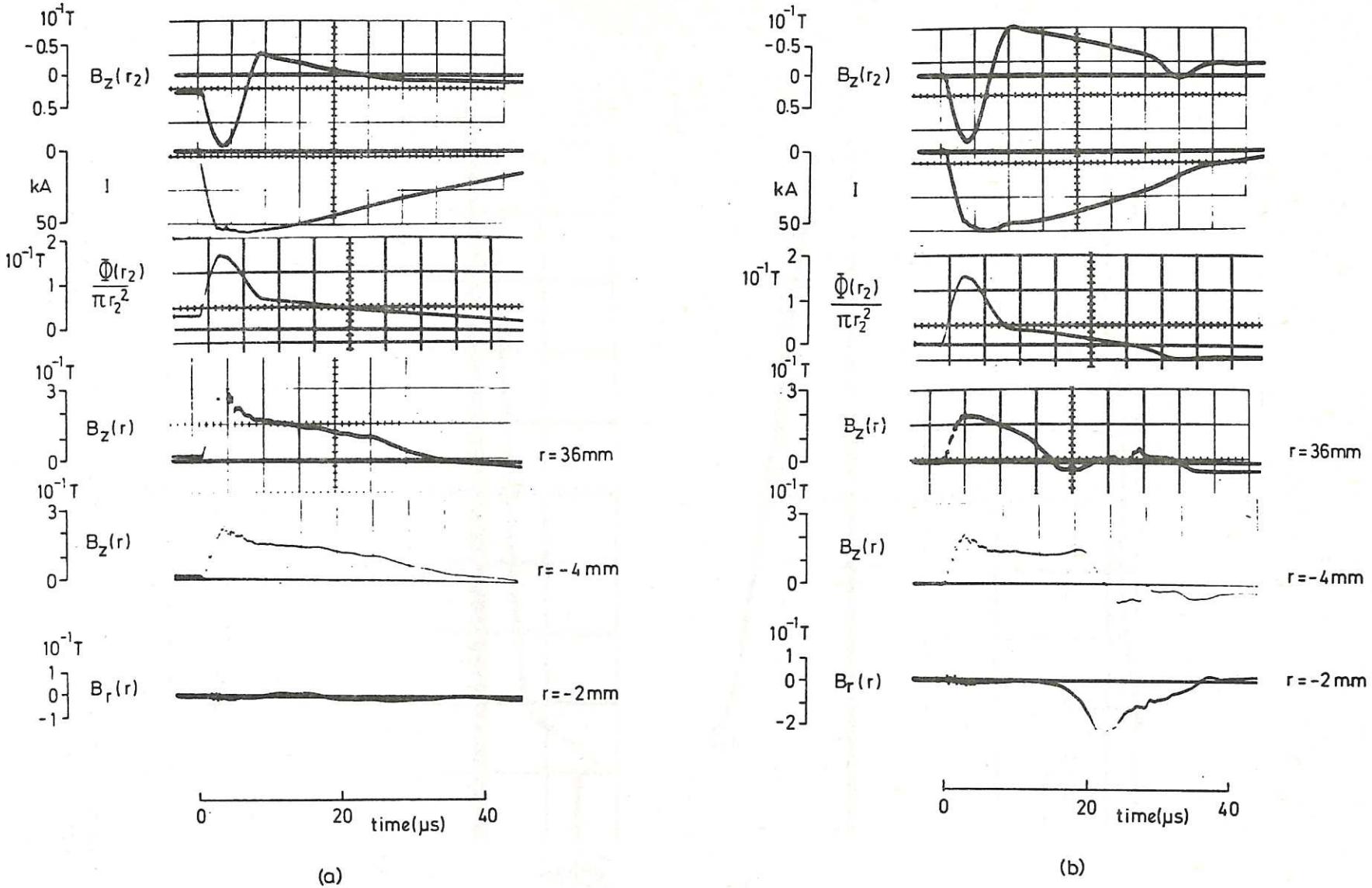

Fig. 21 Field diffusion for two RFPs with the same peak current (60 kA) but a different sign of the total toroidal flux $\Phi(r_3)$ (Section 6.2.1). The B_z-field at the wall, plasma current, flux, the B_z-field at two positions inside the plasma, and B_r in the centre are compared as they evolve in time. (a) The total flux is positive: the magnetic field decays continuously and the reversal of B_z disappears. (b) The total flux is negative: the radius for which B_z reverses contracts and the configuration becomes unstable.

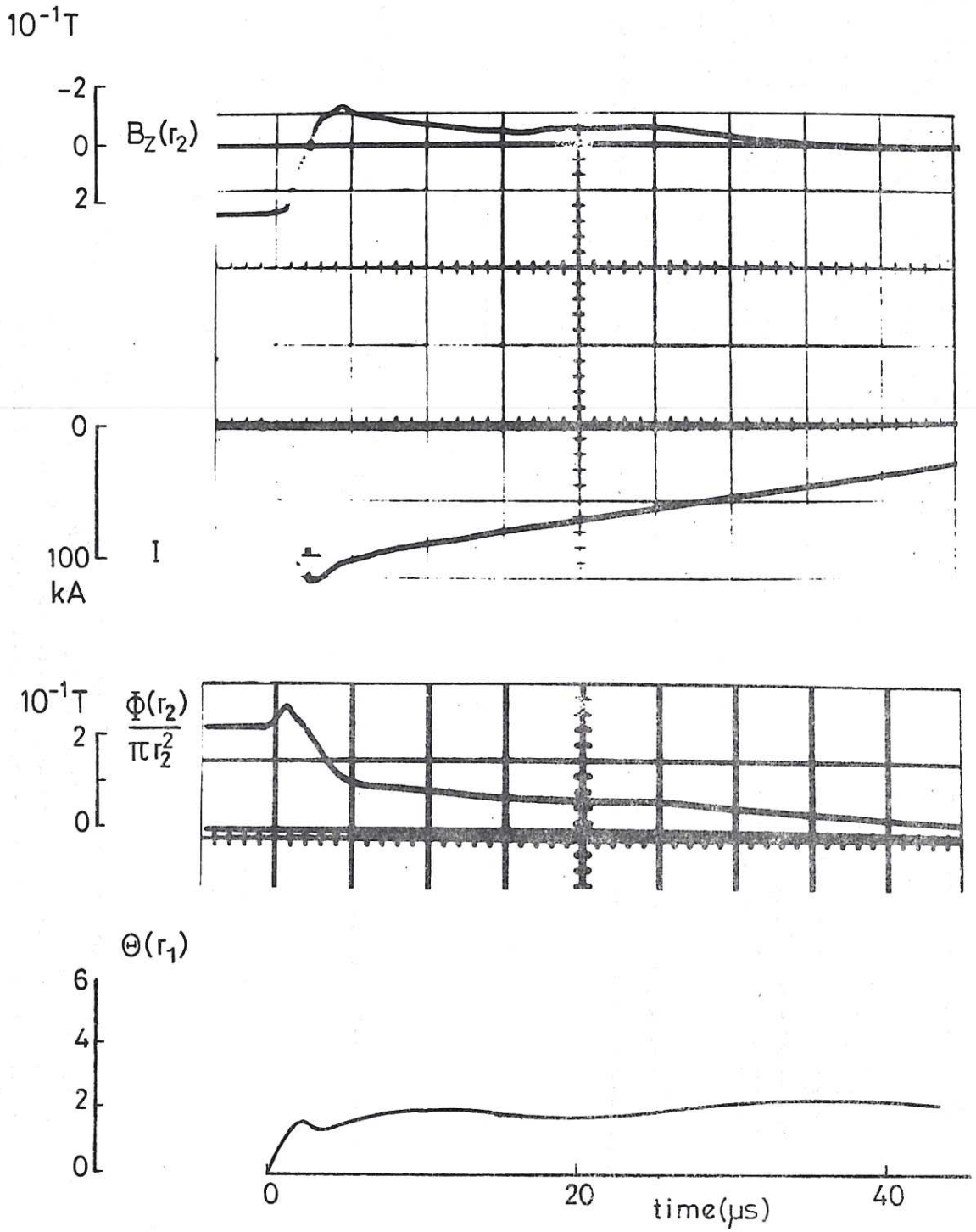

Fig. 22 Main parameters (explained for figure 6) of a weakly compressed RFP, programmed with the mode of figure 1(a) (Section 6.2.2).

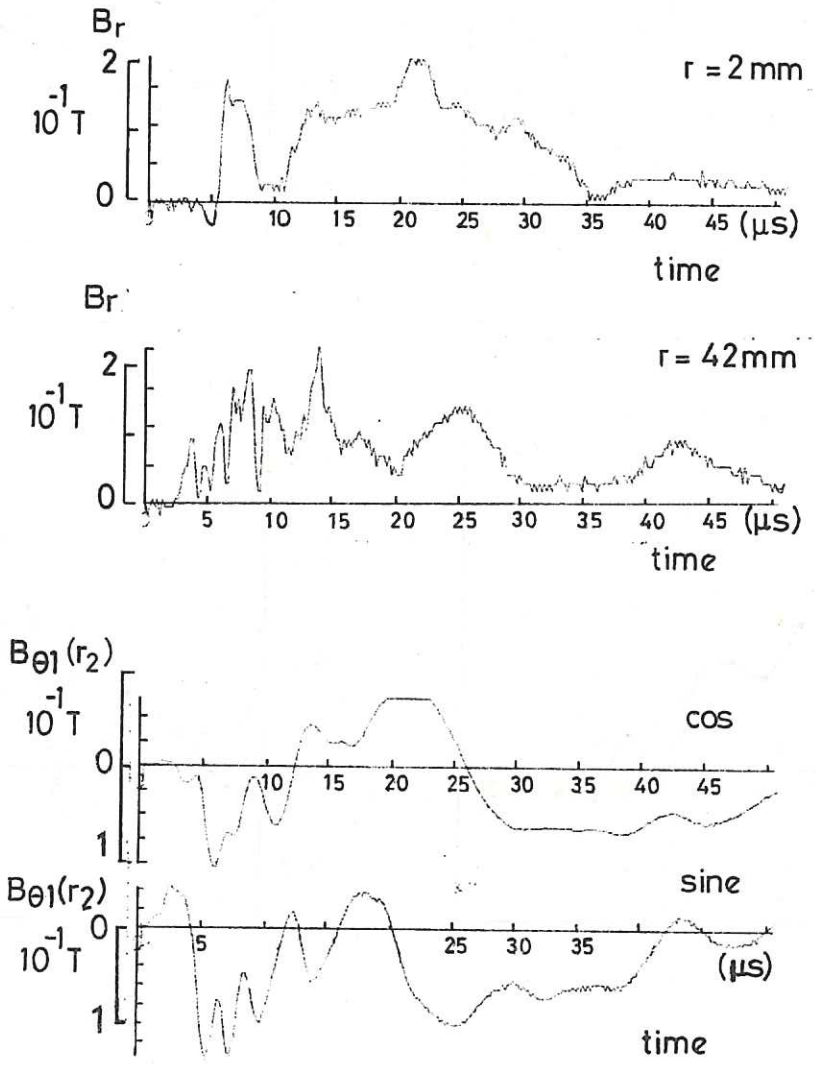

Fig. 23 The radial magnetic field B_r inside the RFP of figure 22 compared with the first harmonics of B_θ obtained with sine and cosine coils outside the plasma. The signals were reproduced with the HBTX-1 Data Acquisition System.

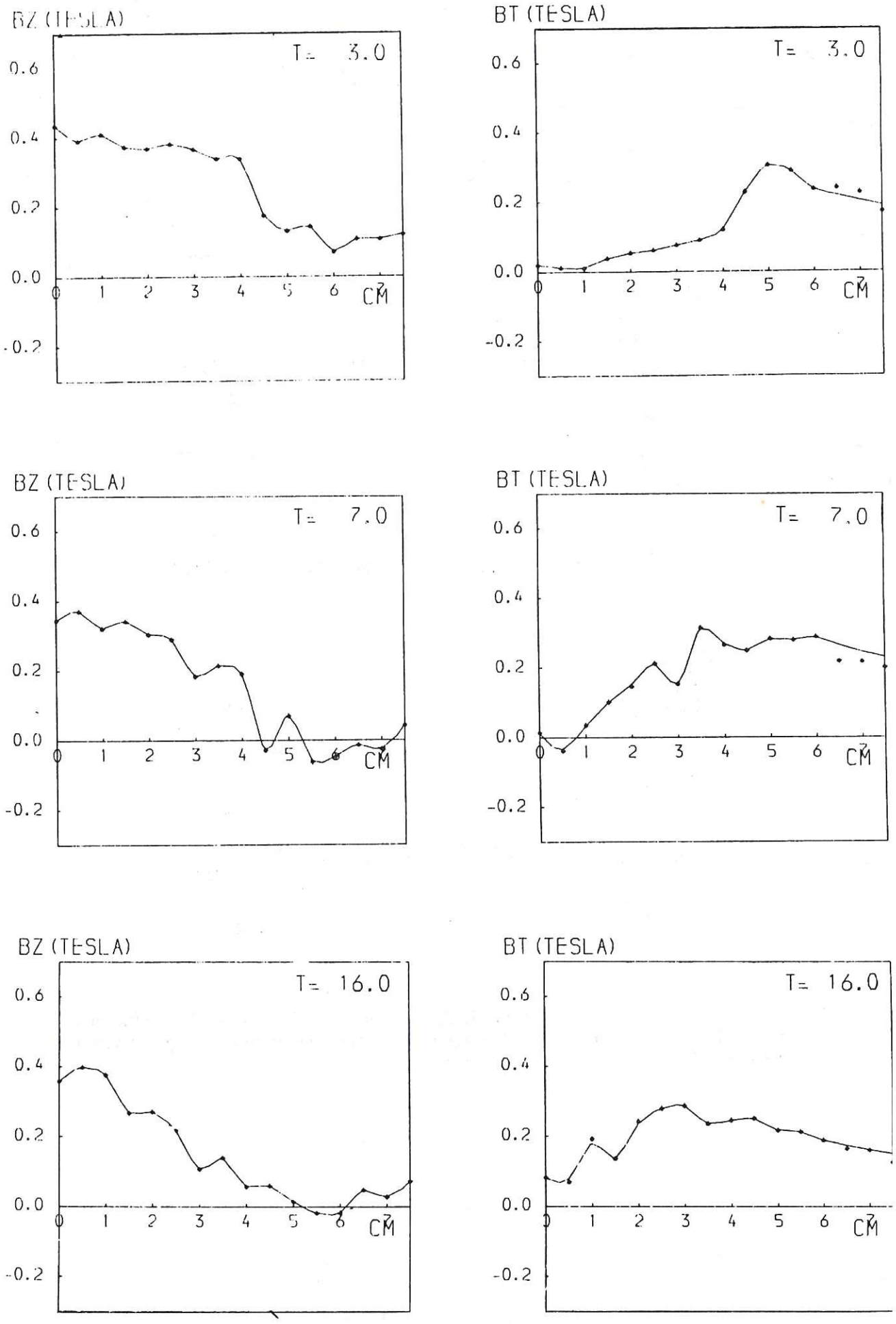

Fig. 24 The magnetic field components B_z (BZ) and B_θ (BT) as a function of radius for the RFP of figure 22, at three points in time. The time (T) is in microseconds, the start of the current corresponds to T = O. (The profiles were drawn by computer; errors in the measured points, 5%, are not accounted for).

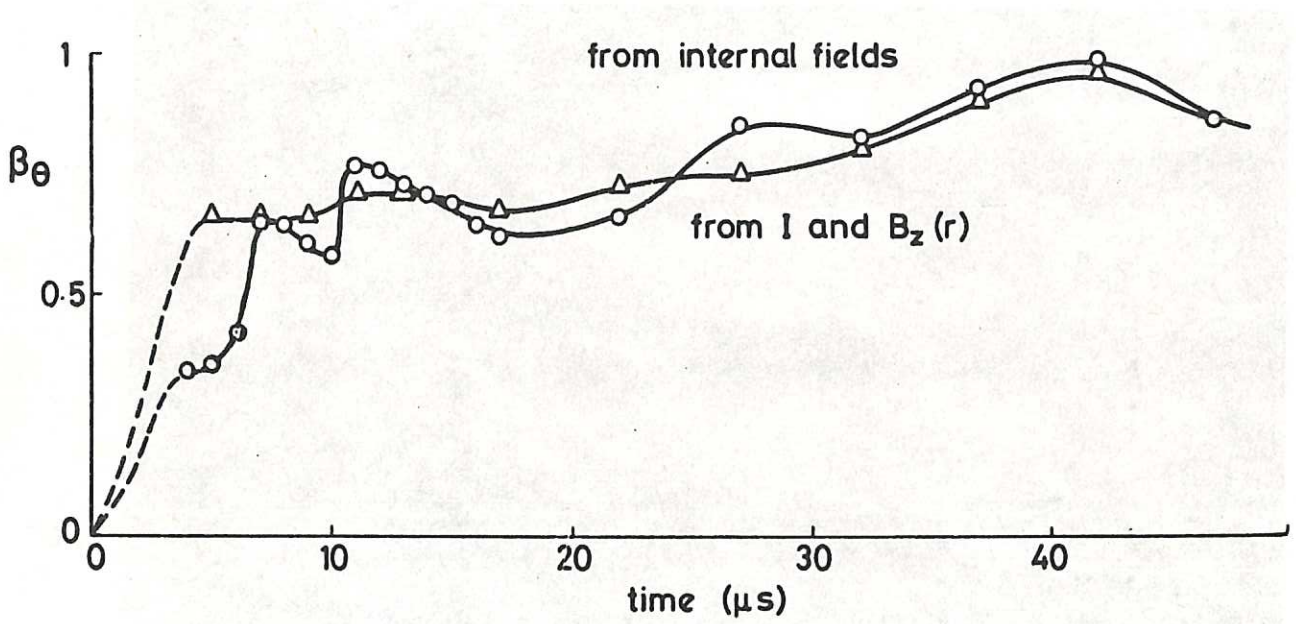

Fig. 25 The time dependence of β_θ for the RFP of figure 22 obtained in the same way as for figure 12(c).

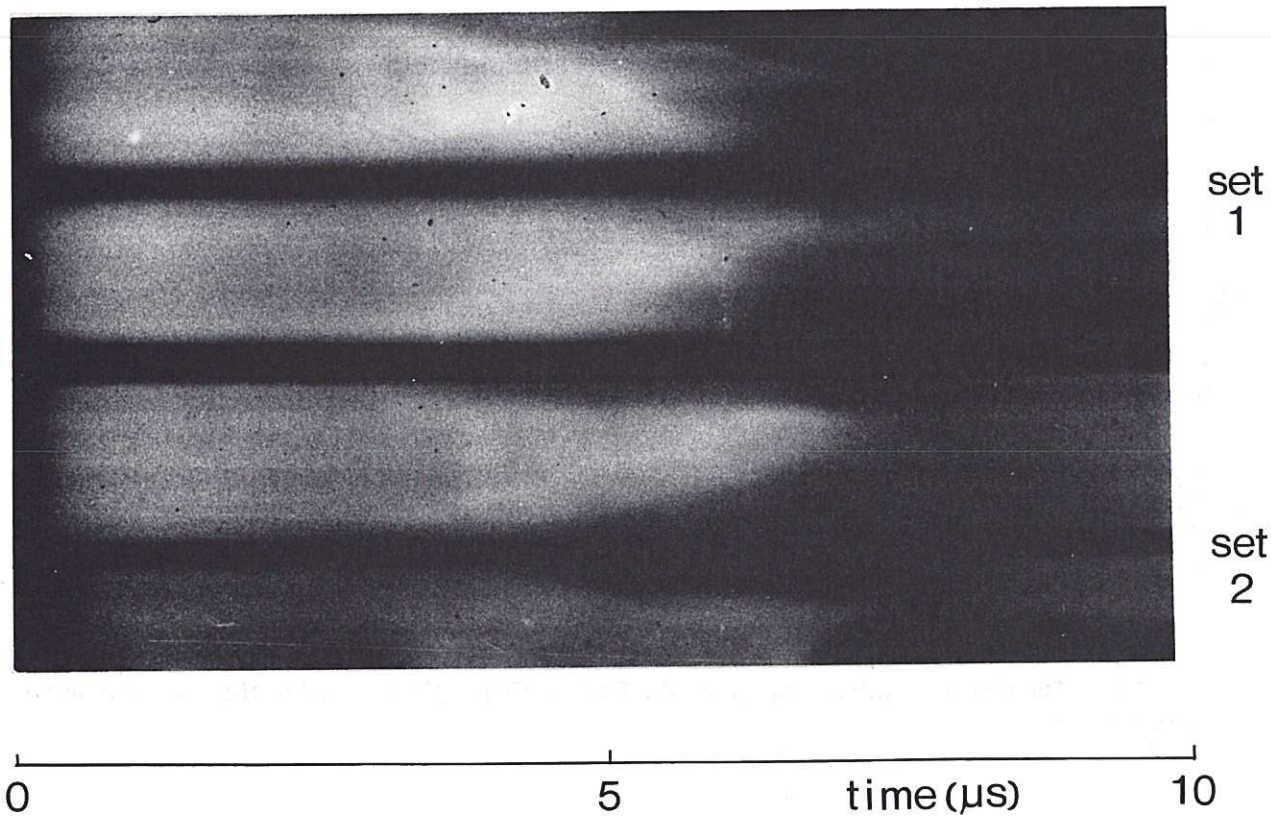

Fig. 26 Streak photographs of the RFP of figure 22. Most details are the same as for figure 9, but two views orthogonal to each other are now given at each position (set 1 and set 2), and the sweep-time is 10 μs.

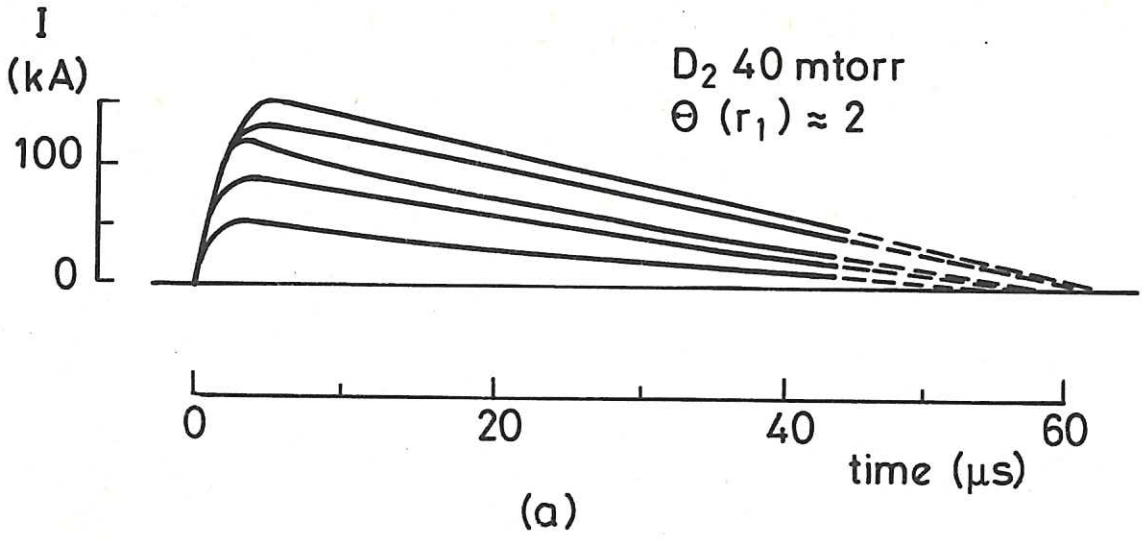

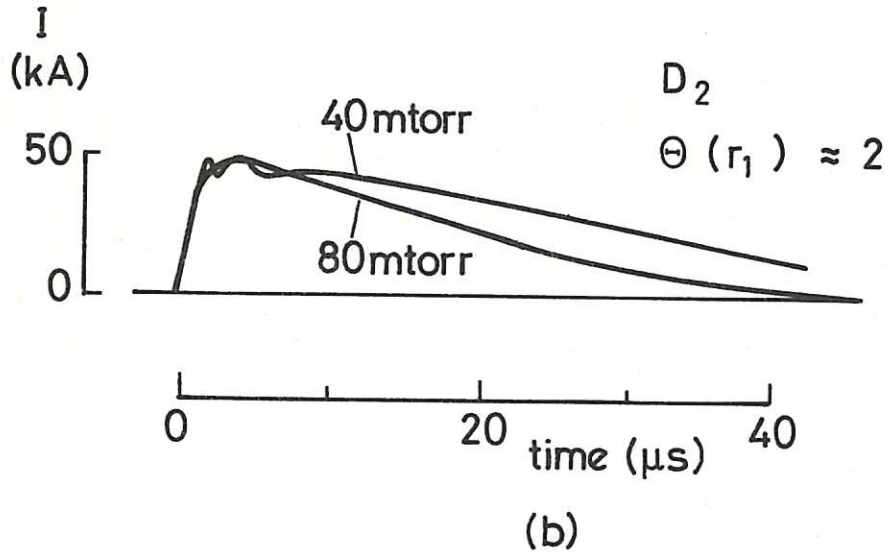

Fig. 27 (a) Comparison of the decay of the plasma current for a series of RFPs in Deuterium with similar pinch ratios and the same filling pressure but different values of the peak current (Section 6.2.3).

(b) Comparison of the decay rate of the current in similarly programmed RFPs in Deuterium for two different values of the filling pressure.

HER MAJESTY'S STATIONERY OFFICE

Government Bookshops

49 High Holborn, London WC1V 6HB
13a Castle Street, Edinburgh EH2 3AR
41 The Hayes, Cardiff CF1 1JW
Brazennose Street, Manchester M60 8AS
Wine Street, Bristol BS1 2BQ
258 Broad Street, Birmingham B1 2HE
80 Chichester Street, Belfast BT1 4JY

Government publications are also available through booksellers